New sulfur based compounds for efficient energy production

Adam Bertrand

Normandie Université

THÈSE

Pour obtenir le diplôme de doctorat

Spécialité CHIMIE

Préparée au sein de l'Université de Caen Normandie

New Sulfur Based Compounds for Efficient Energy Production

Présentée et soutenue par
ADAM BERTRAND

Thèse soutenue le 14/12/2022 devant le jury composé de		
M. MANUEL GAUDON	Professeur des universités, Université de Bordeaux	Rapporteur du jury
MME LORETTE SICARD	Maître de conférences HDR, Université Paris Cité	Rapporteur du jury
M. TRISTAN BARBIER	Maître de conférences, ENSICAEN	Membre du jury
MME CHRISTEL LABERTY-ROBERT	Professeur des universités, Sorbonne Université	Membre du jury
M. FABIEN GRASSET	Directeur de recherche, UNIVERSITE RENNES 1	Président du jury

Thèse dirigée par FRANCK GASCOIN (Laboratoire de cristallographie et sciences des materiaux (Caen))

UNIVERSITÉ CAEN NORMANDIE

ED 591 PSIME

RISMA

Normandie Université

THÈSE

Pour obtenir le diplôme de doctorat

Spécialité CHIMIE

Préparée au sein de l'Université de Caen Normandie

New Sulfur Based Compounds for Efficient Energy Production

Présentée et soutenue par

ADAM BERTRAND

Thèse soutenue le 14/12/2022
devant le jury composé de

M. MANUEL GAUDON	Professeur des universités, Université de Bordeaux	Rapporteur du jury
MME LORETTE SICARD	Maîtresse de conférences HDR, Université Paris Cité	Rapporteur du jury
M. TRISTAN BARBIER	Maître de conférences, ENSICAEN	Membre du jury
M. FABIEN GRASSET	Directeur de recherche, Université de Rennes 1	Membre du jury
MME CHRISTEL LABERTY-ROBERT	Professeure des universités, Sorbonne Université	Membre du jury
M. FRANCK GASCOIN	Professeur des universités, Université de Caen Normandie	Directeur de thèse

Thèse dirigée par FRANCK GASCOIN et encadrée par TRISTAN BARBIER, Laboratoire de cristallographie et sciences des materiaux (Caen)

UNIVERSITÉ CAEN NORMANDIE

ED 591 PSIME

RISMA

REMERCIEMENTS

Tout d'abord, je tiens à très grandement remercier Tristan Barbier et Franck Gascoin pour m'avoir offert l'opportunité de travailler sur ce projet de thèse au laboratoire CRISMAT, à un moment où j'étais proche d'abandonner mes recherches pour un sujet. Je les remercie aussi pour leur disponibilité et leurs soutiens tout le long de celle-ci, malgré les difficultés inattendues auxquelles j'ai dû faire face par rapport à cette capricieuse samsonite. Sans leurs expertises et conseils, je n'aurais sans doute jamais fini par réussir à trouver comment reproduire ce minerai.

Je tiens aussi à remercier mes parents, Justine et Patrick, mes frères, Alec et Scott, et ma sœur, Ines, pour leur support et leur confiance en moi tout le long de mes études supérieures jusqu'à ce jour. Vous avez mes sincères excuses pour ne pas avoir été souvent là avec la distance combinée avec les événements de ces dernières années.

Je remercie aussi sincèrement Benjamin pour son soutien durant la recherche de thèse suivi de ces trois dernières années. En cette longue période compliquée, pas tout le monde aurait décidé de rester jusqu'au bout et n'en a été rendue que plus simple par ta présence.

Je remercie Hugo pour avoir dû me supporter pendant deux ans et demi dans le même bureau. Et, plus sérieusement, les discussions sur nos travers respectifs durant la thèse avec (parfois, peut-être) des solutions l'un pour l'autre, les possibilités de repas à l'essentiel, la sincérité, etc.

Je remercie Cédric pour le soutien mutuel par messages pendant les étrangetés du doctorat alors que nos thèses se concluent bientôt.

Je remercie Laurence Hervé pour l'aide et ses conseils qu'elle m'a apportés plus d'une fois pour la mise en place des multiples méthodes de synthèses que ce projet a nécessitée.

Je remercie Sophie, Stéphanie, Caroline, Jérôme, Sylvie et Fabien pour les formations aux machines et les caractérisations que je ne pouvais toujours faire moi-même.

Je remercie Sylvie Hébert et Denis Pelloquin pour leurs expertises sur le magnétisme et la microscopie.

Merci à Thibault, Lucie, Justine, Martin et Aerman pour leurs aides précieuses en tant que stagiaires pour ces nombreuses synthèses.

Je remercie les autres doctorants et post-doctorants, présents et passés, pour la bonne ambiance du laboratoire.

Je remercie aussi tous mes joueurs de JDR (would they be french speaking or otherwise) pour me permettre d'avoir la possibilité de créer ensemble des histoires sur des chasseurs de vampires, des enfants alsaciens

déménageant en Normandie, de gendarmes français résolvant d'étranges crimes, des shadowrunners extrêmement professionnels tant qu'on les laisse le temps de se préparer, des amis inquiets par la disparition de celle qui maintenait le groupe ensemble, et tant d'autres pendant des périodes où j'avais bien besoin de penser à autre chose. May you all forgive me for not listing all your names, it would take way too much place!

Merci aussi à mes camarades épéistes et notre maître d'armes du SUAPS de Caen pour les séances d'escrime qui ont toujours été agréables et permis de me défouler un peu tous les lundis (auxquels je venais, désolé de ne pas avoir été 100 % assidu…), malgré les difficultés occasionnées par les conditions sanitaires.

Merci à tous mes amis, dispersés à travers le pays (et parfois plus loin encore), que j'ai eu la chance de trouver le temps de revoir ou l'esprit de garder contact, même si vos noms ne sont pas tous cités ici, sachez que vous comptez tous énormément pour moi et je pense souvent à vous d'une manière ou d'une autre, même si je ne le manifeste pas forcément.

.

RÉSUMÉ ÉTENDU EN FRANÇAIS

Les travaux de thèse présentés dans ce manuscrit sont principalement axés sur les diverses méthodes de synthèses développées, afin d'obtenir le composé thioantimoniate $Ag_4MnSb_2S_6$ aussi connu sous le nom de **samsonite.** Ce composé tire son nom de la mine, ou plus exactement de la veine hydrothermale, de Samson en Allemagne, lieu où ce minéral a été découvert (1908). Les raisons pour lesquelles ce composé est le point central de ce projet sont multiples :

- Tout d'abord, ce composé qui présente des éléments abondants et non-toxique n'a jamais été synthétisé en laboratoire jusque-là.
- Sa structure cristalline est l'autre raison pour laquelle nous souhaitons synthétiser ce minéral. En effet, la maille élémentaire de la phase samsonite, représentée sur la Figure i, est complexe (groupe d'espace : $P2_{1/n}$ avec a = 10.3861 Å, b = 8.1108 Å, c = 6.6637 Å, and β = 92.639 °). D'un côté, les atomes d'argent (Ag1 et Ag2 – position de Wyckoff : *4e*) sont très mobiles, mais sans que cela ne provoque de conductivité ionique et d'un autre côté, les atomes d'antimoine (Sb1 – position de Wyckoff : *4e*) sont en configuration AX_3E_1. Cette configuration de l'antimoine met en évidence un doublet non-liant qui permet de drastiquement diminuer la conductivité thermique de réseau, grâce notamment à un effet dit de « rattling » (dû au « frottement » du doublet non-liant). La structure complexe de ce composé, associée au doublet non liant de l'antimoine pourrait donc faire de ce matériau un excellent candidat pour des applications thermoélectriques.

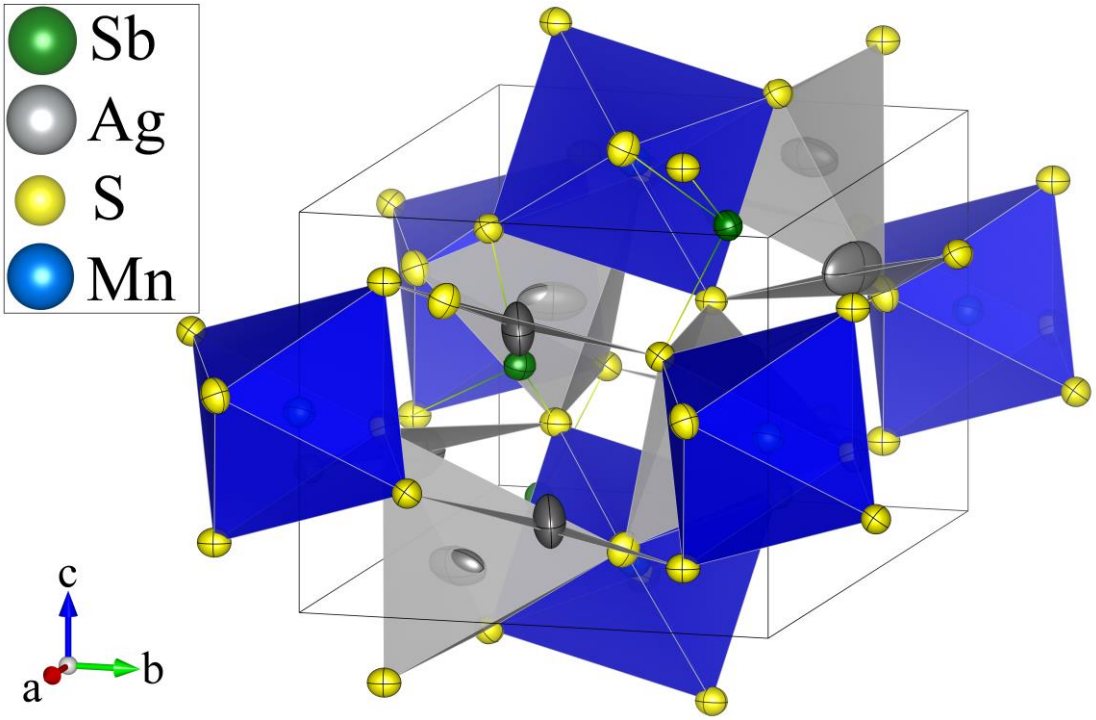

Figure i: *Structure cristalline de la samsonite.*

La thermoélectricité est un concept reliant électricité et chaleur : un transport de chaleur à travers un matériau peut s'appliquer à un semi-conducteur sur lequel un courant est appliqué (effet Peltier) *OU* un courant peut-être généré dans un semi-conducteur auquel est appliqué un gradient de température (effet Seebeck).

Un matériau thermoélectrique performant doit posséder, une conductivité électrique élevée (nécessaire pour limiter les échauffements induits par effet joule), un coefficient Seebeck élevé afin de générer un maximum de tension pour un gradient de température donné, et une conductivité thermique faible (la chaleur ne doit pas être conduite pour pouvoir conserver un gradient de température important). Ces différentes propriétés sont reliées entre elles au travers de la figure de mérite ZT, évaluant la performance des matériaux thermoélectriques :

$$ZT = \frac{\sigma S^2 T}{\kappa}$$

Avec T représentant la température (en Kelvin (K)), S représentant le coefficient Seebeck (en Volt par Kelvin ($V.K^{-1}$)) qui définit le voltage généré par la différence de température, σ représentant la conductivité électrique (en Siemens par Mètre ($S.m^{-1}$)) et, enfin, κ représentant la conductivité thermique (en Watt par Mètre par Kelvin ($W.m^{-1}.K^{-1}$).

De nombreuses applications industrielles mettant en jeux des matériaux thermoélectriques sont d'ores et déjà commercialisées. Il existe bien des déshumidificateurs, des mini-frigos ou du matériel électronique qui fonctionnent avec ce type de système. Malheureusement, le rendement des matériaux étant faible (~10 %) par rapport aux autres sources énergétiques préexistantes (par exemple, un ZT d'environ 20 est nécessaire pour atteindre la puissance d'un moteur Stirling), ces utilisations persistent à être très limitées. La communauté scientifique s'efforce donc de synthétiser de nouveaux matériaux, composés d'éléments abondants et non-toxiques, présentant de meilleures performances thermoélectriques.

Ces travaux de thèse impliquent donc des **synthèses**, le **traitement des poudres**, des méthodes de **frittage**, l'analyse systématique des **structures** et des **microstructures** ainsi que des caractérisations **magnétiques** et de **transport**.

Le premier chapitre de ce manuscrit est dédié aux synthèses à hautes températures. Premièrement, la méthode dite : « conventionnelle » pour l'obtention de binaires, ternaires et quaternaires sulfurés, à savoir, la synthèse par **voie solide** sera décrite. Cette voie de synthèse implique simplement de chauffer un mélange de poudres à de hautes températures pour forcer la diffusion des atomes et ainsi former une nouvelle phase. Cette voie de synthèse est relativement simple à mettre en place, mais elle implique de nombreux, longs et fastidieux essais avant l'obtention d'un composé monophasé. En effet, les faibles vitesses de diffusion des éléments engendrent de longs temps de recuit (pouvant être supérieur à 1 mois) et

généralement des broyages et pastillages intermédiaires sont nécessaires afin d'assurer une bonne homogénéité de l'échantillon. De plus, cette voie de synthèse, privilégiée pour la synthèse de phases oxyde, nécessite certaines précautions pour l'obtention de composés sulfurés (travail en boîte à gants, nécessité de sceller des tubes de préalablement sous vide). Cette voie de synthèse conventionnelle favorise l'obtention des phases les plus thermodynamiquement stables, c'est ainsi et sans surprise que le composé majoritaire obtenu par cette méthode est la pyrargyrite (Ag_3SbS_3), accompagnée de traces de sulfure de manganèse (MnS).

En effet, un minerai proche en composition, la pyrargyrite, dont des synthèses hors équilibres ont déjà été rapportées, semble thermodynamiquement plus stable. L'obtention systématique de la phase pyrargyrite lors de synthèse dites « conventionnelles » représente donc un défi supplémentaire pour l'obtention de la phase samsonite sans que ce composé « secondaire » et très difficile à décomposer n'apparaisse. Ceci est donc une occasion pour mieux appréhender et utiliser des méthodes de synthèse dites : **« hors équilibre »** pour synthétiser ce composé de manière monophasée.

Une méthode de synthèse expérimentée pour l'obtention de la phase samsonite est la synthèse par **sels fondus.** Il s'agit d'une variante de la méthode de flux qui est généralement utilisée comme post-traitement pour homogénéiser une synthèse réalisée par voie solide. On utilise un sel inorganique, qui a une température de fusion plus faible que celles des précurseurs, comme solvant ionique. Les conditions spéciales de cette méthode de synthèse permettent de se placer à des températures plus faibles que celles utilisées lors de synthèse par voie solide. De plus, la nature du solvant permet de précipiter des composés hors de l'équilibre thermodynamique. Malheureusement, cette méthode de synthèse ne s'avère pas efficace pour l'obtention de la phase samsonite, car la formation, une fois de plus, de la phase pyrargyrite (Ag_3SbS_3) et du sulfure de manganèse (MnS) ne permettent pas l'obtention du composé désiré. Cependant, d'autres composés furent formés lors de l'utilisation de cette méthode.

Le premier fut le composé $MnSbS_2Br$, qui fut formé pendant une tentative de synthèse de la samsonite par sel fondu avec $MnBr_2$ en tant que solvant et réactif.

Afin d'éviter l'apparition systématique de la phase pyrargyrite lors des synthèses de la samsonite, des tentatives de substitution ont été expérimentées. C'est ainsi que trois autres composés ont été formés :

- Un composé ayant également la structure du composé tétraédrite (de formule générale $Cu_{12}Sb_4S_{13}$) $(Ag, Cu)_{10}Mn_2Sb_4S_{13}$, mais une composition exacte difficile à identifier.
- Un ternaire, $MnSb_2S_4$ (dont l'optimisation de la synthèse sera conduite par Martin Leproult dans un stage, puis une thèse en continuation de celle-ci).
- Et enfin, la wassonite (TiS), un composé dont la seule synthèse mentionnée dans la littérature est une synthèse par voie solide de 2 mois qui mène à deux phases différentes, une stable et une

métastable. Les résultats obtenus par la méthode de synthèse par sels fondus sont représentés dans la Figure ii :

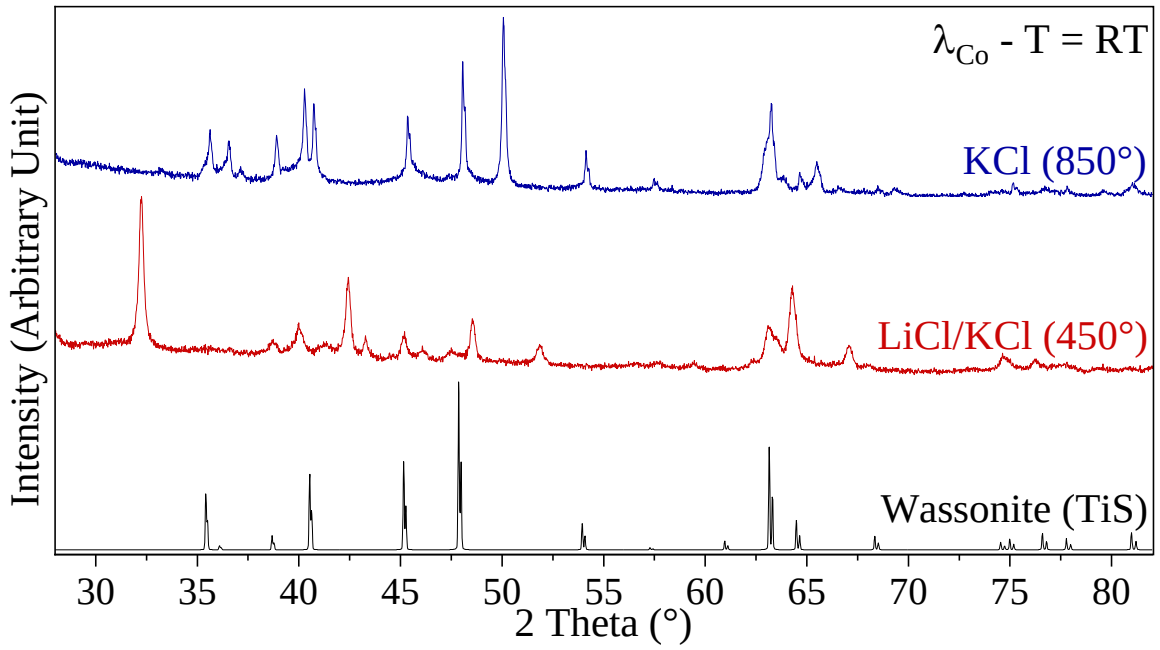

Figure ii: *Diagramme de Diffraction des Rayons X (DRX) des composés formés par la méthode de synthèse par sels fondus accompagné d'un scan simulé de la wassonite (minerais de sulfure de titane (II)) (ICSD : 25561).*

Le second chapitre de ce manuscrit sera consacré à une autre méthode de synthèse utilisant des températures plus basses : la synthèse **hydrothermale**. Le nom de cette méthode a une origine géologique, puisqu'elle était d'abord utilisée pour décrire les conditions dans lesquelles des minerais (dont la samsonite) étaient formés sous terre grâce aux conditions de pressions et températures « exotiques » (car très éloigné de ce qui est communément observé lors de synthèses conventionnelles) sous-terraines dans des poches d'eau sous forme de gaz. Le terme a ensuite été utilisé lorsque des conditions similaires tentent d'être répliquées dans un contexte de laboratoire. Au fil du temps, deux perspectives sur la méthode hydrothermale se distinguent :

- Tout d'abord la méthode « douce », qui implique des températures inférieures à 250 °C où le véritable apport est la forte température dans un système fermé qui maintient la quantité d'eau présente dans celui-ci.
- La méthode « dure », quant à elle utilise des températures proches, ou supérieure, au point critique de l'eau (voie hydrothermale) ou du solvant utilisé (voie solvothermale), dans ce cas, températures et pressions sont des facteurs prédominants pour l'obtention des composés désirés.

Cette méthode a l'avantage d'être économe en énergie et en temps par rapport à la synthèse par voie solide et permet d'obtenir des composés métastables (ou hors équilibre). Cependant, celle-ci n'est pas triviale, car elle est fortement sensible aux variations des paramètres utilisés (précurseurs, volumes,

minéraliseurs, concentrations, cycles thermiques, température (montrée en exemple dans la Figure iv), …) et a une tendance à former de multiples phases, nécessitant en conséquence de nombreuses expérimentations pour une optimisation de la synthèse du composé recherché. Dans le cas de la phase samsonite, l'obtention de cette dernière nécessite des précurseurs acétates pour l'argent et le manganèse (nécessitant d'être ajouté en excès) et un composé thioantimoniate du nom de Sel de Schlippe ($Na_3SbS_4.9H_2O$) comme précurseurs d'antimoine et de soufre. Ce sel n'étant plus produit de manière commerciale, il a été nécessaire de le synthétiser de manière rapide et efficace au laboratoire. Un protocole expérimental impliquant de l'eau, du soufre, Na_2S et Sb_2S_3 dans un broyeur planétaire suivi d'une filtration et d'une évaporation sous vide permet une synthèse efficace (monophasé, homogène, comme montré dans la Figure iii, et avec un rendement d'environ 90 %). La méthode de synthèse développée durant cette thèse, permet un gain de temps important (quelques heures comparées à plusieurs jours par rapport aux méthodes précédemment rapportées) ainsi qu'un gain important de rendement (90 % au lieu des 30 % des méthodes précédemment rapportées).

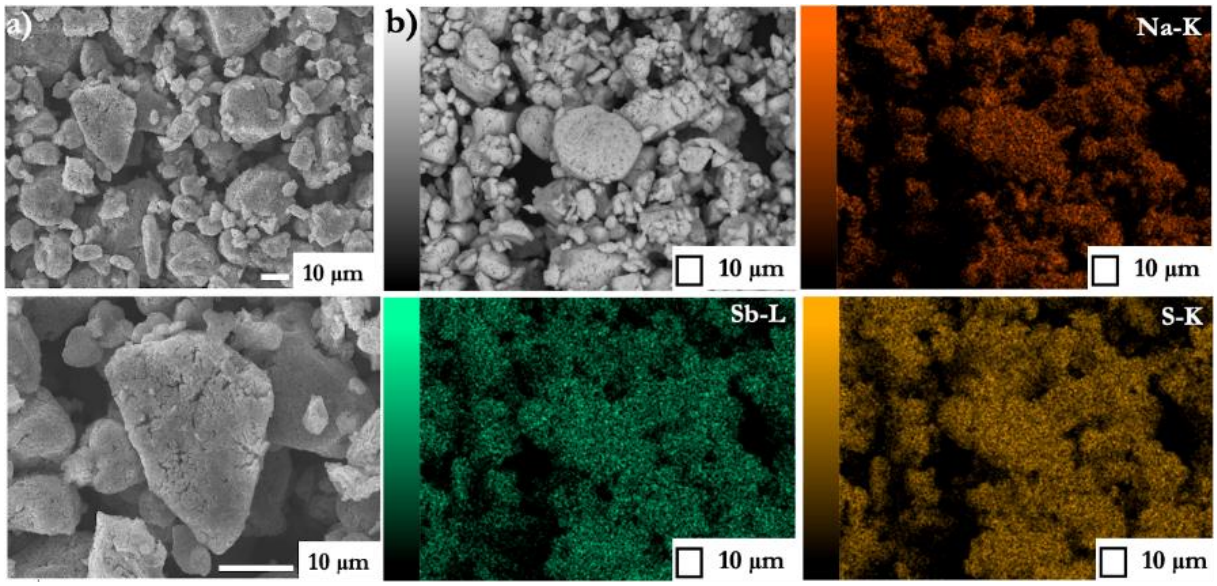

Figure iii: *Images Microscopie Electronique à Balayage (MEB) du sel de Schlippe a) avec un grossissement x1000 et x2500 b) avec un mapping EBSD de Na, Sb et S.*

Les trois précurseurs ont été dissous dans l'eau sous forte agitation avant d'être introduits dans une bombe hydrothermale. Cette dernière est ensuite rapidement chauffée à 180 °C et maintenue pendant 24 heures avant un refroidissement qui s'effectue grâce à l'inertie du four. La poudre obtenue est un mélange entre la phase samsonite (97 %) et la phase pyrargyrite (3 %). Malgré le pourcentage élevé de phase samsonite obtenu, le composé ternaire (Ag_3SbS_3) est tout de même toujours présent. Il convient également de mentionner que le temps de synthèse globale est relativement long, car cette méthode nécessite la synthèse préalable du sel de Schlippe. Une autre méthode de synthèse fut donc explorée avec l'objectif d'obtenir seulement la phase samsonite.

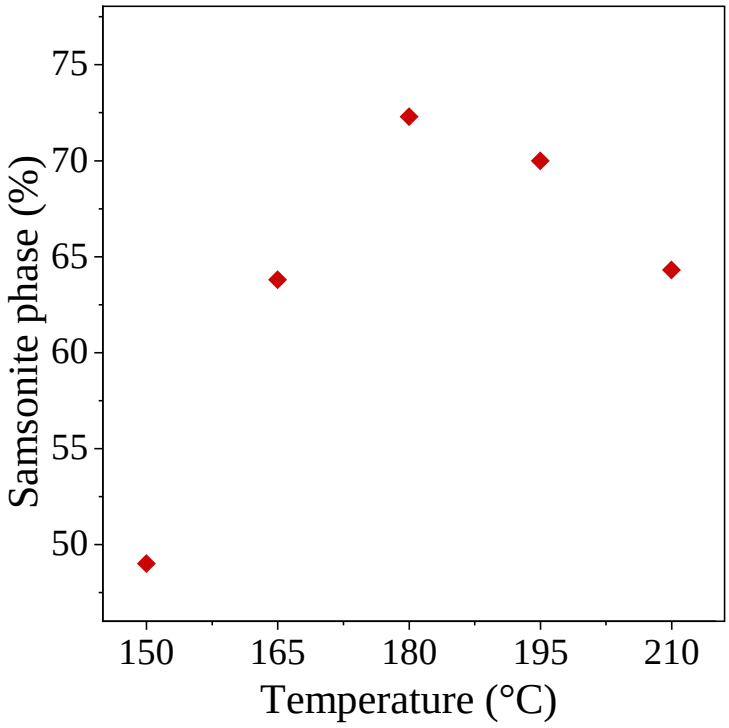

Figure iv : *Evolution de la formation de la phase samsonite en fonction de la température de plateau.*

Ainsi, le chapitre 3 est donc dédié à une autre méthode de synthèse dont le mécanisme principal est la précipitation hors équilibre de matériaux : **la synthèse polyol**. Celle-ci consiste en l'utilisation de précurseurs dans un solvant organique composé de multiples fonctions alcool. La forte température d'ébullition, permettant une précipitation dans des conditions exotiques est un des points communs avec la synthèse hydrothermale, mais ici, le solvant joue aussi un rôle d'agent réducteur pendant la synthèse. Cette méthode a des avantages similaires à la synthèse hydrothermale, mais est aussi souvent utilisée dans des cas où le contrôle de la morphologie des grains formés durant la synthèse est primordial. Cependant, la synthèse polyol partage les inconvénients de la méthode hydrothermale. En effet, si le nombre de paramètres à contrôler restent inférieurs à ceux de la synthèse hydrothermale, ils engendrent malgré tout de grandes variations dans les composés obtenus, de plus, la nature organique des solvants utilisés et la possibilité de leur auto-réduction rend cette méthode plus polluante avec l'impossibilité de réutiliser les solvants. Le protocole expérimental optimal mis en place dans cette étude fut l'utilisation d'acétate d'argent, acétate de manganèse, acétate d'antimoine et du soufre dans une solution de 3-aminopropan-1-ol. Le mélange a été chauffé sous azote dans un montage à reflux pendant 3h30min puis refroidie à l'air ambiant sous une agitation magnétique forte et constante. Ce protocole s'avère être aussi aussi efficace que la synthèse hydrothermale puisque la poudre formée est composée en quasi-majorité de samsonite (95 %) mais avec des traces d'alliages plutôt que la phase pyrargyrite (dyscrasite (Ag_3Sb) à 4 % et d'antimoine à 1 %), comme le montre l'affinement Rietveld appliqué à la diffraction des rayons X de la Figure v. Avec

deux méthodes de synthèse efficaces de la samsonite maintenant maîtrisées, l'attention s'est ensuite tournée sur l'étude du matériau et de ses propriétés.

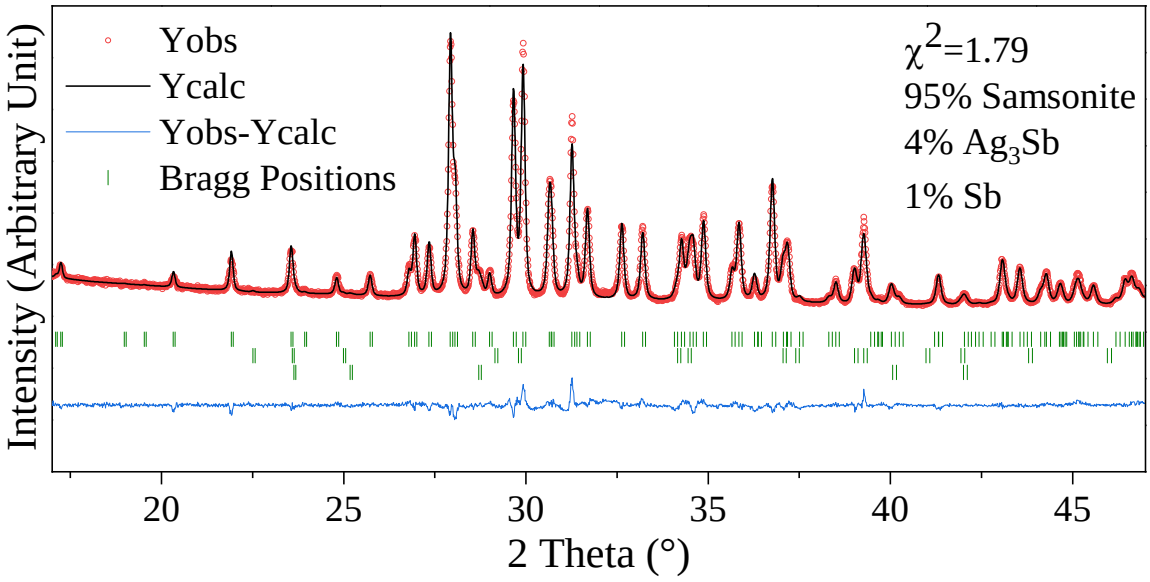

Figure v: *Diagramme DRX d'un composé samsonite synthétisé par la méthode polyol.*

Dans ce quatrième chapitre, l'attention a été mise sur les propriétés de la samsonite synthétique. Ce chapitre sera également consacré à la comparaison des structures et microstructures engendrées par les modes de synthèse, les propriétés physico-chimiques seront également comparées et discutées. En effet, même si sa découverte date de 1910 et que sa structure cristalline a été précisément caractérisés par Luca Bindi et Michel Evain, peu d'informations précisent existent sur les propriétés physicochimiques de ce composé. Ceci est probablement dû à sa rareté et sans applications facilement apparentes.

En conséquence, ce chapitre apporte de nouvelles informations sur le composé. Suite à une étude en Analyse Thermogravimétrique et Calorimétrie Différentielle à Balayage (ATG-DSC), complémentée par une étude de multiples DRX en température, une température de **décomposition** d'environ 160 °C pu être déterminée.

Le **comportement magnétique** du matériau fut aussi déterminé en fonction de la température et du champ magnétique appliqué à celui-ci. La samsonite est donc un composé paramagnétique à fluctuations antiferromagnétiques avec une transition à environ 7 K. Le caractère (II+) des atomes de manganèse a pu être confirmé grâce à leur moment magnétique, déterminé à partir de la susceptibilité du composé et sa température de Curie. De plus, une hystérèse magnétique à bas champs a été observé ; comme le montre la Figure vi, permettant de déterminer en conséquence la coercivité et la rémanence magnétique du composé à 5 K.

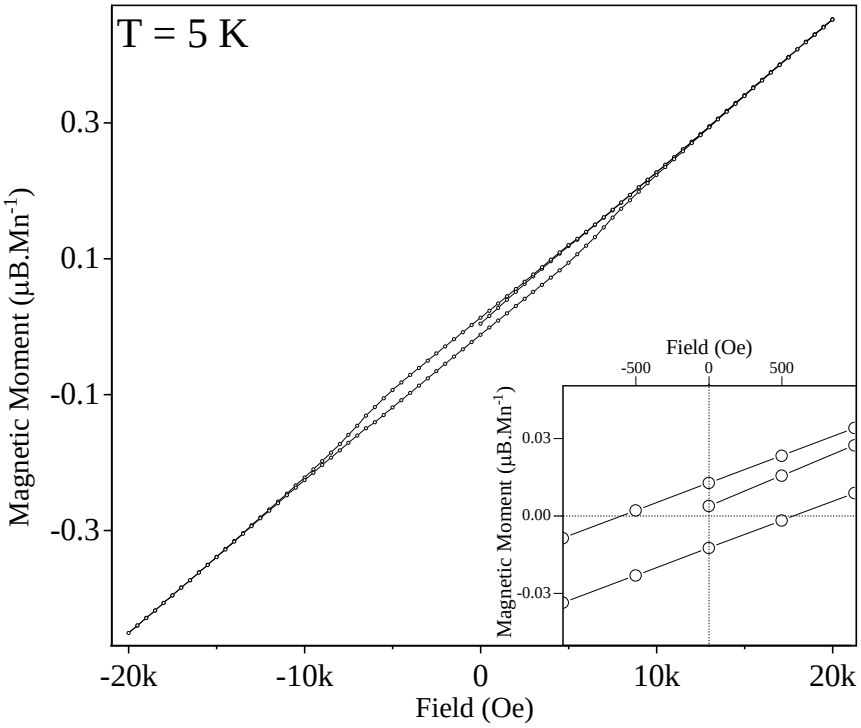

Figure vi: *Moment magnétique de la phase samsonite en function du champ magnétique appliqué à une température constante de 5 K.*

Une comparaison entre les **morphologies** des composés de synthèse hydrothermale et polyol est effectuée via la microscopie à balayage électronique et granulométrie. Avec les informations limitées sur le composé (pas d'indices de réfraction ou d'absorption rapportés), seuls une information générale pouvait être tirée par la granulométrie, mais la tendance de grains issus du processus polyol étant inférieurs à ceux obtenus via la synthèse hydrothermale. En addition à celle-ci, une étude au microscope électronique à balayage (dont certaines des images représentatives peuvent être observées en Figure vii) permis de déterminer une taille moyenne (790 nm pour la synthèse hydrothermale et 890 nm pour la synthèse polyol) et des formes des grains formés (des plaques pour le processus polyol et des bâtons avec la synthèse hydrothermale).

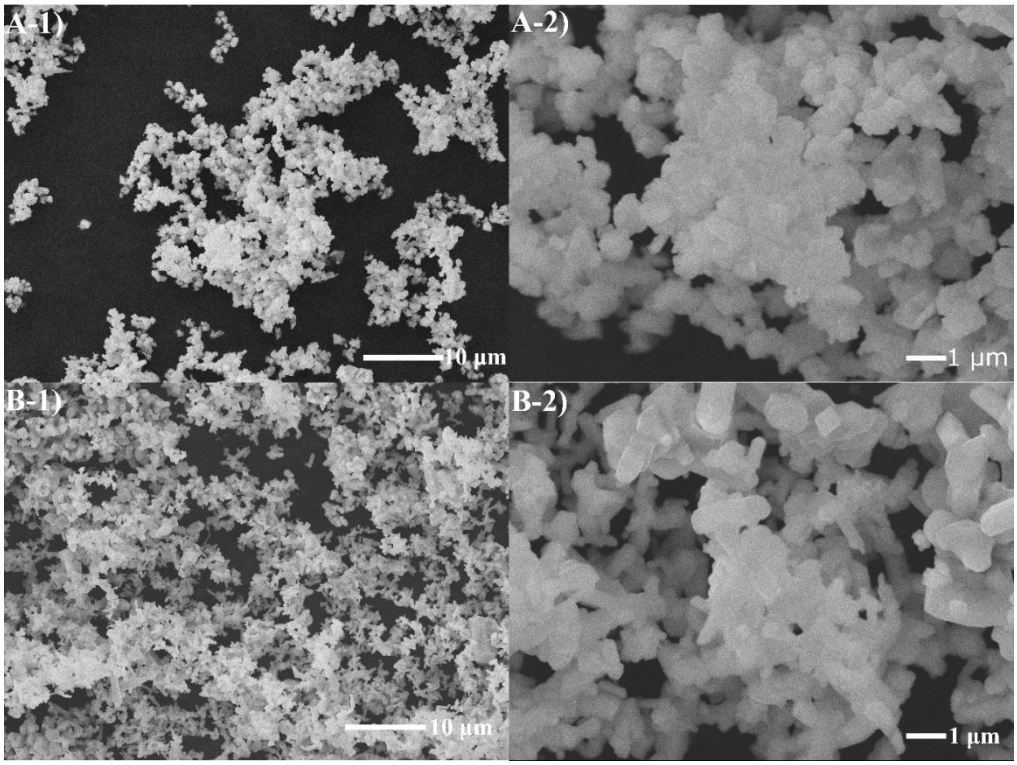

Figure vii: *Images MEB des poudres synthétisées via A) méthode hydrothermale et B) Synthèse polyol à un grossissement de 1) x2 000 et 2) x10 000.*

Concernant les propriétés déjà rapportées, la phase samsonite de synthèse pu être comparée à la **structure cristalline** rapportée par Bindi et Evain avec la méthode Gram-Charlier, avec une analyse, complémentée par une analyse via « fonction de distribution de paires » qui est une méthode faisant fi des paramètres instrumentaux et permettant de se concentrer uniquement sur les distances inter-atomes.

Des tentatives pour obtenir un composé dense, permettant d'estimer correctement les propriétés de transport de la samsonite, furent testées, à travers le **frittage** à haute température, le « Spark Plasma Sintering » (SPS) et par presse isostatique, mais malheureusement, les tests furent peu concluants. La décomposition à basse température du composé impliquant que la pression fut le paramètre primordial pour une densification efficace. Une densité de 80 % environ seulement fut atteignable sans décomposition notable ou instabilité de la pastille, ou du barreau, formé.

Par rapport aux propriétés thermoélectriques du composé, malheureusement, le manque de densité et une trop haute résistivité électrique font que celle-ci ne peuvent être déterminées. Cependant, la résistivité électrique étant supérieure à 60 MΩ indique clairement que la samsonite est probablement trop isolant pour être effectif en tant que matériau thermoélectrique. Des modifications de la composition de la phase pourraient être envisagées pour améliorer celles-ci.

TABLE OF CONTENTS

Remerciements i

Résumé étendu en Français iii

Introduction 1

A. Thermoelectricity 1

B. Samsonite 2

I. High-Temperature Synthesis 7

A. State of the art 7

I.A.1. Solid State Synthesis 7

I.A.2. Molten Salt Synthesis 7

B. Results and discussion 9

I.B.1. Solid State Synthesis 9

I.B.2. Molten Salt Synthesis 10

C. Conclusion 19

II. Solvothermal Synthesis 21

A. State of the art 21

B. Experimental Section 27

C. Results and discussion 28

II.C.1. Influence of Solvent 28

II.C.2. Influence of Volume 32

II.C.3. Influence of Precursors 34

II.C.4. Synthesis of Schlippe's Salt 39

II.C.5. Influence of concentration 42

II.C.6. Influence of heating cycle 43

II.C.7. The eventuality of (sulf)oxide formation 45

II.C.8. Optimal solvothermal synthesis protocol for samsonite phase and conclusions 46

III. Polyol Synthesis 49

A. State of the art 49

B. Experimental Section 51
C. Results and discussions 53
III.C.1. Influence of Atmosphere 53
III.C.2. Influence of solvent 55
III.C.3. Influence of precursors 59
III.C.4. Influence of the concentration 61
III.C.5. Influence of stirring speed 62
III.C.6. Influence of the heating cycle 64
III.C.7. Mechanisms behind the polyol synthesis 66
IV. Physical Properties of Samsonite 69
A. State of the art 69
B. Characterization and sintering techniques 70
C. Results and discussion 72
IV.C.1. X-Ray Diffraction and Pair Distribution Function 72
IV.C.2. Decomposition study (ATG-DSC and in-situ XRD) 77
IV.C.3. Magnetic properties 85
IV.C.1. Grain morphologies 88
IV.C.2. Sintering 90
IV.C.3. Thermoelectric properties 93
Conclusion 97
Bibliography 99
Appendix I
Résumé en Français IX
Summary in English IX

LIST OF FIGURES

Figure 1: Photograph of samsonite crystals from the Samson mine.[9] 2
Figure 2: crystal structure of the samsonite. 3
Figure 3: Schematic diagram of the Solid State Synthesis reaction of a disulfide compound with A and B as metals. 7
Figure 4: Schematic diagrams of the formation of product particle P from reactant particles A and B by (a) solution-precipitation and (b) solution-diffusion processess[22] 8
Figure 5: Heating cycle for molten salt synthesis. 9
Figure 6: Room temperature XRD pattern of solid-state synthesis and simulated patterns of Ag_3SbS_3 (COD: 1011162), $AgSbS_2$ (COD: 1509521), and MnS (COD: 9005930). 10
Figure 7: Room temperature XRD patterns from synthesis with molten chlorides and simulated patterns of Ag_3SbS_3 (COD: 1011162), $AgSbS_2$ (COD: 1509521), and MnS (COD: 9005930). 11
Figure 8: Room temperature XRD pattern from molten salt synthesis and simulated patterns of Ag_2S (COD: 1544685) and Sb_2S_3 (COD: 9007051). 12
Figure 9: Room temperature XRD pattern from molten salt synthesis with $MnBr_2$ as a solvent and simulated patterns of AgBr (ICSD: 65061) and $MnSbS_2Br$ (COD: 1528449). 13
Figure 10: Room temperature XRD patterns of "$Ag_{4-x}Cu_xMnSb_2S_6$" tetrahedrite compounds. 14
Figure 11: Room temperature XRD pattern of "$Ag_{0.8}Cu_{3.2}MnSb_2S_6$". Red scatters correspond to the experimental data, the black line corresponds to the Rietveld simulation which has been performed by using two distinct tetrahedrite phases (i.e., using slightly different cell parameters); finally, the blue line points out the difference between the experimental and the calculated data, and the green scatters highlight the Bragg position. 15
Figure 12: Room temperature XRD pattern of Molten Salt Synthesis and simulated pattern of $MnSb_2S_4$. 17
Figure 13: Room temperature XRD pattern of the synthesis method to attempt synthesizing $TiSb_2S_4$ and simulated patterns of Ti_3S_4 (ICSD: 25562) and Sb (COD: 9008575). 17
Figure 14: room temperature XRD pattern of the synthesis method to attempt to synthesize TiS and simulated pattern of the wassonite phase (mineral TiS) (ICSD: 25561). 18
Figure 15: Variation of pressure according to temperature and pure water fill with blue zone being the domain explored in this study and orange zone being the supercritical domain.[21] 21
Figure 16: Variation of the dielectric constant of pure water according to pressure and temperature.[21] 22
Figure 17: a graphic representation of evolution under the LaMer model of (a) the nuclei number (———) and their size (-------) (b) the concentration of complexes (with C_{sat} the saturation

concentration, C_{min} the concentration at which point the precipitation process starts and C_{max} the maximum supersaturation reached by the precursor) and (c) the speed of growth (-------) and the speed of nucleation (———). In all graphs, every step is represented by I: rise of concentration, II: nucleation-growth, III: growth, IV: Oswalt Rippening. [28] 23
Figure 18: Potential structure types of polysulfide complexes. [34] 24
Figure 19: General complexes formed during hydrothermal synthesis with M the metal, X an anion with an n- charge, h the hydrolysis ratio of the cation, α the number of water molecules on the first hydration shell, z the charge of the cation, q the hydrolysis ratio of the anion. [24] 24
Figure 20: picture of a digestive pressure vessel [16] and its various pieces..... 26
Figure 21: representation of $[H_3NCH_2CH_2NH_2][Ag_2SbS_3]$ along the ab plane. 29
Figure 22: Room temperature XRD Pattern obtained from powder synthesized in ethylenediamine compared to simulated patterns of hybrid silver thioantimoniate (COD: 4312632) and samsonite (COD: 9010235). 30
Figure 23: Room temperature XRD pattern obtained from the solvothermal synthesis with 2,2-DMP and theoretical patterns of pyrargyrite (COD: 1011162) and samsonite (COD: 9010235) phases. ..31
Figure 24: Room temperature XRD pattern obtained from the solvothermal synthesis with xylenes and theoretical patterns of pyrargyrite (COD: 1011162) and samsonite (COD: 9010235) phases. ..31
Figure 25: Room temperature XRD Patterns for solvothermal synthesis with ethanol and water compared to two simulated patterns of pyrargyrite (COD: 1011162) and samsonite (COD: 9010235) phases. 32
Figure 26: Room temperature XRD patterns of hydrothermal synthesis according to water fill. 33
Figure 27: Room temperature XRD patterns of powders synthesized by hydrothermal process, simulated patterns of the samsonite (COD: 9010235), the silver sulfide (COD: 1544685), and antimony oxide phases (COD: 9007587). 34
Figure 28: Samsonite phase formed according to the manganese/stoichiometry ratio. 36
Figure 29: Room Temperature XRD pattern of the powder obtained by hydrothermal synthesis with chloride precursors and the simulated patterns of the pyrargyrite phase (COD: 1011162). 37
Figure 30: Room Temperature XRD pattern of powder obtained from hydrothermal synthesis with nitrate precursors and simulated patterns of pyrargyrite (COD: 1011162) and silver sulfide (COD: 1509709). 37
Figure 31: Room temperature XRD patterns of powder obtained through hydrothermal synthesis with nitrate and acetate precursors. 38
Figure 32: Room temperature XRD patterns of stirred and unstirred reactive mixtures compared to theoretical scans of pyrargyrite (COD: 1011162) and samsonite phases (COD: 9010235). 39
Figure 33: powder X-Ray diffraction patterns of Schlippe's Salt with D8 ADVANCE. 40

Figure 34: SEM images a) with x1000 and x2500 magnification b) with EDS-Elemental mapping of Na, Sb, and S. 41
Figure 35: DSC-TGA curves of Schlippe's Salt under nitrogen flux. Heating rate = 3 °C/min. each horizontal line represents the number of water molecules present in the structure (9 at 100%, 0 at 66.16%). 41
Figure 36: Room temperature XRD patterns of powders obtained through hydrothermal synthesis according to assumed produced product compared to solvent volume. 42
Figure 37: Evolution of the proportion of the samsonite phase in powder obtained from hydrothermal synthesis according to maximum temperature. 43
Figure 38: Comparison of room temperature XRD patterns between powders obtained through hydrothermal synthesis with and without a sulfur source present. 45
Figure 39: SEM images with EDS-Elemental mapping of Ag, Mn, Sb, and S. 46
Figure 40: General presentation of the polyol process 49
Figure 41: General synthesis mechanisms during the polyol process where M is the solvated metal and “O—O” is the polyol compound. 50
Figure 42: Room temperature XRD patterns of powder obtained through polyol synthesis without a controlled atmosphere and simulated patterns of pyrargyrite (COD: 1011162) and samsonite (COD: 9010235) phases. 54
Figure 43: Room temperature XRD pattern of the powder obtained through polyol synthesis under pure oxygen with simulated patterns of the pyrargyrite phase (COD: 1011162) and the silver sulfide phase (COD: 1544685). 54
Figure 44: Room Temperature XRD Patterns of powder obtained through polyol synthesis with tetraethylene glycol according to temperature plateau. * are peaks related to the samsonite phase. 56
Figure 45: Room temperature XRD patterns of powders obtained through the polyol synthesis with propan-1,3-diol as a solvent and simulated patterns of silver sulfide (COD: 1544685), pyrargyrite (COD: 1011162), and samsonite (COD: 9010235) phases. 57
Figure 46: Room temperature XRD pattern of the powder obtained from polyol synthesis with aminopropanol as a solvent. 58
Figure 47: Suggested mechanism during the polyol process for manganese with “S—S” is the aminopropanol combined with the sulfur precursor. 59
Figure 48: Room temperature XRD pattern from powder obtained through polyol synthesis with Schlippe's salt as a precursor and the simulated pattern of the samsonite phase (COD: 9010235)... 59
Figure 49: Room temperature XRD pattern obtained from power synthesized through polyol process with excess sulfur and simulated patterns of myrargyrite (COD: 9002733) and samsonite (COD: 9010235) phases. 60

Figure 50: Room temperature XRD pattern of powder obtained through Polyol synthesis with sulfide precursors with simulated patterns of Ag_3SbS_3, MnS, and $AgSbS_2$. 61
Figure 51: $Zr_5O_8(SO_4)_2$ synthesis rate according to stirring speed. [72] 62
Figure 52: Room temperature XRD patterns of powders obtained according to their stirring speed during the polyol synthesis process. 63
Figure 53: Samsonite phase present in powder obtained from polyol process according to plateau duration. 64
Figure 54: Room temperature XRD patterns of powders obtained by polyol process depending on the cooling method. 65
Figure 55: Non-harmonic probability density isosurfaces of Ag1 and Ag2 for samsonite at 100 K, RT, and 400 K.[4] 69
Figure 56: Representation of two crystals -a) and b)- representative of samsonite shape. The same letter means the faces are of the same crystal shape. 70
Figure 57: Full Room Temperature XRD pattern of powder obtained polyol synthesis and its refinement, done through the Rietveld Model. 74
Figure 58: Full Room Temperature XRD pattern of powder obtained hydrothermal synthesis and its refinement, done through the Rietveld Model. 74
Figure 59: Diagram of samsonite phase synthesized through polyol process obtained through the Pair Function Distribution 76
Figure 60 : Diagram of samsonite phase synthesized through hydrothermal process obtained through the Pair Function Distribution 76
Figure 61: DSC–TGA curves of samsonite in Nitrogen. Heating rate = 3 °C.min^{-1} 78
Figure 62: In-Situ XRD patterns of Polyol synthesized samsonite powder according to temperature. 80
Figure 63: DSC–TGA curves of samsonite in Nitrogen from Figure 52, zoomed in on the 150-175 °C domain. Heating rate = 3 °C.min^{-1}. 81
Figure 64: DSC–TGA curves of silver sulfide and antimony sulfide mix up to 300 °C. Heating rate = 3 °C.min^{-1}. 83
Figure 65: The pseudobinary system Ag_2S-Sb_2S_3. All assemblages are in equilibrium with vapor. Phase relations involving the stephanite phase (Ag_5SbS_4) and pyrostilpnite (Ag_3SbS_3) are inferred from the behavior of minerals. [95] All compositions are in atomic percent. The red line represents the domain studied through DSC-TGA. 84
Figure 66: Magnetic susceptibility of the samsonite phase according to temperature with a constant field of 100 Oe. 85

Figure 67: Magnetic moment of the samsonite phase according to the magnetic field from 0 Oe to 50 000 Oe with a constant temperature of 5 K. 86
Figure 68: Magnetic moment of the samsonite phase according to the magnetic field from -20 000 Oe to 20 000 Oe with a constant temperature of 5 K. 87
Figure 69: Magnetic moment of the samsonite phase according to the magnetic field from -50 000 Oe to 50 000 Oe with a constant temperature of 20 K. 87
Figure 70: Distribution of size according to the volume of the powder present in the solvent. 88
Figure 71: SEM images of powders obtained from A) Polyol Synthesis and B) Hydrothermal Synthesis. Pictures were both taken at a 1) x2 000 and 2) x10 000 magnification. 89
Figure 72: SEM images with EDS-Elemental mapping of Ag, Mn, Sb, and S for A) Hydrothermal and B) Polyol Synthesis. 90
Figure 73: The heating cycle of the Spark Plasma Sintering process with a constant 5kN Force. 91
Figure 74: Heating and pressure cycle of the Spark Plasma Sintering process. 91
Figure 75: Room Temperature XRD patterns of samsonite synthesized through polyol synthesis before and after SPS treatment following Figure 74's heat and pressure cycle. 91
Figure 76: Heating and pressure cycle of the Spark Plasma Sintering process. 92
Figure 77: Heating and pressure cycle of the Spark Plasma Sintering process. 92
Figure 78: Room Temperature XRD patterns of the samsonite powder before and after sintering through isostatic pressing. 93
Figure 79: Evolution of the Seebeck Coefficient, electrical conductivity, and thermal conductivity according to carrier concentration.[96] 94
Figure 80: Room Temperature XRD pattern from powder obtained through hydrothermal synthesis and the simulated pattern of $Na_3Zn_4O(AsO_4)_3 \cdot 6H_2O$ I

LIST OF TABLES

Table 1: Melting points of some alkali metals salts according to literature (in °C).....8
Table 2: Salts, atmosphere, and heating cycle used.....11
Table 3: Average EDS composition and theoretical tetrahedrite composition.....16
Table 4: Physical properties of the solvents used 29
Table 5: Comparison of phase proportions according to filling fraction.....33
Table 6: Samsonite proportions synthesized according to the assumed amount synthesized.....42
Table 7: Samsonite phase synthesized dependent on the duration of rising temperature slope at 180 °C. 44
Table 8: Dependence of the samsonite phase proportion against dwell-time duration at a fixed temperature of 180 °C 44
Table 9: Non-exhaustive list of properties of various organic solvents.....51
Table 10: Dependence of the samsonite phase proportion against the assumed amount synthesized through the polyol process in 100mL. 61
Table 11: Proportions of samsonite and pyrargyrite phases according to speed. 63
Table 12: General crystal data of the synthetic samsonite phase via polyol process compared to litterature[10]. 73
Table 13: General crystal data of the synthetic samsonite phase via hydrothermal process compared to litterature[10]. 73
Table 14: Atomic coordinates of samsonite phase synthesized through polyol process obtained from D8 diffractometer.....75
Table 15: Atomic coordinates of samsonite phase synthesized through hydrothermal process obtained from D8 diffractometer. 75
Table 16: Atomic coordinates of samsonite phase synthesized through both processes and isotropic displacement parameters (B_{iso}) according to the synthesis process used obtained from the Rigaku Smartlab diffractometer 77
Table 17: Evolution of the proportion of the samsonite and pyrargyrite phase according to temperature. PT is an abbreviation of “Post Treatment” 79
Table 18: Evolution of the samsonite phase’s cell parameters according to temperature. 79

INTRODUCTION

INTRODUCTION

A. Thermoelectricity

Thermoelectric materials are compounds able to take advantage of the thermoelectric effect in a practical context. They can be used in everyday life situations, such as dehumidifiers or small-sized coolers. However, they may also be needed in specific environments like, for example, electric supplies in space probes (NASA GPHS-RTG). It can be defined from two perspectives:

- The **Peltier effect**, which is the transport of heat as an electric current is applied to semiconductors.
- The **Seebeck effect**, which is the transport of electrons in semiconductors as a gradient of temperature is applied to them.

Both have quite a lot of potential as unwanted generated heat has always been an issue in energy consumption and there are applications possible for heating and/or cooling systems. However, efficiency is the true factor that will determine the possibility of these systems to be working. This can be determined through the dimensionless figure of merit ZT, defined as such: [1]

$$ZT = \frac{\sigma S^2 T}{\kappa}$$

Where T is the temperature (in Kelvin (K)), S is the Seebeck coefficient (in Volt per Kelvin ($V.K^{-1}$)) representing the voltage generated by the difference in temperature, σ is the electrical conductivity (in Siemens per Meter ($S.m^{-1}$)) and κ is the thermal conductivity (in Watt per Meter per Kelvin ($W.m^{-1}.K^{-1}$)).

So far, known materials have reached a ZT up to around 3 (beyond in specific thin films experimental settings), but for a truly competitive compound, the ZT would need to be beyond those values.[2] As such, while applications already do exist, they are rather limited compared to other more power-efficient options. Potential is present in wasted heat recovery in systems that do produce such loss. Automobiles and the heat produced by combustion engines are a source of energy recovery. Unfortunately, as of now, the small efficiency means that uses have been rather scarce.

Coolers have also been mentioned previously as a current application, but it is always in a small, portable context because the replacement of traditional coolers becomes less and less worth it as scale increases. This means that research is focused on finding new materials with better efficiency. From the equation previously mentioned about the figure of merit, lowering thermal conductivity or

electrical resistivity is the strongest means to do so. Different aspects are aimed that having promises for greater thermoelectric performances: nanostructures (which can reduce the total thermal conductivity),[3] anisotropy,[4] « imperfections » in the structure (such as defects, interfaces, vacancies…),[5] and complex crystal structures (favoring phonon scattering, thus inducing lower thermal conductivity).[6]

However, while new structures are being discovered, minerals have been studied in the past to assess their thermoelectric properties.[7] Therefore, investigating natural compounds that may already have promising structures could lead to these properties or much better ones!

B. Samsonite

Samsonite (**$Ag_4MnSb_2S_6$**) is a mineral that can be naturally found in hydrothermal veins (Figure 1 shows such crystals grown in natural conditions). It was found inside the Samson vein of Sankt Andreasberg (Germany) in 1908 and its composition was determined in 1910. The name was chosen based on the location of this first discovery.[8] It has been found in other silver mines since but this compound has been, so far, never synthesized through laboratory conditions.[9]

Figure 1: *Photograph of samsonite crystals from the Samson mine.*[9]

The samsonite mineral has a rather complex crystal structure, as represented in Figure 2, (space group: $P2_{1/n}$ with a = 10.3861 Å, b = 8.1108 Å, c = 6.6637 Å, and β = 92.639 °).[10] It also has useful particularities, such as mobile silver atoms that do not induce ionic conductivity[10] (which would be optimal for thermoelectric use as elements such as copper or silver tend to migrate to the borders of the material used, degrading it consequently). It also has electron lone pair of **Sb^{3+} atoms in an AX_3E_1** configuration, which can be seen in Figure 2, which makes this phase highly promising for thermoelectric applications.[10]

Indeed, authors have shown through the tetrahedrite phase, that the electron lone pair of Sb^{3+} may explain the intrinsically ultralow thermal conductivity of $Cu_{12}Sb_4S_{13}$. In its case, the SbS_3 pyramid and the lone pair provokes a bonding asymmetry in the S_3SbCu_3 structure.[11] It could be assumed that a similar effect would be witnessed in the samsonite phase due to that common aspect.

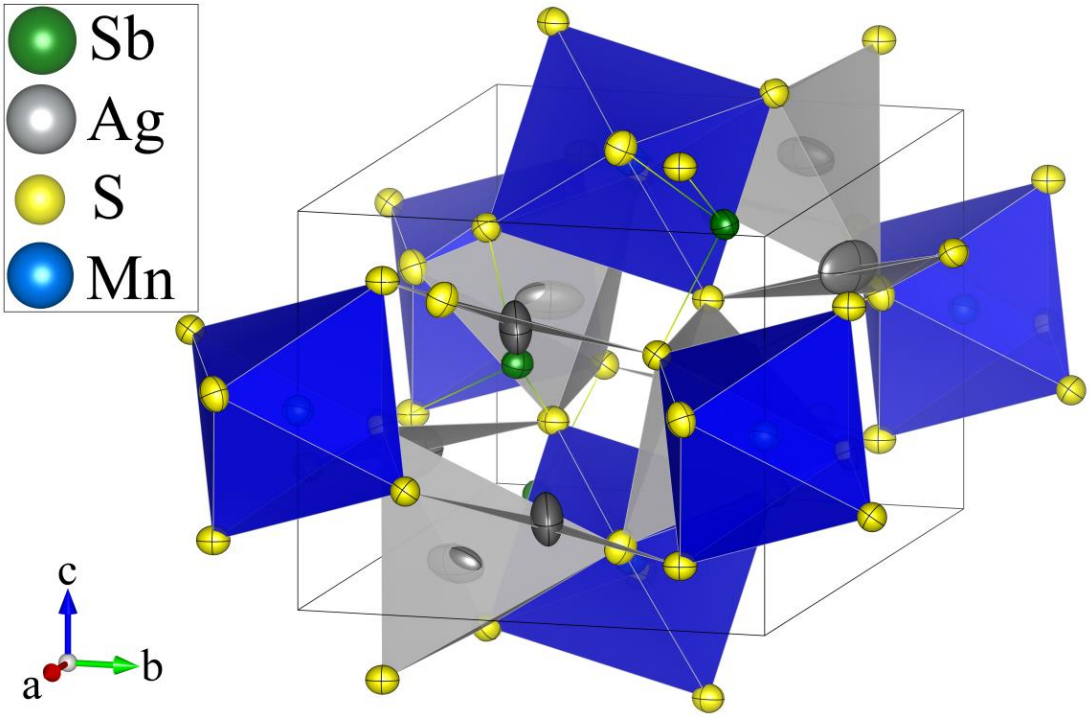

Figure 2: *crystal structure of the samsonite.*

However, the mineral has, so far, never been synthesized in an experimental setting. Such synthesis faces a great difficulty that is bypassing the formation of the pyrargyrite phase (Ag_3SbS_3) which is a ternary sulfide compound that has been shown in the literature to be easily formed with precursors that will inevitably be necessary to reach a samsonite phase in solution based processes[12]. As further proof, should you look to purchase the mineral, it will often also have pyrargyrite crystals attached to it as they tend to grow in the same veins.

The main goal of this thesis will be to find an efficient way to synthesize this mineral, to avoid completely the formation of the pyrargyrite phase (or at least reach an optimal amount where its presence can be considered negligible), and try to understand the mechanisms behind the formation of the compound in the conditions in which it can appear. Then, to estimate its thermoelectric properties as well as the magnetic ones.

This manuscript is divided into 4 parts:

Part I will focus on high-temperature syntheses. In these systems, the temperature set up during the process is usually strongly above 200 °C. Starting with the classical solid-state synthesis and estimating its limitations, then going to the more exotic conditions of molten salt synthesis to try to

bypass these issues. This part will also mention additional compounds that were found during the process and deserved rapid studies.

Part II will then shift to solvent-based synthesis and lower temperature (usually below 250 °C). This part will be dedicated more specifically to the solvothermal process. Attention will be paid to the influences of the various parameters and the mechanisms of hydrothermal synthesis involved in the formation of the compounds obtained with it.

Part III tackles the polyol process, which has numerous common points with solvothermal synthesis. A stronger focus on the mechanisms will be done through deductions of the various cycles used and why this synthesis method seems to be the most efficient among those experimented.

Part IV concludes with a study of the properties of the samsonite phase while comparing them to what was found in the natural mineral. As most of the data reported comes from the early XXth century, it is seldom and rather inaccurate which makes this a great opportunity to re-establish the characteristics of the newly synthesized quaternary sulfide.

PART I : HIGH TEMPERATURE SYNTHESIS

I. HIGH-TEMPERATURE SYNTHESIS

A. State of the art

I.A.1. Solid State Synthesis

Solid State Synthesis, also known as Ceramic Route, is the method usually used for the synthesis of many types of materials, including polysulfide compounds. Mechanisms involved in the reaction are thus summarized in Figure 3:

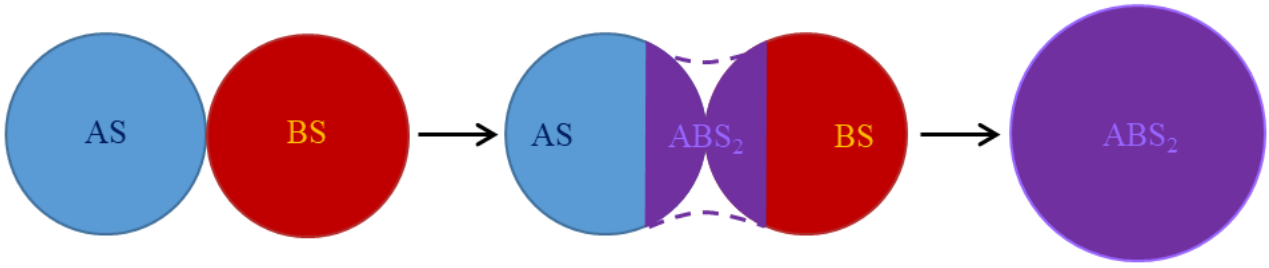

Figure 3: Schematic diagram of the Solid State Synthesis reaction of a disulfide compound with A and B as metals.

This method has the great advantage of being the **easiest one to set up** as it only involves pelleting and heating the precursors (with sometimes a necessary preliminary treatment depending on said precursors such as a short ball-mill process for powder homogenization or such). It also has **very few parameters** to tune for optimization as it is mostly influenced by the size and purity of precursors, the atmosphere, and the heating cycle.

However, this method only results in the formation of the most **thermodynamically favorable** compounds and rather large-sized grains.[13] The mechanisms behind this method also rely heavily on the solid-solid diffusion of atoms between grains which means risks of inhomogeneity, a spread-out size distribution, and the need for a long heating cycle with high temperatures.[14] This means that the range of temperature usually needed may lead to the degradation of the samsonite phase. Also, as the mineral was formed in a hydrothermal vein, it is uncertain if it can be formed in these conditions in the first place and more thermodynamically stable compounds will always be formed instead.

However, despite these potential issues, complex sulfides and chalcogenides have been successfully synthesized through this method so investigating it is a necessity. [15–21]

I.A.2. Molten Salt Synthesis

Molten Salt Synthesis is a method that involves precursors mostly used for solid-state synthesis and a large number of salts. In this case, **salts serve as a solvent**, unlike the flux method where it is often rather used as an additive, and in small quantities. As the melting temperature of salts used are usually low and the process is only hours long, much less energy is necessary compared

to the solid-state reaction. This method follows the mechanisms of the **precipitation** or the **diffusion** process, depending on the solubility of the precursors used, as shown in Figure 4, which are bound to be faster than the only solid-solid diffusion that is involved during solid-state synthesis, making it a method that is used more in the range of hours instead of days.

In this case, the salt has many properties that differentiate it strongly from water or organic solvent. It has a strong ionic conductivity and allows for better homogeneity and control over the size and shape of the particles formed.[22]

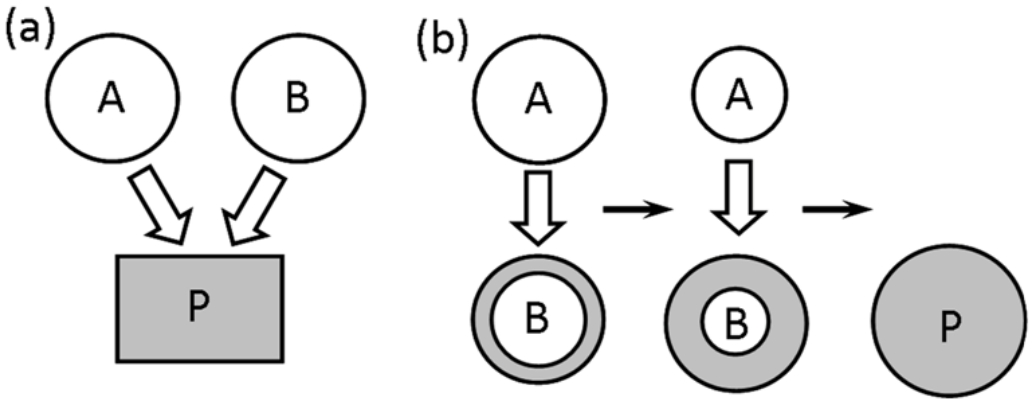

***Figure 4**: Schematic diagrams of the formation of product particle P from reactant particles A and B by (a) solution-precipitation and (b) solution-diffusion processess[22]*

The main reason molten salt synthesis was decided to be used here is due to the exotic conditions for precipitation caused by the molten salt that may bring enough energy to bypass the pyrargyrite phase formation, and be more favorable to the synthesis of the samsonite phase.

Depending on the solvent used, a wide range of temperatures can be explored through this method. It can range from lower than 200 °C to above 1000 °C, as shown in Table 1.[23,24] This allows for a better range of possibilities than the solid-state reaction could.

***Table 1:** Melting points of some alkali metals salts according to literature (in °C).*

Cation\Anion	*Nitrate*	*Sulfate*	*Carbonate*	*Chloride*
Li	225[23]	857[23]	723[23]	510[24]
Na	307[23]	884[23]	858[23]	770[24]
K	334[23]	1076[23]	893[23]	775[24]
Eutectic Li-Na	195[23]	532[23]	500[24]	554[24]
Eutectic Na-K	225[23]	830[23]	704[23]	657[24]
Eutectic Li-K	125[24]	530[24]	488[24]	356[24]

Reactions between the precursors and the solvent are a possibility that, on one hand, may impact negatively the compound that is aimed by introducing unwanted elements into the structure. On the

other hand, also opens the potential of more easily adding an element in the structure that may be difficult to incorporate into a regular context. This better ease to do so can be justified by the excess amount of said element present in the environment and the previously mentioned exotic conditions set up by the molten salt.[25]

B. Results and discussion

I.B.1. Solid State Synthesis

In order to experiment with the solid-state synthesis, the following heating cycle was used on a stoichiometric mix of binary sulfides Ag_2S, MnS, and Sb_2S_3:

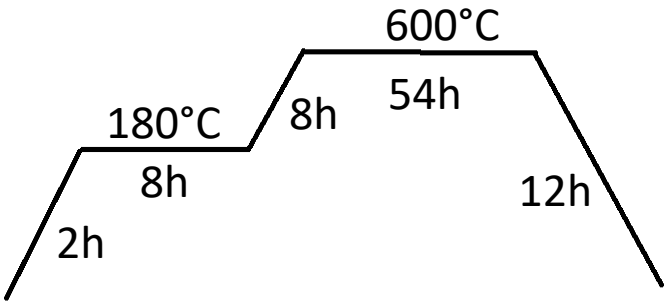

Figure 5: *Heating cycle for molten salt synthesis.*

To determine the phases in presence of the synthesized powder, X-Ray Diffraction (XRD) was used. The data were collected at room temperature with three different devices. For a first assessment, through a diffractometer MPD PANALYTICAL [copper/cobalt anode (for limiting the fluorescence generated by the Mn element), X'Celerator detector], in reflection configuration. Data were collected from 10 up to 80°. Then, for powders that seemed to have more relevant information to be revealed from more precise data than previously recorded, data were collected through a diffractometer Bruker D8 ADVANCE [copper anode, monochromatic Ge 111, Lynx Eye detector], in reflection configuration. Data were collected from 8 up to 100° with a step size of 0.009198°, and a step time of 1.7 s. A diffraction pattern of a standard LaB_6 powder was also registered under the same conditions in order to obtain the instrumental broadening of these diffractometers. The peak shape was then corrected from the instrumental broadening using the aforementioned calibration acquisition. Those data were then refined using the FullProf and WinPlotr software package.[26,27] For the structure refinement, the systematic error correction (zero-point shift and asymmetry) was applied, and the background was adjusted using a polynomial function. Concerning the crystallographic structure, the lattice parameters, atomic positions, and isothermal temperature factor (B_{iso}) were also refined.

The resulting product exhibits different phases such as Ag_3SbS_3, $AgSbS_2$, and unreacted MnS, as shown in Figure 6. Similar results were obtained **regardless of temperatures and time** spent during the heating cycle (from 500 to 700 °C, from 15 to 54 h).

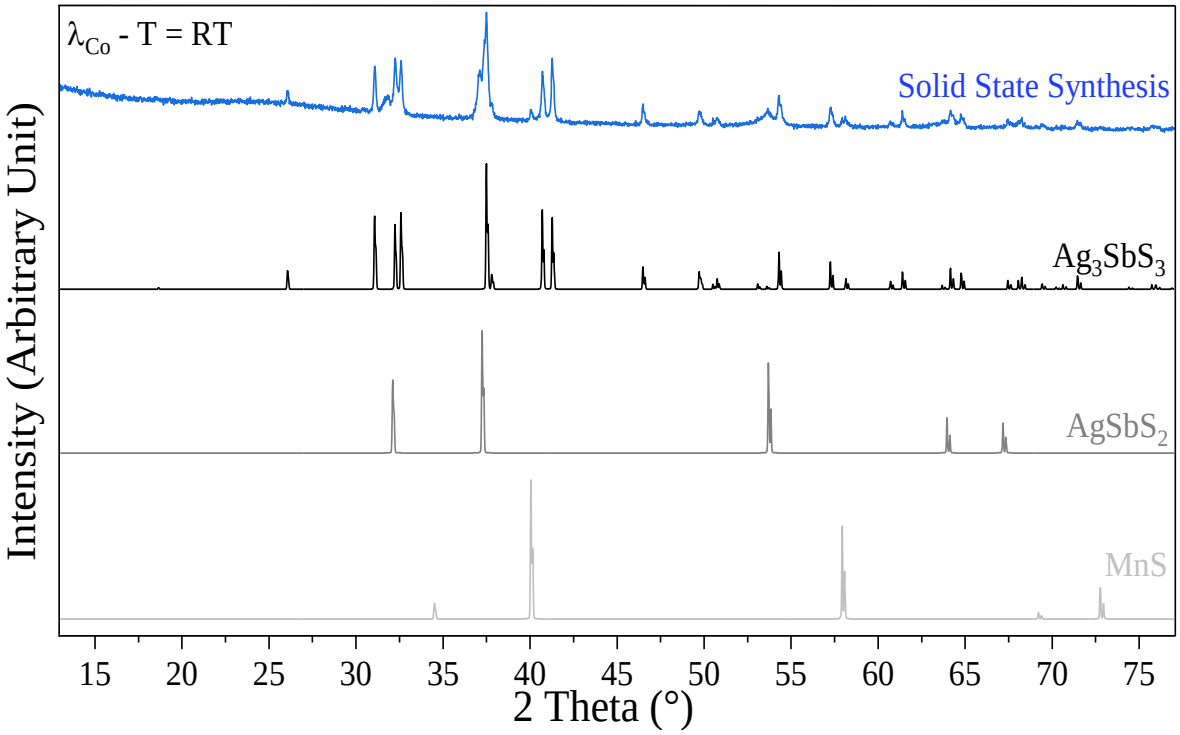

Figure 6: *Room temperature XRD pattern of solid-state synthesis and simulated patterns of Ag_3SbS_3 (COD: 1011162), $AgSbS_2$ (COD: 1509521), and MnS (COD: 9005930).*

What can be assumed here is that the **thermodynamically favorable compound is the pyrargyrite phase** (Ag_3SbS_3), making it so that only Ag_2S and Sb_2S_3 react with each other while MnS remains. Hence, the following equilibrated reaction may happen:

$$2\,Ag_2S + Sb_2S_3 + MnS \rightarrow Ag_3SbS_3 + AgSbS_2 + MnS$$

Unfortunately, this implies that the **samsonite phase cannot be reached** through this method. As such, if this range of temperature is still to be explored, it needs to be in conditions that allow for thermodynamically unfavorable compounds to appear.

I.B.2. Molten Salt Synthesis

I.B.2.a) Samsonite

The following general experimental protocol was set up to form the samsonite phase through molten salt synthesis. Careful attention has been made of the potential reactivity between the precursors and the vessel used or the atmosphere in which the reaction happens:

Binary sulfides Ag_2S, MnS, and Sb_2S_3 were mixed in with an alkali-based salt with an Ag/A molar ratio of 1:9 (where A = Li or K) for 10 minutes inside an agate mortar under a controlled Argon

atmosphere. The mixed powder was then heated up above these salts' boiling points. A summary of the experiments performed is gathered in Table 2.

Table 2: Salts, atmosphere, and heating cycle used.

Salt(s)	*Atmosphere*	*Temperature (°C)*	*Duration (hours)*
LiCl/KCl	Vacuum	500	24
KCl	Vacuum	850	24
Li(NO₃)/Na(NO₃)	N_2	215	3

A vacuum was set up by enclosing the powder into a sealed silica tube. The N_2 atmosphere was set up with constant flux during the synthesis. The nitrate-based synthesis is shorter than the experiments made under chloride-based salts due to the formation of gases that made it preferable to interrupt the process earlier than the others.

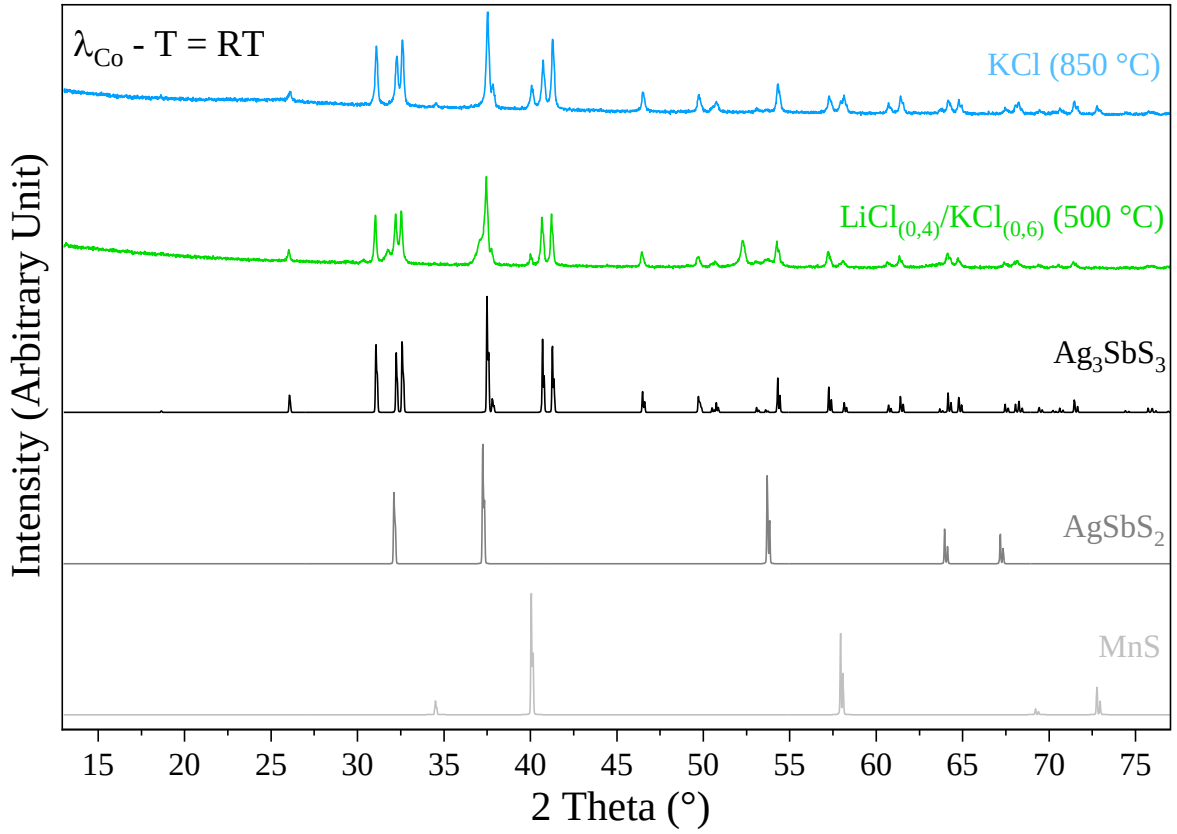

Figure 7: Room temperature XRD patterns from synthesis with molten chlorides and simulated patterns of Ag_3SbS_3 (COD: 1011162), $AgSbS_2$ (COD: 1509521), and MnS (COD: 9005930).

As Figure 7 clearly shows, unfortunately, the use of **a different solvent does not seem to affect significantly the final products obtained.** In regard to the LiCl and KCl eutectic mix, the result is the same as the one obtained using the solid-state synthesis. In the case of lone KCl as a solvent, it

can be noticed that the $AgSbS_2$ phase is no longer present. The most likely reason for such change could be some precursor reacting with the solvent and/or staying in the solvent as a solution and somehow was washed away during the centrifugation process.

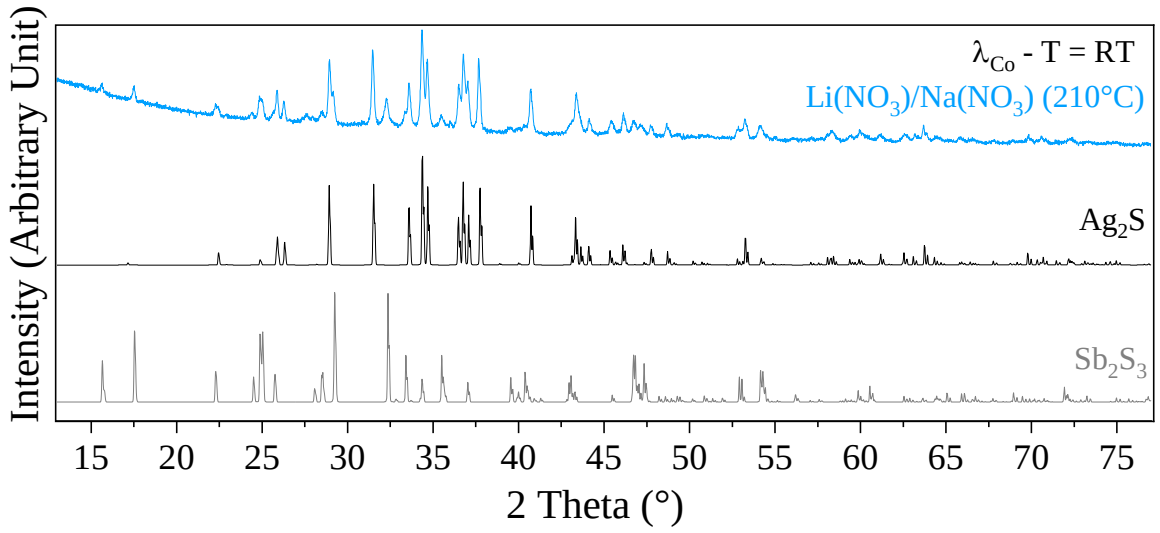

***Figure 8**: Room temperature XRD pattern from molten salt synthesis and simulated patterns of Ag_2S (COD: 1544685) and Sb_2S_3 (COD: 9007051).*

In the case of the Lithium / Sodium nitrate eutectic, as shown in Figure 8, **compounds do not seem to have reacted** as only silver sulfide and antimony sulfide can be found. As such, lower temperatures, unfortunately, do not appear to be a possibility in the case of molten salt synthesis.

As an unreactive molten salt synthesis did not seem to lead to the expected compounds, an attempt was made with a salt involving one of the elements in the samsonite phase. Thus, manganese was decided as the fitting element in a hope that the high concentration of the element may favor the formation of the samsonite phase over the pyrargyrite one. The following experimental protocol has been set up:

Binary sulfides *Ag_2S, Sb_2S_3, and MnS* in *stoichiometric amounts* for the $Ag_4MnSb_2S_6$ phase were mixed in with manganese bromide *($MnBr_2$)*. An $Ag_4MnSb_2S_{4(theo)}$ / $MnBr_2$ *volumetric ratio of 1:1* has been set up, and powders homogenization has been performed through 10 minutes of grinding inside an agate mortar under a controlled Ar_2 atmosphere. The resulting powder is then sealed into a silica tube under a vacuum. The tube was then *heated up to 798 °C at 50 °C/h and then maintained for 336 h (14 days)* before being let to *cool down along with the inertia of the muffle furnace*.

However, through XRD analysis, as shown in Figure 9, it seems to mostly contain **AgBr, $MnSbS_2Br$, and unknown compounds** due to unidentified peaks. It may also be pointed out that attempts have been made to figure out which unknown compound may be obtained, but such a problem has not been elucidated so far.

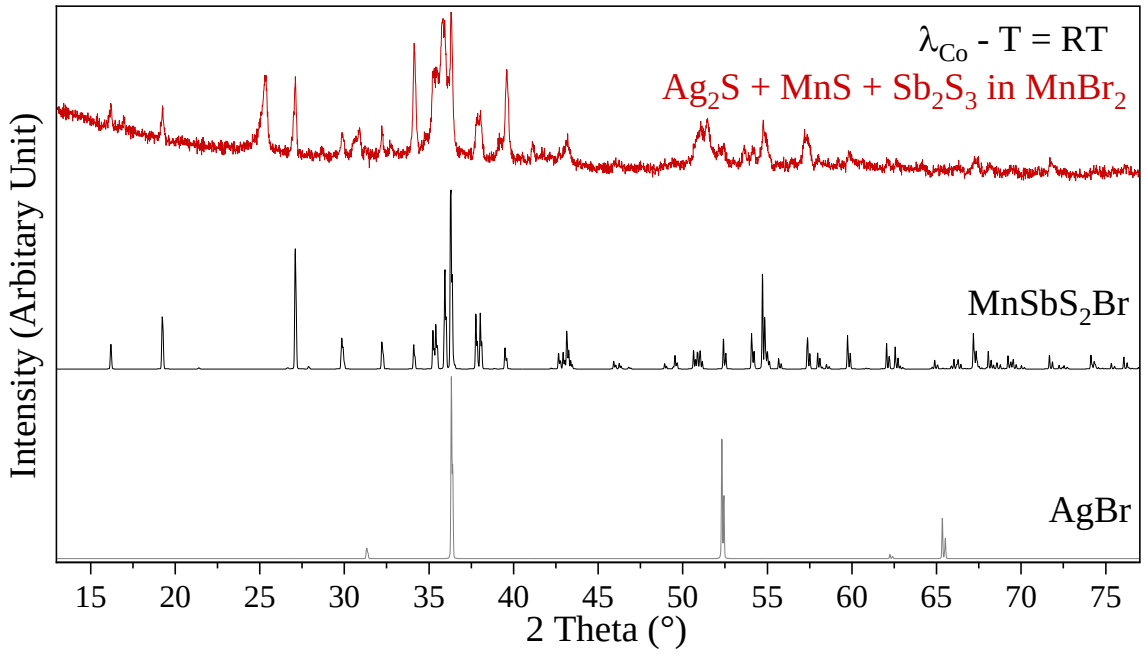

***Figure 9**: Room temperature XRD pattern from molten salt synthesis with $MnBr_2$ as a solvent and simulated patterns of AgBr (ICSD: 65061) and $MnSbS_2Br$ (COD: 1528449).*

I.B.2.b) Other compounds (tetrahedrite, titanium (II) sulfide)

Due to the unpredictable nature of this method, **unanticipated (new) compounds were found**. While they are not the focus of this manuscript, it was considered a necessity to display those compounds and the perspectives that can be considered from them.

As a strict samsonite phase was not possibly synthesized by using such an experimental setup, attempts were made with the aim to find atoms that may suit the samsonite phase better and facilitate its formation compared to the pyrargyrite phase. Through this method, additional compounds were able to be found with these substituted atoms.

The first attempt was to substitute some silver atoms with copper. This led to the formation of the **tetrahedrite phase** (nominal composition of $Cu_{12}Sb_4S_{13}$). The following protocol was used:

Binary sulfides Ag_2S, Cu_2S, MnS, and Sb_2S_3 *in stoichiometric amounts for the* $Ag_{4-x}Cu_xMnSb_2S_6$ were mixed in with *potassium chloride* with an *(Ag + Cu) / K molar ratio of 1: 9* for 10 minutes inside an agate mortar under a controlled Ar_2 atmosphere. The resulting powder was then sealed into silica tubes under a vacuum. The tubes have been then heated up to 850 °C at 25 °C/h and then maintained for 24 h before being let to cool down along with the inertia of the oven.

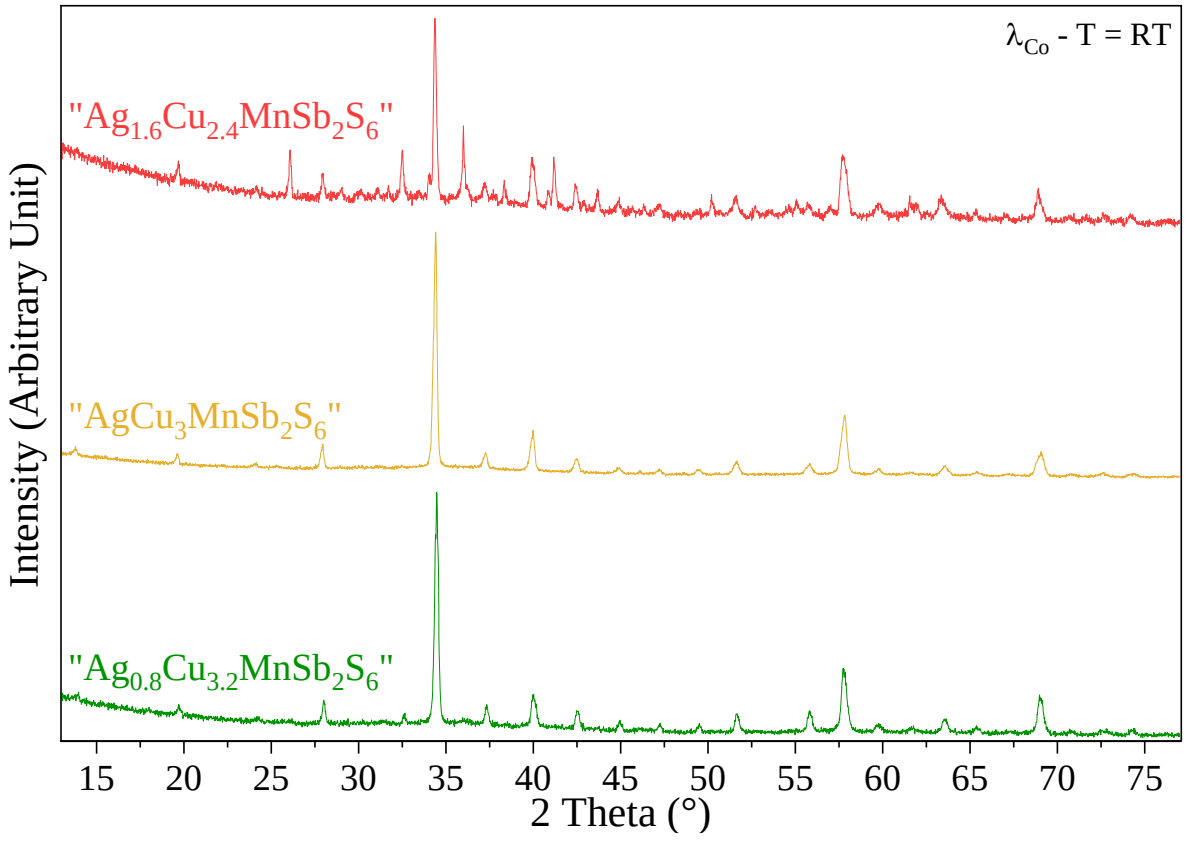

Figure 10: *Room temperature XRD patterns of "$Ag_{4-x}Cu_xMnSb_2S_6$" tetrahedrite compounds.*

As can be seen in Figure 10, it seems like impure compounds start appearing for x < 2.4 in $Ag_{4-x}Cu_xMnSb_2S_6$, and values above lead to a pure tetrahedrite. However, a more thorough X-ray diffraction acquisition of the "$Ag_{0.8}Cu_{3.2}MnSb_2S_6$" compound shows that there are **actually two different tetrahedrite compounds** being formed, as established in Figure 11. Such behavior may be explained by a composition deviation which therefore led to tetrahedrite phases exhibiting different cell-parameters.

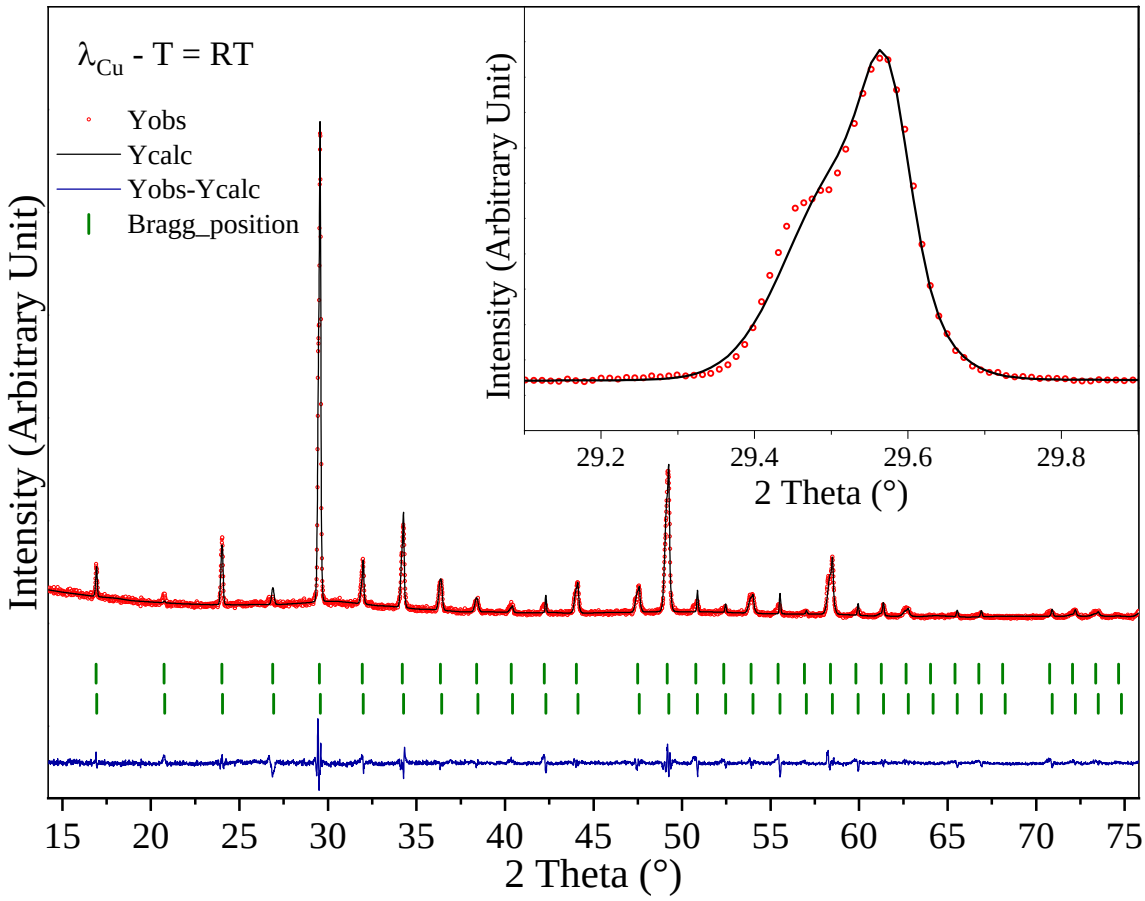

Figure 11: *Room temperature XRD pattern of "$Ag_{0.8}Cu_{3.2}MnSb_2S_6$". Red scatters correspond to the experimental data, the black line corresponds to the Rietveld simulation which has been performed by using two distinct tetrahedrite phases (i.e., using slightly different cell parameters); finally, the blue line points out the difference between the experimental and the calculated data, and the green scatters highlight the Bragg position.*

From Scanning Electron Microscopy (SEM) and Energy Dispersive Spectrometry (EDS) analysis, it can be further uncovered that these are probably tetrahedrite phases with a different composition: one with manganese and another without it. Such an assumption may be explained by the different cell parameters deduced from the Rietveld refinements (a_1 = 10.4745(5) Å; a_2 = 10.4553(8) Å). However, from what is expected from a tetrahedrite compound, the **average percentage uncovered does not make any sense**, as shown by the comparison between the theoretical composition and the ones observed in Table 3:

Table 3: Average EDS composition and theoretical tetrahedrite composition.

Atoms (%)	*Phase 1*	*$(Cu_{10,5}Ag_{3,5})Sb_4S_{13}$*	*$(Cu_7Ag_3)Cu_2Sb_4S_{13}$*	*Phase 2*	*$(Cu_{7,5}Ag_{2,5})Mn_2Sb_4S_{13}$*
Ag	13	11.3	10.3	5	8.6
Cu	29	33.9	31	43	25.9
(Ag + Cu)	42	45.2	41.3	48	34.5
Mn	0	0	0	4	6.9
Sb	20	12.9	13.7	13	13.8
S	38	41.9	44.8	34	44.8

Assuming that antimony atoms are the most accurate, it could be assessed that the general composition for those two phases might be $(Cu^+, Ag^+)_{10-\delta}(Cu^{2+})_{2-\varepsilon}Sb_4S_{13-5.4}$ and $(Cu^+, Ag^+)_{10-\delta}(Cu^{2+}, Mn^{2+})_{2-\varepsilon}Sb_4S_{13-7.6}$ respectively where δ and ε are vacancies in respectively the M^{+1} and M^{+2} sites.

Binary sulfides Ag_2S, Cu_2S, MnS, and Sb_2S_3 in stoichiometric amounts for the $Ag_{4-x}Cu_xMnSb_2S_6$ were mixed in with potassium chloride with an (Ag + Cu) / K molar ratio of 1:9 for 10 minutes inside an agate mortar under a controlled Ar_2 atmosphere. The mixed powder was then sealed inside a silica tube under a vacuum. The tube has then been heated up to 850 °C at 25 °C/h, and then maintained for 24h before being let to cool down along with the inertia of the oven.

In the following experiments, ternary compounds were attempted to be made in order to **bypass the formation of Ag_3SbS_3**. In combination with the idea of substituting manganese, multiple compounds were attempted. As such, Molten Salt syntheses of **XSb_2S_4** with X = Mn, Ti, Fe, Zn, or Cu were tried out. Noticeable results only appeared in the case of manganese and titanium.

Indeed, the **$MnSb_2S_4$ phase was synthesized**, albeit impure (traces of an unknown compound may also have been observed in the XRD diagram shown in Figure 12), through this synthesis method. It might be mentioned that the monoclinic form of $MnSb_2S_4$ ($C2_{/m}$ space group) has solely been observed despite the existence of the orthorhombic form (Pnam space group).

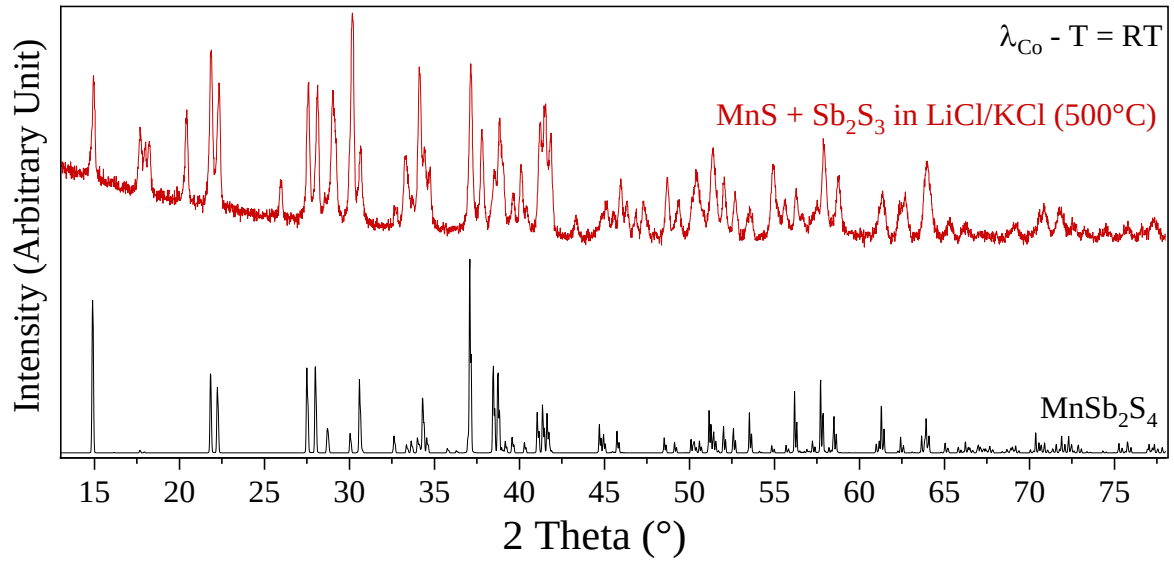

Figure 12: Room temperature XRD pattern of Molten Salt Synthesis and simulated pattern of $MnSb_2S_4$.

In the case of $TiSb_2S_4$, titanium sulfide (TiS) was **not available for purchase**, so the protocol was modified to use elemental titanium and sulfur instead.

However, while the formation of $TiSb_2S_4$ was the outcome expected, the main compounds formed were TiS_x and Sb from the **decomposition of Sb_2S_3**, as evidenced in Figure 13.

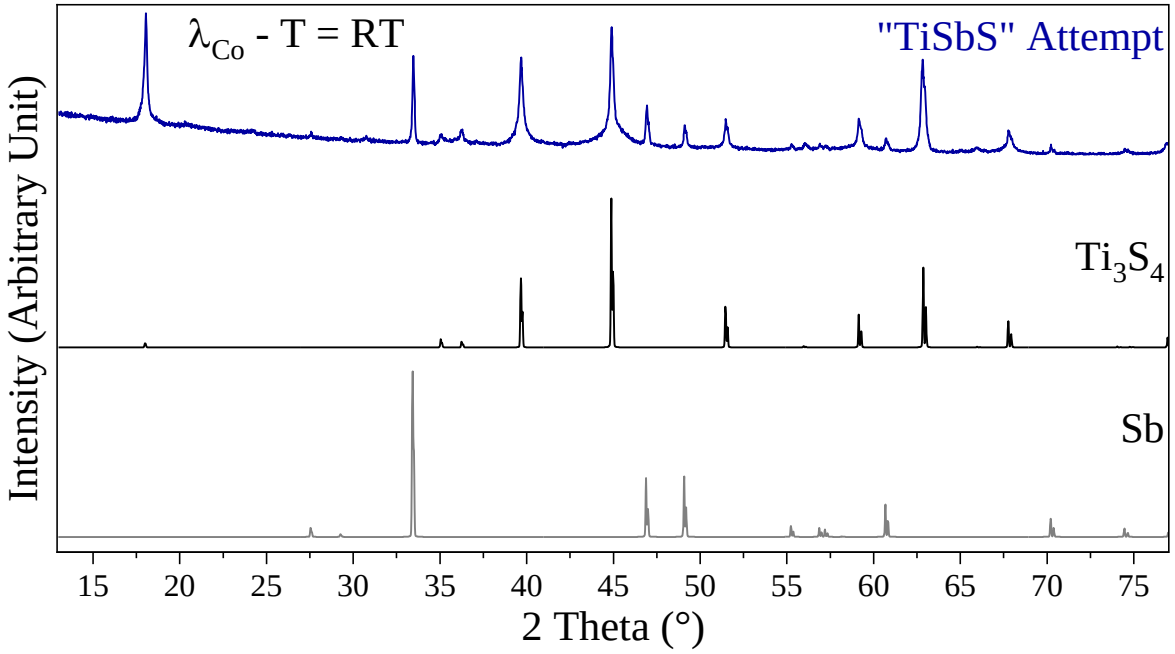

Figure 13: Room temperature XRD pattern of the synthesis method to attempt synthesizing $TiSb_2S_4$ and simulated patterns of Ti_3S_4 (ICSD: 25562) and Sb (COD: 9008575).

As such, the possibility of synthesis of titanium (II) sulfide was considered and tested out with two different solvents:

- *Protocol A:*

Titanium and Sulfur in *stoichiometric amounts for the TiS phase* were mixed in with potassium chloride using a Ti / K molar ratio of 1: 9 for 10 minutes inside an agate mortar under a controlled Ar_2 atmosphere. The mixed powder was then sealed inside a silica tube under a vacuum. The tube has then been heated up to **850 °C at 25 °C/h**, and then maintained for 24 h before being let to cool down along with the inertia of the oven.

- *Protocol B:*

Binary sulfides Sb_2S_3 and metallic Ti in *stoichiometric amounts for the* $TiSb_2S_4$ were mixed in with KCl and LiCl with an Sb / (K + Li) molar ratio of 1: 9 (where A = Li or K) for 10 minutes inside an agate mortar under a controlled Ar_2 atmosphere. The mixed powder was then sealed inside a silica tube under a vacuum. The tube was then heated up to **450 °C at 25 °C/h** and then maintained for 24 h before being let to cool down along with the oven's inertia.

Unfortunately, additional attempts with only titanium and sulfur have not led to a single-phase compound but led to promising results which can be optimized. These first results, as compared in Figure 14, show that a higher temperature might be necessary for the formation of the compound (a temperature of 450 °C only produces Ti_xS_y variants) so modifications of the heating cycle may lead to better results.

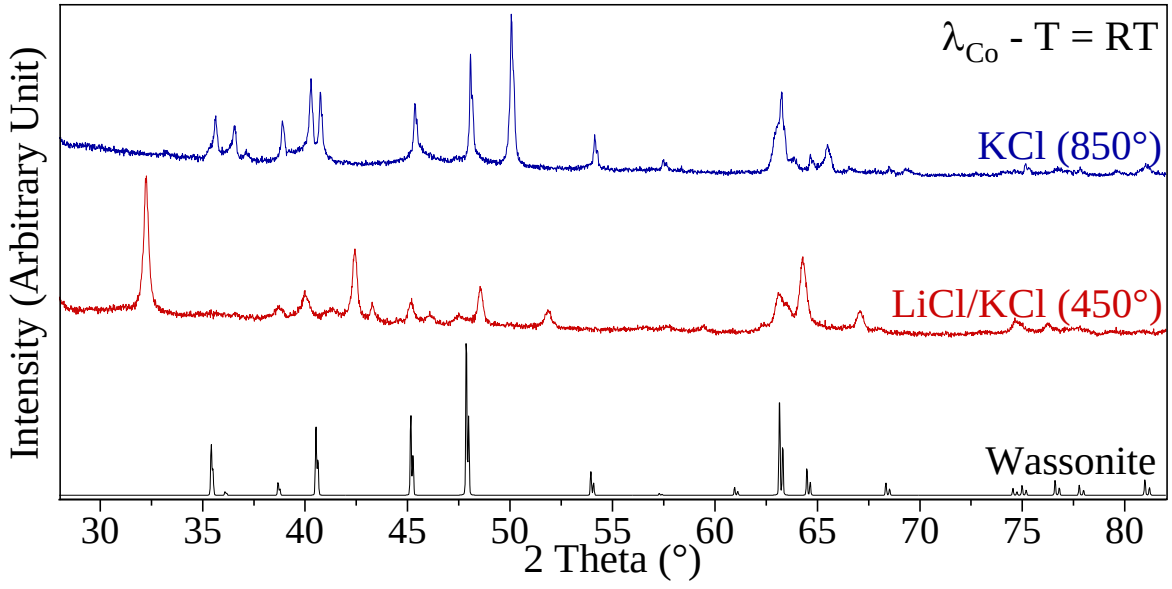

Figure 14: *room temperature XRD pattern of the synthesis method to attempt to synthesize TiS and simulated pattern of the wassonite phase (mineral TiS) (ICSD: 25561).*

C. Conclusion

While diverse binary and ternary compounds have been formed, **the samsonite phase could not be reached**, either in the case of solid-state or molten salt synthesis. Indeed, as the phases mainly obtained through these two synthesis processes are the **most thermodynamically stable**, it seems that even the peculiar conditions brought by the molten salts are not enough to induce the formation of the samsonite phase.

Additionally, a corrected pure synthesis of manganese and silver-doped tetrahedrite has **the potential to be reached** rather easily. The major drawback for a correct process to form this material is the necessity of finding out the exact composition of the phases formed, which will allow for the use of the correct amounts of precursors that may lead to a single-phase compound. Supplementary elemental analysis through various methods (*i.e.*, Inductively Coupled Plasma – ICP or such) may be necessary to reach that crucial information.

Synthesis of a pure $MnSb_2S_4$ phase was then optimized by Martin Leproult (Ph.D. student who will continue working on that subject) and attempts were made the use the compound as a precursor to form the samsonite phase along with silver sulfide. Unfortunately, $MnSb_2S_4$ ended up **being decomposed into MnS as Ag_3SbS_3 was formed instead**.

In the case of titanium sulfide, as the compound has recently been made single-phase through hydrothermal synthesis and washing with fluoric acid, it shows that reaching an **optimal synthesis is an existing possibility**. Multiple options can be explored here, such as the control of the heating cycle or the solvent used. Also, as a polymorphic compound, a more thorough study of the metastable and the stable phases may lead to interesting results.

PART II :

SOLVOTHERMAL SYNTHESIS

II. SOLVOTHERMAL SYNTHESIS

A. State of the art

Hydrothermal synthesis is a process that involves precipitation **in water** maintained at a temperature **above 100 °C and 1 bar** inside of a closed system. As the name implies, the conditions are like the hydrothermal veins where minerals like the samsonite ore can be found. Indeed, the term "hydrothermal" is first used by Mr. Roderick Murchison in a geological context in 1840. It describes the effects of higher pressure and temperature while in presence of subterranean water on mineral formation.

In 1845, the first model of hydrothermal synthesis is set up by Mr. Schafhäult with a simple closed metal box containing an aqueous solution and heated up above 100 °C to synthesize microcrystals of quartz. Ever since the system has been perfected to make safer setups and explore a wider range of hydrothermal synthesis. This has reached a point where two variants of hydrothermal synthesis can be considered:

- The *"soft" hydrothermal synthesis*, still involves systems going above 100 °C but **not much above 250 °C**.
- The *"hard" hydrothermal synthesis*, with systems that can be considered above 200 °C and often **beyond the critical point** of water (374 °C).

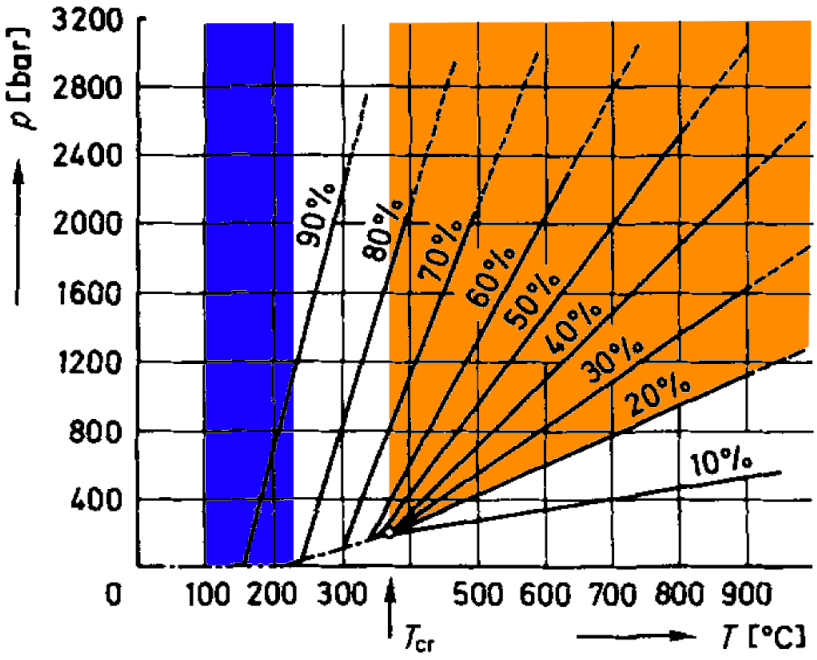

Figure 15: *Variation of pressure according to temperature and pure water fill with blue zone being the domain explored in this study and orange zone being the supercritical domain.*[21]

In the case of this study, our focus will be mostly on the *"soft" variant* due to the equipment available on-site, as shown in Figure 15.

However, at temperatures **lower than 200 °C**, the pressure **does not have any major effect** on the compound obtained, it is mostly the change in kinetics, solvent properties, and the formation of hydrogen bonds that have, in this range, a major influence. [28]

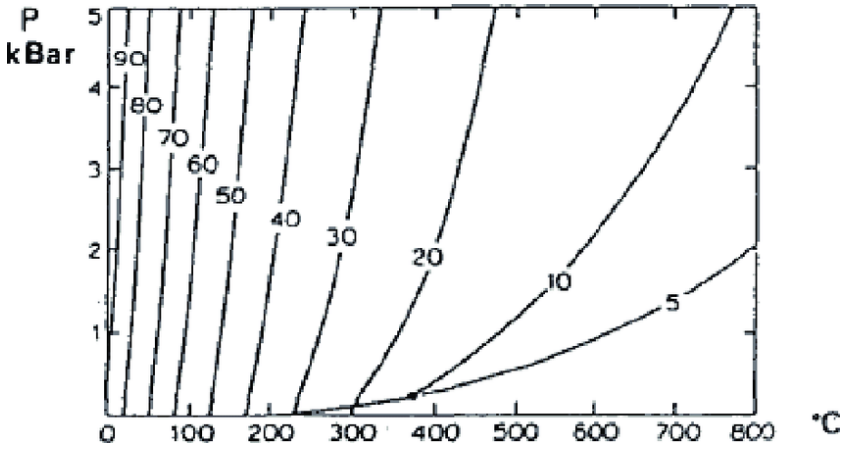

Figure 16: *Variation of the dielectric constant of pure water according to pressure and temperature.* [21]

These exotic parameters allow for a **low dielectric constant**, as shown in Figure 16, which leads to dissolution and precipitation processes that would not be possible in a normal setting. [29] In these conditions, phases that cannot be reached with classic methods, such as solid-state synthesis, are more easily attainable, such as **metastable, or completely new, phases**.[30]

Despite these exotic conditions it can be assumed that the rules of precipitation are not changed in any way. According to the model of LaMer and Denigar,[31] there are **4 successive steps**: the rise of concentration, germination, growth, and ripening. The general behavior is summarized in Figure 17.

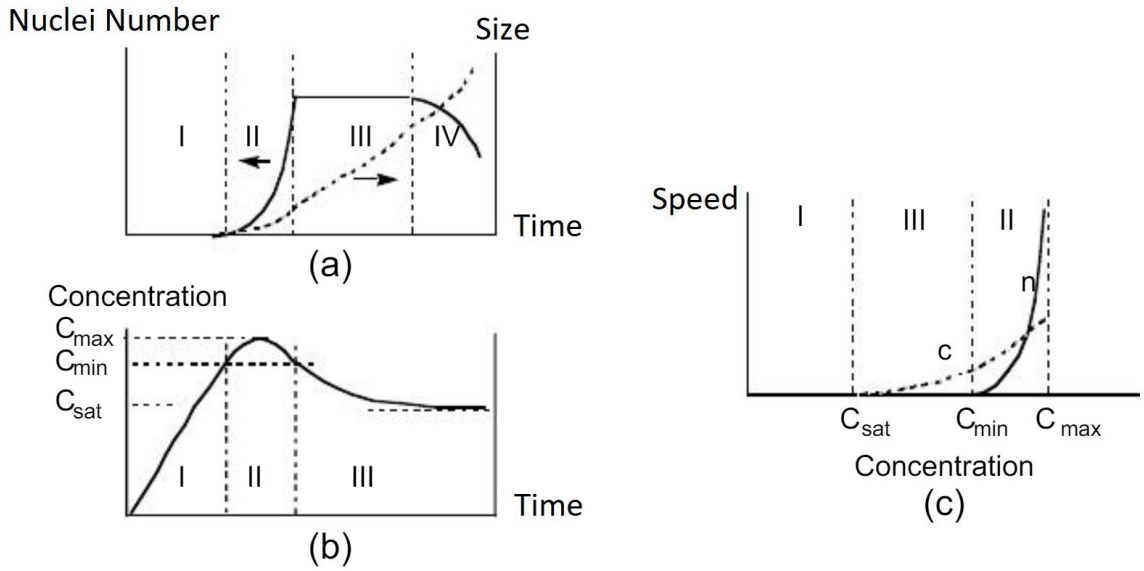

Figure 17: *a graphic representation of evolution under the LaMer model of (a) the nuclei number (———) and their size (-------) (b) the concentration of complexes (with C_{sat} the saturation concentration, C_{min} the concentration at which point the precipitation process starts and C_{max} the maximum supersaturation reached by the precursor) and (c) the speed of growth (-------) and the speed of nucleation (———). In all graphs, every step is represented by I: rise of concentration, II: nucleation-growth, III: growth, IV: Oswalt Rippening.* [28]

To correctly synthesize the samsonite phase, attempting to understand the mechanisms behind each phase is an important aspect to reach the correct conditions.

First of all, the behavior of the dissolved anion and cations in the solution. They are both subject to potential reactions of solvation and hydrolysis with water, but also to react with each other. At this moment, complexes with a null charge could be formed.[32]

These complexes are the ones considered in Figure 18, following the mechanisms of Figure 19 and, once the solution will have reached a concentration of C_{min}, the nucleation reactions will start and stop when the concentration goes back below the value. Most of the reactions reported in the literature about this process are condensation reactions, such as oxolation and olation, which could mean that using a solvent such as water, might lead to the impossibility of synthesizing sulfide compounds in these conditions. However, it has been reported (admittedly in organic compounds, which means that the model may not be completely applicable here)[33] that dissolved **sulfur anions can substitute themselves for oxygen** during condensation reactions, thanks to its larger range of possible oxidation states.

Unfortunately, elemental sulfur is not soluble in water, so precursors that may allow the introduction of these sulfide anions will be necessary. The dissolution of these compounds would lead to the following hydrolysis:

$$S^{2-} + H_2O \leftrightarrow HS^- + OH^-$$

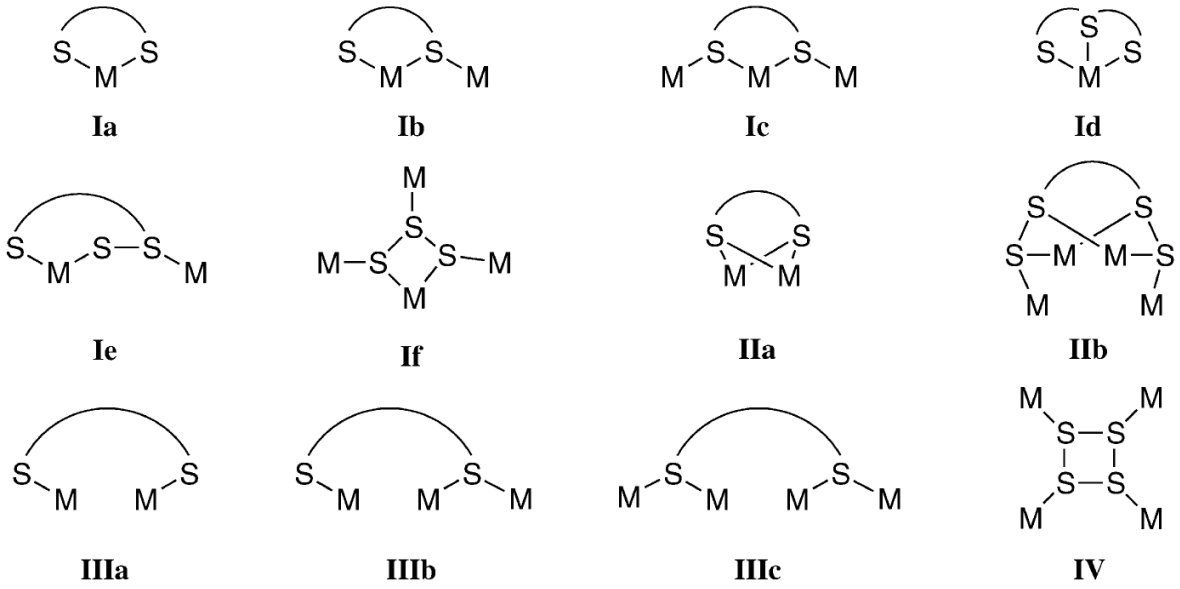

Figure 18: Potential structure types of polysulfide complexes. [34]

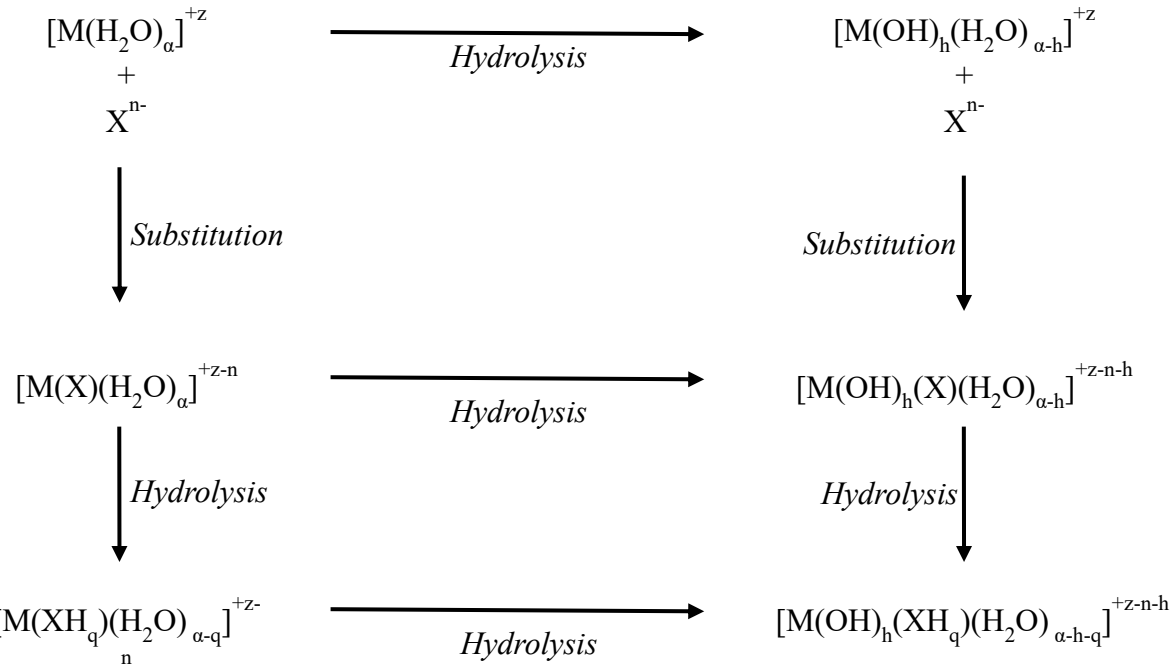

Figure 19: General complexes formed during hydrothermal synthesis with M the metal, X an anion with an n- charge, h the hydrolysis ratio of the cation, α the number of water molecules on the first hydration shell, z the charge of the cation, q the hydrolysis ratio of the anion. [24]

Meaning that the pH of the solution, at the start of the process, will always be in the basic domain. [35] This may be an aspect to take into consideration as hydrothermal synthesis is often strongly tied to the pH evolution during synthesis.

However, as the possibility of oxygen reactions is not null, the focus will be done to check if an oxysulfide variant of samsonite is not produced instead of a completely sulfide-based compound.

While the process of growth starts at C_{min}, it only becomes predominant once the concentration lowers to below that value but stays above the concentration of saturation. In this situation, the solution is not concentrated to form new nuclei, but the remaining complexes can still react to the remaining particles, inducing their growth.

Finally, once the concentration nears the C_{sat}, the smaller particles will dissolve back to complexes to maintain a constant concentration, those can then react again with the bigger particles and continue increasing their size. This mechanism is known as the Oswalt ripening.[36]

The formation of complex sulfide compounds in the context of hydrothermal synthesis has an underlying issue. Certainly, the fact that many phases are stable in this system means that it **can easily be locked into a specific kind of system**. This includes the pyrargyrite phase which, as previously mentioned, is already known to be easily synthesized[12], but also binary sulfides, such as Ag_2S[37], MnS[38], and Sb_2S_3.[39] As such, starting with these binaries or even the metallic elements would be unwise. The major focus to be put on in an attempt of reaching a single-phase compound will be through the use of precursors that will decompose in the solution and allow for an **exchange of ions**.[40]

The term "solvothermal synthesis" is often used in cases where a solvent other than water is used or to describe the whole process, regardless of the kind of solvent used. Popular organic solvents used for chalcogenide synthesis **are amino-based**, usually chosen for their basic nature (ethylenediamine[41–44], diaminopropane[45,46], diethylenetriamine[47]….). However, they are not the only ones either, more classical solvents such as **alcohols** have also been successfully used to form these kinds of compounds.

"Mineralizers" are compounds that are used in a solvothermal process to **favor the synthesis of the aimed mineral** without necessarily being part of the final product. The term is rather broad as the functionality and the purpose of what someone considers a mineralizer can end up being a little complicated to correctly estimate. It can be a salt used at saturation to modify the inherent solubility of the solvent.[48] It can also be other solvents, used in a lesser amount to influence parameters such as viscosity or the boiling point.[45] It can be one of the precursors, used in an excess amount to favor certain reactions by influencing the equilibrium between products and reactants.[41]

Another aspect of synthesis to take into account is the heating method used. There are two major ways of heating the autogenic system:

- The *"conventional" method*, where the system is heated up with a conventional oven with electric resistances. In this case, the heating-up process is made with a temperature gradient. This heating method necessitates at least a multiple-hour-long heating cycle.

- The *"microwave-assisted" method* is heated up with microwaves, allowing for a more homogeneous heating of the reactive mixture. In this situation, additional care must be given to the type of solvent used during the process due to the dielectric constant and it is evolution dependent on temperature.[49] Heating cycles involved with this method are usually much shorter and would last a couple of hours at most.

The systems used in "soft" hydrothermal synthesis are specific autogenic systems. The vessel is made of stainless steel and contains an insert made of polytetrafluoroethylene (PTFE).[50] The whole system is thus called a "bomb". The stainless steel allows for easy and homogenous conduction of heat and the PTFE insert is a non-reactive material that will not produce unwanted by-products. The system as a whole can sustain temperatures **up to 250 °C** and can sustain pressure **up to 200 bar**. These limits are good enough to allow us to fully explore the domain of "soft" hydrothermal synthesis.

These hydrothermal bombs are then inserted into a conventional heating block with resistors that has up to 6 slots that can be filled simultaneously.

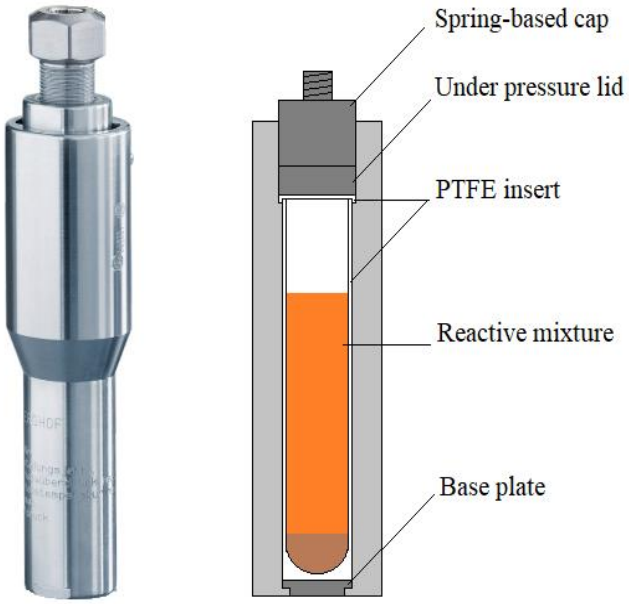

Figure 20: *picture of a digestive pressure vessel [16] and its various pieces.*

While this method is often used for the formation of many oxides and hybrid compounds [28,47,51–54] complex sulfides made through this process are rather seldom, mostly around binary materials and control of their shape and size.[37]

B. Experimental Section

A core issue with a proper way to explain a clear experimental protocol of solvothermal synthesis is the number of parameters that are involved and may have an influence on the obtained powders:

- Solvents
- Precursors
- Mineralizers
- Volume occupied by the mixture inside the insert
- Concentration
- Temperature
- Rising slope speed
- Decreasing slope speed
- Plateau length
- Heating method
- Starting conditions

Those are 11 different parameters to be considered. For a complete proper assessment of their influence, the number of experiments needed would be difficult to set up (2048 if we assumed each parameter had only two options (which is not the case for most of them)).

Adding to this issue of a too large scope to explore correctly, a surprising additional parameter appeared during testing: The initial state of the reactive mixture before synthesis. It was discovered that, for a mixture that was stirred for 10 minutes before being introduced into the hydrothermal autogenic system, results would be vastly different from mixtures that were simply introduced directly into the PTFE insert. Due to this, many attempts were now to be considered irrelevant in hindsight and necessitated many of those to be remade. This issue will be discussed further in *section II.C.3*.

All these aspects taken into consideration, here is the experimental protocol used:

1) Add *PRECURSORS (and potential ADDITIVES)* in a *VOLUME* of *SOLVENT*. The solution is stirred for 10 minutes with magnetic agitation.
2) The mixture is then added to the PTFE insert of 25 mL. The hydrothermal bomb is then heated up following a programmed *HEATING CYCLE* in a conventional heating block.
3) The solution was then filtered to recover the powder and washed with water or ethanol (depending on the *SOLVENT* used).

In this setup, when a *TUNABLE PARAMETER* is modified, all others are fixed with the assumption of their potential optimal configuration. It is then assumed that the variations observed when modifying this single parameter has always the same effect independently of the other parameters in place. This approach is flawed for obvious reasons as, in regards to solvents alone, all the reactions behind the formation of complexes described previously are clearly going to be vastly different from one to another and assuming that, for example, the influence of the heating cycle is the same for xylenes or water could be considered short-sighted. However, it is a necessary compromise for effective research of an optimal path to the synthesis of the samsonite phase.

Studies of the phases in presence inside of the powder synthesized were done through XRD, similarly to the protocol first described in *section I.B.1*.

C. Results and discussion

Multiple syntheses with varying parameters have been done **(176 iterations)** and will now be discussed with the most relevant data and regrouped around each varying and relevant parameter.

As such, parameters from which nothing could be correctly assessed or not enough data could be gathered will not be mentioned here. For example, due to difficulties with the microwave hydro/solvothermal devices available, the influence of the heating method cannot be correctly discussed here.

In the case of “mineralizers” or “starting conditions”, those are parameters that are interlocked with many others so, while they do not get their specific sections, they will still be mentioned when relevant, across the discussion of the experimental results.

Once all parameters have been discussed, an optimal synthesis protocol is suggested with a first characterization of the product obtained with it.

II.C.1. Influence of Solvent

To begin with, a major parameter to investigate has been the solvent. It is the media in which the reaction is going to occur. Focusing on the most efficient of these will help greatly in limiting the scope of necessary tweaking of parameters.

The various solvent experimented with were chosen to try different configurations: Xylenes were chosen as an oxygen-free solvent. Ethylenediamine was chosen as, in literature, it is the most popular organic solvent to be used in the solvothermal synthesis of chalcogenide compounds. 2,2-Dimethoxypropane (2,2-DMP) was chosen to use its property as a water scavenger to guarantee a water-free system. Ethanol was chosen as an easily accessible solvent with a low boiling point.

Finally, water is an even more accessible solvent and much less polluting than the other organic compounds that have been mentioned previously. Also, the samsonite mineral has been found in specifically hydrothermal veins, so synthesis with this solvent should be theoretically possible.

Table 4: *Physical properties of the solvents used*

Properties	*Water*[55]	*Ethanol*[55]	*Ethylenediamine*[55]	*Xylenes*[56]	*2,2-DMP*[57]
Chemical formula	H_2O	C_2H_6O	$C_2H_8N_2$	C_8H_{10}	$C_5H_{12}O_2$
Molar mass ($g.mol^{-1}$)	18.01	46.07	60.10	106.16	104.15
Density at 20 °C ($g.cm^{-3}$)	0.99821	0.7893	0.8995	0.87	0.847
Viscosity at 20°C (mPa.s)	1.002	1.3611	1.4568	0.76	N/A
Boiling Temperature (°C)	100	78.5	116.5	140	83

Results obtained from this variety of solvents have been highly interesting as they also strongly vary from solvent to solvent:

In regard to ethylenediamine, its role in the synthesis seemingly has not only been as a solvent but also as a reactive compound. Indeed, the major product obtained from this process has not been an inorganic compound but a hybrid. To be more precise a multi-layered $[H_3NCH_2CH_2NH_2][Ag_2SbS_3]$, that has been already reported in the past: [58]

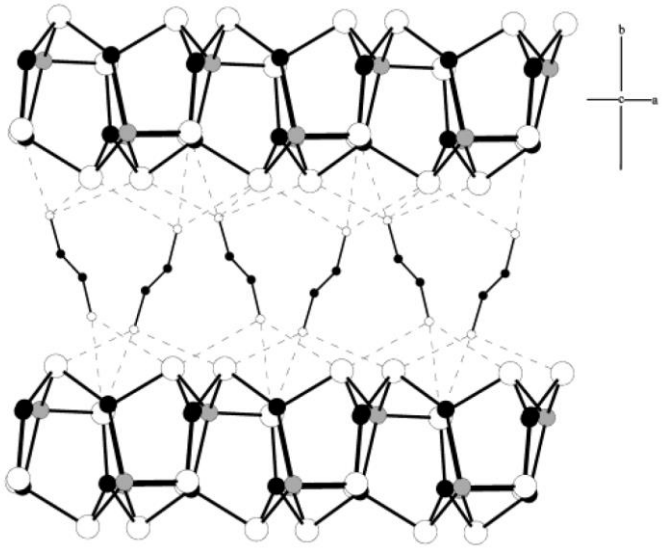

Figure 21: *representation of $[H_3NCH_2CH_2NH_2][Ag_2SbS_3]$ along the ab plane.*

Despite, multiple attempts with other parameters being shifted, **manganese does not seem to have been involved with the reaction**, unfortunately, which means that reaching samsonite through this solvent is not viable. The **samsonite phase could not be found** as only unidentifiable peaks could be seen, as shown in Figure 22.

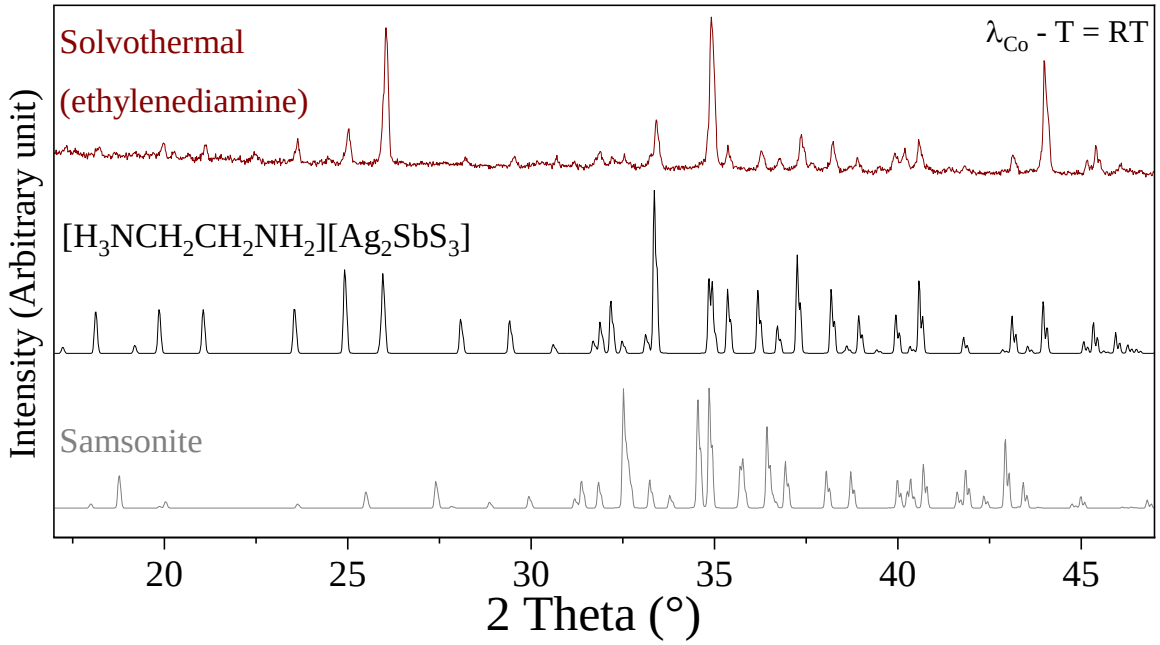

Figure 22: *Room temperature XRD Pattern obtained from powder synthesized in ethylenediamine compared to simulated patterns of hybrid silver thioantimoniate (COD: 4312632) and samsonite (COD: 9010235).*

Additionally, the Teflon vessels that were used during the process seemed to have been damaged by the process. As such, using this solvent, even if it was an efficient one, might seem to be unsuitable for this experimental setup.

2,2-DMP is the most intriguing result among all the solvents used as, while the pyrargyrite phase is clearly apparent, other peaks are not identifiable but are most definitely **not related to the samsonite phase**, as can be noticed in Figure 23. Attempts to identify the unknown phases synthesized have been performed but no satisfactory results have been reached so far.

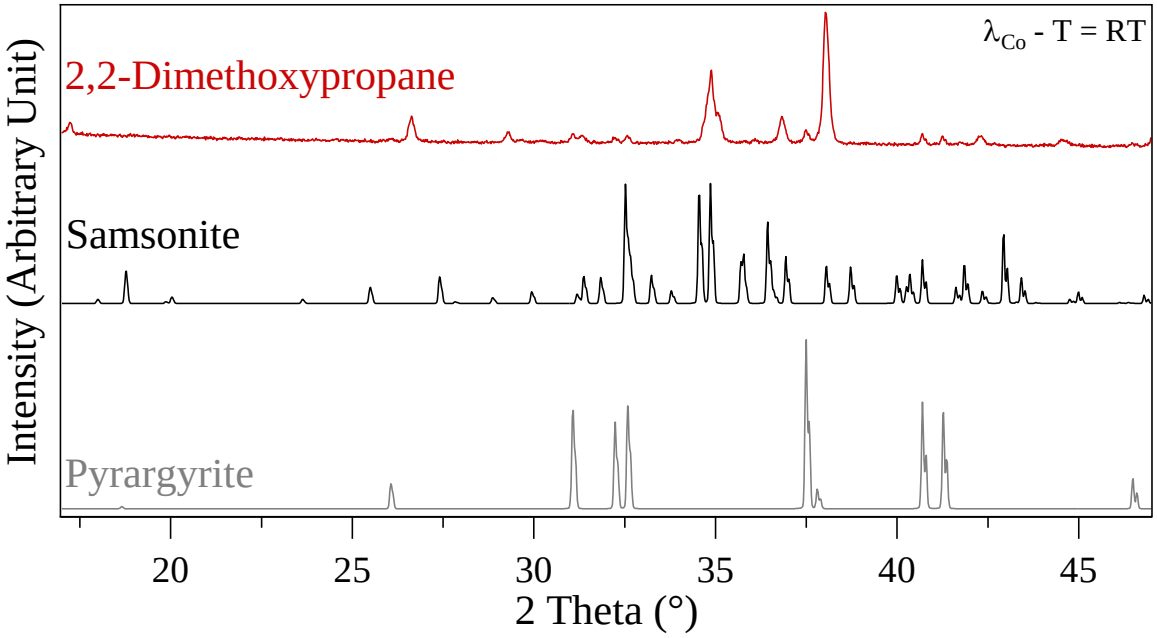

Figure 23: *Room temperature XRD pattern obtained from the solvothermal synthesis with 2,2-DMP and theoretical patterns of pyrargyrite (COD: 1011162) and samsonite (COD: 9010235) phases.*

The mix of **xylenes proved to be a rather inefficient solvothermal solvent** for the formation of the quaternary sulfide as XRD did not show the presence of any peaks related to that phase, as shown in Figure 24.

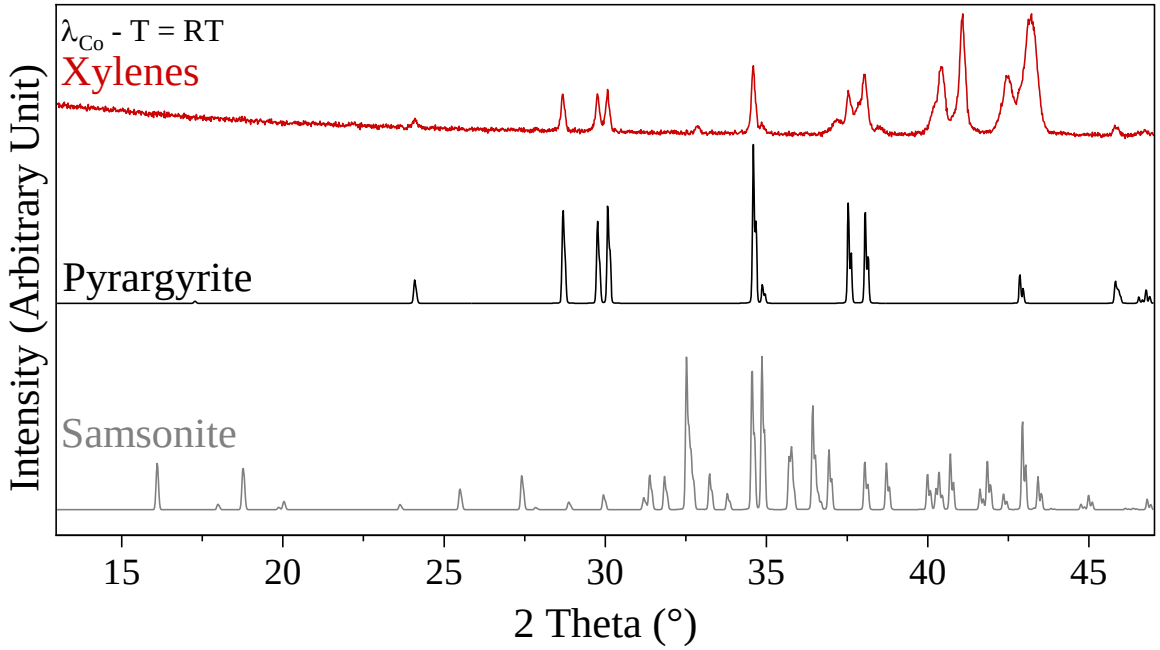

Figure 24: *Room temperature XRD pattern obtained from the solvothermal synthesis with xylenes and theoretical patterns of pyrargyrite (COD: 1011162) and samsonite (COD: 9010235) phases.*

Both cases where samsonite could be witnessed through XRD patterns, as shown in Figure 25, were when ethanol and water were used as solvents. **Water is the most efficient method** as it is the one

that leads to the formation of the **most of samsonite phase synthesized**. It is, however, not perfect, as the presence of an unwanted pyrargyrite phase is still in the produced powder.

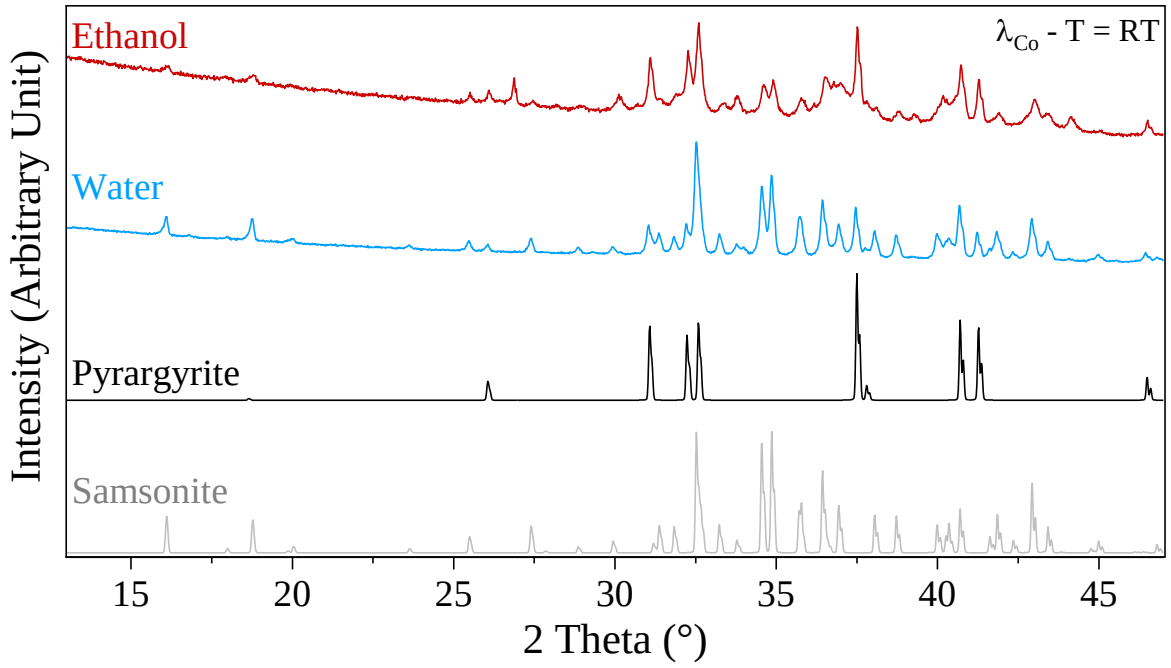

Figure 25: *Room temperature XRD Patterns for solvothermal synthesis with ethanol and water compared to two simulated patterns of pyrargyrite (COD: 1011162) and samsonite (COD: 9010235) phases.*

Therefore, all following tuning of experimental parameters will be done with water and the synthesis process will be referenced in this manuscript as "hydrothermal".

An interesting aspect to note is, whatever the solvent that was used, there were no situations where oxide or oxysulfide compounds were seemingly formed. While the presence of potential oxide will be further discussed in *II.C.7*, it is rather worthy to notice that the oxygen being present, or not, in the solvent **does not** lead to the formation of any unwanted compound in that regard.

II.C.2. Influence of Volume

As this reaction happens in a closed system (especially in the case of "soft hydrothermal synthesis", this is irrelevant in "hard" as the critical point is reached and the solvent becomes a supercritical fluid), a change of the filling fraction (for a same concentration of precursors) may be influential during the synthesis. Based on the density of the solvent at the critical point, **its behavior will be different according to the filling fraction.** In the case of water, the density at the critical point is 0.32 g.cm^{-3}. Consequently, for a filling fraction below 32 %, the volume of liquid lowers until reaching the critical point at 374 °C (which cannot be reached with the current setup used during this thesis), the opposite happens with a filling fraction above 32 %. At the filling fraction of 32 %, the volume stays constant.[29]

In order to correctly estimate the potential influence of this parameter, the same experience has been made with different fills. The amount of precursors used was always modified accordingly to fit the same concentration which, evidently, lead to a different amount of powder obtained. The water filling fractions used were respectively 15, 32, 70, and 87%. The last one was determined as the maximum filling fraction possible for the vessel without a critical rise of pressure that could have damaged the system.

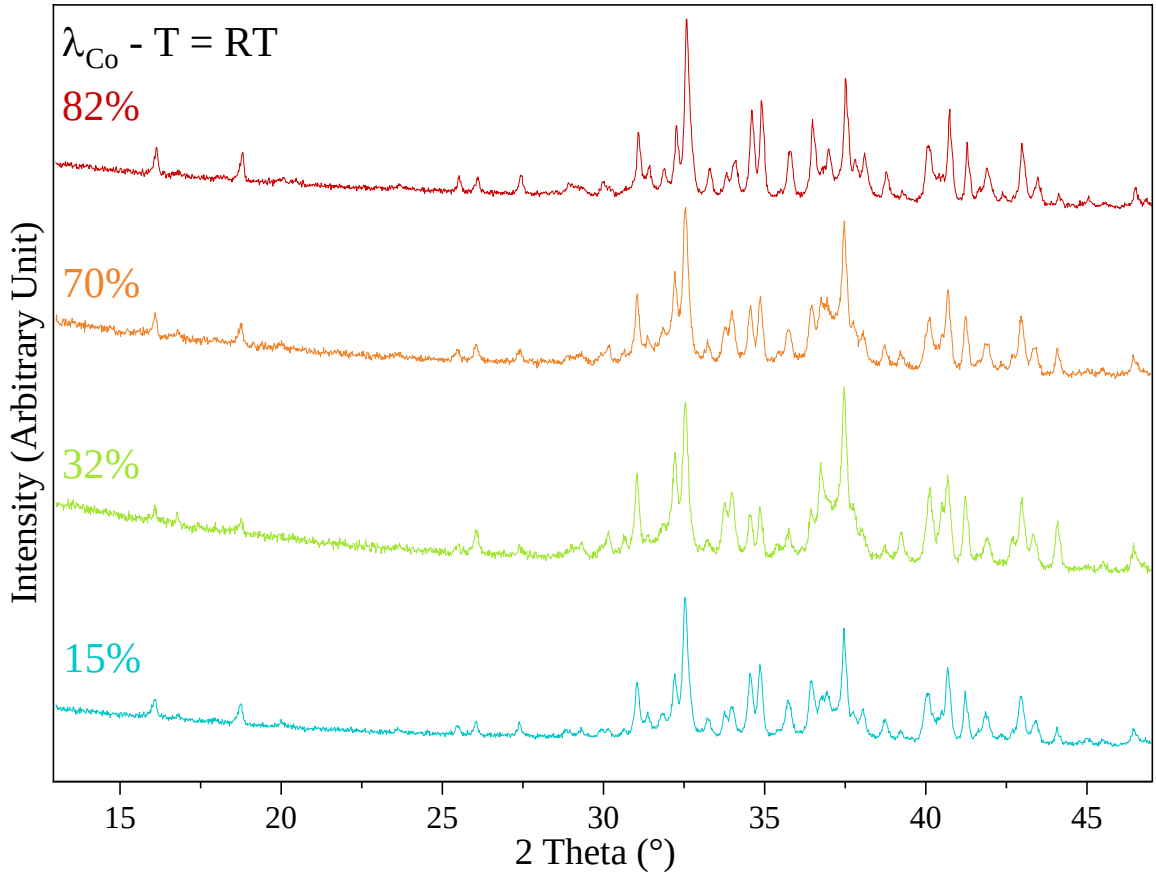

Figure 26: *Room temperature XRD patterns of hydrothermal synthesis according to water fill.*

The amount of samsonite present in the powders was estimated through a Rietveld refinement of XRD patterns shown in Figure 26 and led to the following results:

Table 5: *Comparison of phase proportions according to filling fractions.*

Volume	*15%*	*32%*	*70%*	*87%*
Samsonite Phase (%)	52	42	60	67

A significant drop in the quantity of samsonite formed can be observed with the lowering of the volume. More precisely, **the more distant the fill was from the 32% filling fraction**, the most efficient the synthesis process was. A way to interpret such results could be that the further we get

from the "stable" configuration of the system, the more efficient it is at synthesizing the quaternary compound. Additionally, while the shift may not be significant enough in most cases to be considered influential in "soft" hydrothermal processes, the variation in pressure might actually be a factor in this specific case.

II.C.3. Influence of Precursors

A crucial compound necessary in the formation of the samsonite phase has been found, it has been the thioantimoniate precursor $Na_3SbS_4 \cdot 9H_2O$, also known as "**Schlippe's salt**". This inorganic salt releases thioantimoniate anions in the water, instead of the sulfide and antimony-only precursors previously used. As the compound is no longer available for purchase, details about its synthesis are further explored in the following section *II.C.4*. When comparing it to the use of thiourea and antimony acetate in an "all acetate" attempt does not lead to any formation of the samsonite phase, as the gathered XRD patterns in Figure 27 show:

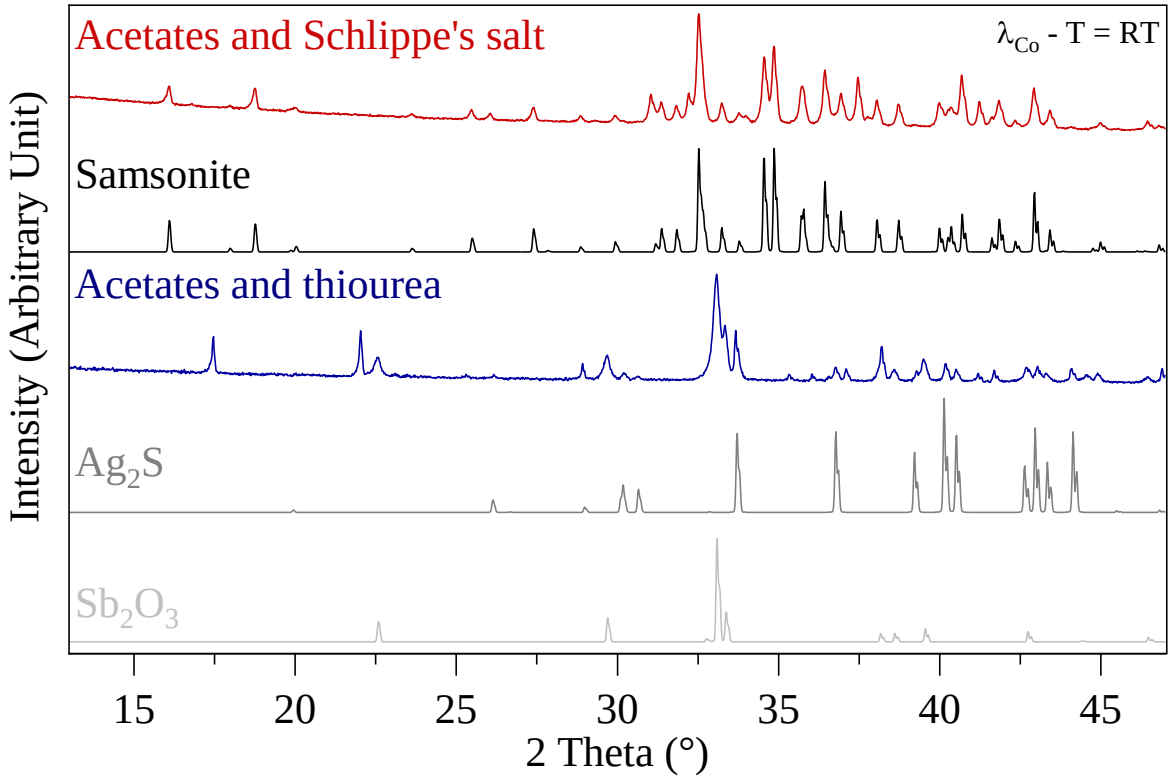

Figure 27: *Room temperature XRD patterns of powders synthesized by hydrothermal process, simulated patterns of the samsonite (COD: 9010235), the silver sulfide (COD: 1544685), and antimony oxide phases (COD: 9007587).*

More than just not making any samsonite phase, it seems that **oxide compounds were formed** as peaks seemingly related to Sb_2O_3 are present in the XRD pattern. As a single-phase samsonite compound was still not reached, though, further exploration of this synthesis method was necessary. With the pyrargyrite phase being the other phase present, an attempt was made to increase

significantly the presence of the manganese phase in the solution with an aim to "force" the formation of the quaternary sulfide above Ag_3SbS_3.

The idea behind it was the following: As the antimony sulfide anion stabilizes with the following reaction in water: [59]

$$SbS_4^{3-} + 2e^- \leftrightarrow SbS_3^{3-} + S^{2-}$$

Then, there are 3 sulfur atoms to which the cations present in the solution can attach themselves. These cations, in our situation, are manganese and silver. If Ag^+ attaches itself to one of these atoms, then the reaction is over as silver nullifies the charges of that atom. However, should Mn^{2+} take its place, then that manganese atom could still reattach itself to another thioantimoniate anion and the reaction would continue. If all sulfide compounds react with silver, then you get Ag_3SbS_3 without any possibility to reach something else. As such, the idea behind this excess amount of manganese is to increase the chances of manganese always getting at least one of these branches and reattaching to another thioantimoniate. Knowing that we need, at least, to have 4 silver equivalents in all experiments, the following equation arises:

$$P_{S-Mn-S}(x) = \frac{x^2}{(x+4)^2}$$

$P_{S\text{-}Mn\text{-}S}$ is the probability of two sulfurs attaching themselves to manganese and x is the equivalent of manganese present in the autogenic system. This equation is quite simplified as it makes a few assumptions: the precursors are constantly present at equal proportions during the synthesis, the manganese that attached itself to an SbS_3^{3-} will always be the one that reacts with the other anion, and does not consider any potential steric effect from the size of the associating anions.

Consequently, it could be assumed that an efficient amount of manganese could be determined by resolving the following equation:

$$P_{S-Mn-S}(x) = \frac{1}{3} = \frac{x^2}{(x+4)^2}$$

$$\leftrightarrow 3 = \frac{(x+4)^2}{x^2}$$

$$\leftrightarrow 0 = 16X^2 + 8X - 2 \left(with\ X = \frac{1}{x}\right)$$

$$\leftrightarrow X = \frac{\sqrt{3}-1}{4}$$

$$\leftrightarrow x = \frac{4}{\sqrt{3}-1} \approx 5.46$$

As such, tests up to 600 % of manganese added to the solution have been done. A Rietveld refinement has been then performed to estimate the amount of the samsonite and summarized in the following graph:

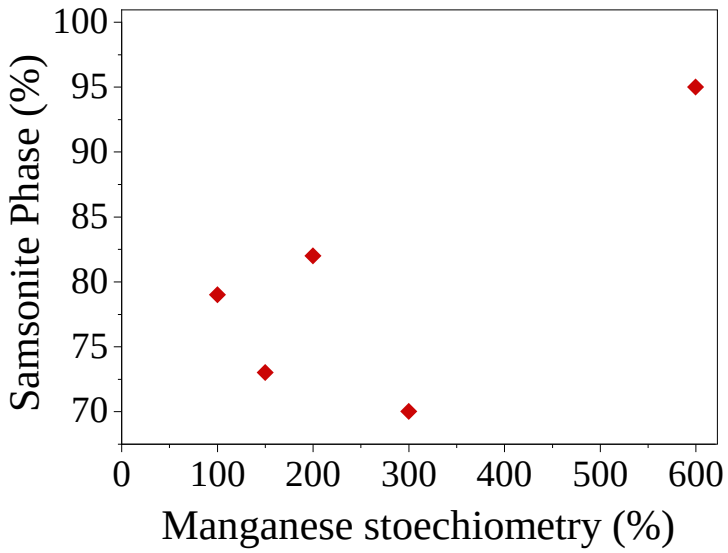

Figure 28: Samsonite phase formed according to the manganese/stoichiometry ratio.

As Figure 28 shows, **a raise in the samsonite phase produced as the amount of manganese is increased is noticeable**. This is not incoherent with the conditions in which the mineral can be found as manganese carbonate crystals are known to grow near samsonite crystals.

Other attempts were made with **nitrate** or **chloride** precursors together with Schlippe's salt, but **neither leads to the synthesis of the wanted compound**, as established from the XRD patterns obtained in Figures 29 and 30:

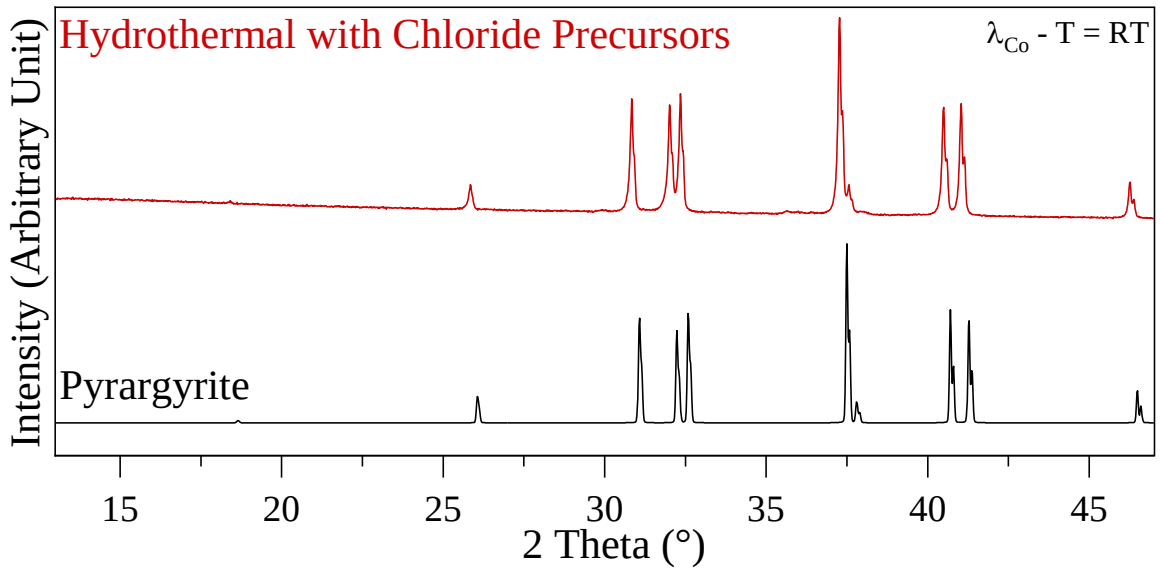

Figure 29: *Room Temperature XRD pattern of the powder obtained by hydrothermal synthesis with chloride precursors and the simulated patterns of the pyrargyrite phase (COD: 1011162).*

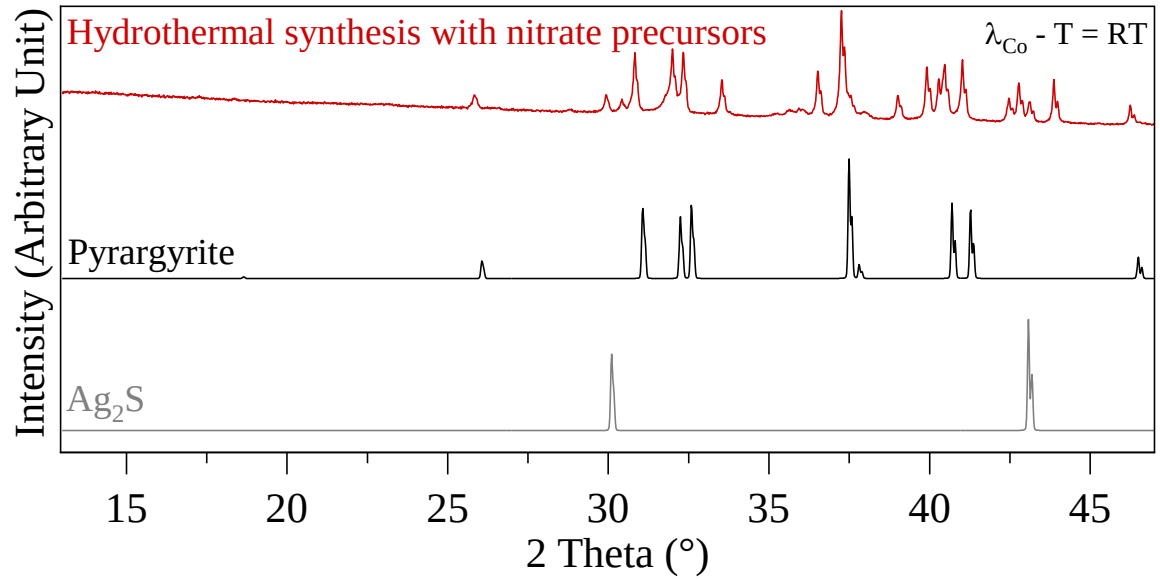

Figure 30: *Room Temperature XRD pattern of powder obtained from hydrothermal synthesis with nitrate precursors and simulated patterns of pyrargyrite (COD: 1011162) and silver sulfide (COD: 1509709).*

In both cases, only Ag_3SbS_3 was seen in the XRD patterns. More specifically regarding the attempt based on chloride precursors, no manganese compounds were precisely observed. The most probable scenario is that the **manganese** stayed in the solvent (water) and **has not reacted** with the rest of the system. It has been reported in the past that manganese can have difficulties condensing under hydrothermal conditions due to its behavior in water, mainly remaining in a solvated form, regardless of the pH in the system. [60] For the pattern obtained with nitrate precursors in Figure 30, while the pyrargyrite phase seems to be a major phase and the easiest to identify, others are more complicated.

Indeed, the low peak intensity together with the probable overlapping peaks, makes the identification of the phases relatively complicated. Silver sulfide and a mix of other compounds of the $Ag_xSb_yS_z$ system seem to be the most likely, but nothing can be asserted for certain. However, it is obvious that the samsonite phase was not made under these conditions.

An additional attempt has been carried out to try and get the best of both worlds by using silver nitrate (for its better solubility compared to the really low value of silver acetate) and an excess amount of manganese acetate (as acetate is still the only precursor that had worked so far) and results were not particularly superior to the acetate only version of the experiment as only 52 % of the samsonite phase for 47 % if the pyrargyrite phase (wt.):

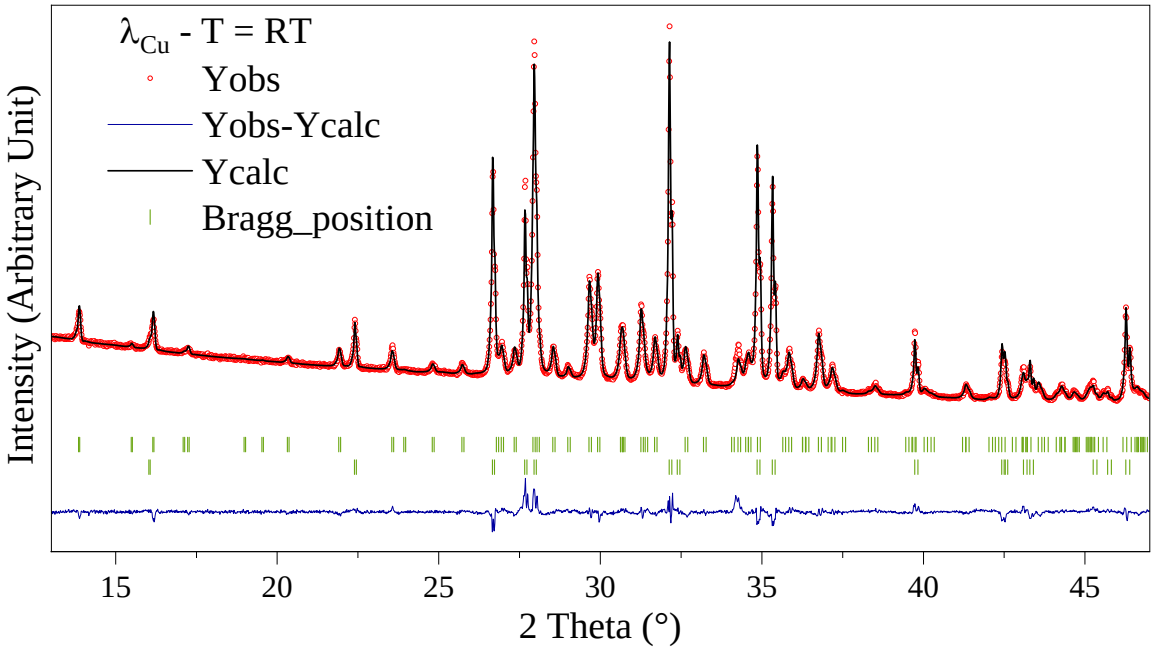

Figure 31: *Room temperature XRD patterns of powder obtained through hydrothermal synthesis with nitrate and acetate precursors.*

Nature of the precursors aside, another highly influential parameter that has been mentioned previously in the experimental section needs to be addressed: the **dissolution** of compounds before the heating cycle. Indeed, many of the experiments done to assess the influence of parameters during this synthesis have all extremely similar results, only leading to **ternary compounds at best**.

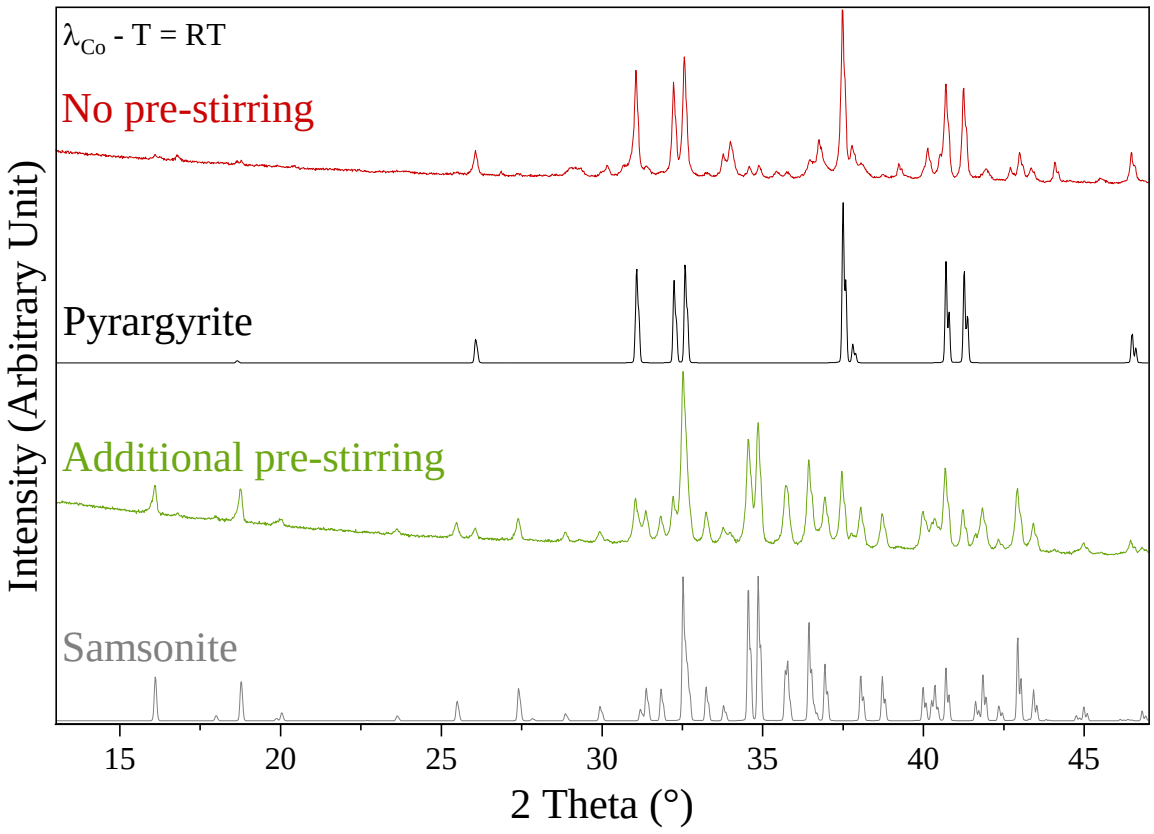

Figure 32: *Room temperature XRD patterns of stirred and unstirred reactive mixtures compared to theoretical scans of pyrargyrite (COD: 1011162) and samsonite phases (COD: 9010235).*

The nature of this change is difficult to accurately assess. In the case of the most functional synthesis, silver acetate is the only precursor with low solubility. A possibility might be that the particles of silver acetate are **more dispersed and of smaller size** than without previous agitation, allowing for a higher reactivity. It might also be the undissolved precursor particles formed from the agitation that create a unique setup for adequate reactions. A further study of the reactive mixture at its initial state would be necessary to understand correctly the mechanisms involved.

II.C.4. Synthesis of Schlippe's Salt

More recently, Schlippe's salt was used as **antimony *and* sulfur precursors** for hydrothermal synthesis.[53,61,62] The latter precursor which is freely soluble in water, compared to other classic antimony precursors, offers the great benefit of having the sulfur already attached to it (with the formation of the anion SbS_4^{3-}).[53] This means, in this situation, that an excess of sulfur is also present during the synthesis, and such excess could act as a mineralizer and help during the nucleation and growth process.[41] Unfortunately, as the compound is no longer available for commercial purchase and has a short shelf life due to rapid decomposition (which can be slowed down with storage in a light-less and cold environment)[63], a synthesis protocol had to be set up for **a fast and efficient**

formation of the compound for use in hydrothermal synthesis. After multiple attempts, the following process was published in *Dalton Transactions*: [64]

A mixture of binary Na_2S (Alpha Aesar, 97 %, 1.93 g, 24.7 mmol), Sb_2S_3 (Sigma-Aldrich, 98 %, 2.82 g, 8.26 mmol), and elemental S (Alpha Aesar, 99.5 %, 0.533 g, 16.6 mmol) was introduced, into 9 mL of distilled water inside a 45 mL tungsten carbide jar containing 48 tungsten carbide balls with a diameter of 5 mm (49.7 g). The mixture was then milled at 450 rpm for 2 hours (divided into 8 cycles of 15 minutes, each separated with a minute-long break to let the system cool down). The resulting solution was washed and filtered with deionized water. The dark brown powder obtained of unwanted products (Na_2SO_4 and Sb_2O_3) was discarded. The filtrate was then dried through rotary evaporation to force the precipitation of the salt.

This **new rapid and scalable synthesis method** presented herein resulted in a satisfying yield of around 90 % in mass for only a four hours long process, which is far higher than the 30 % yield obtained by a multiple days long protocol of dissolution, precipitation, and recrystallization.[61]

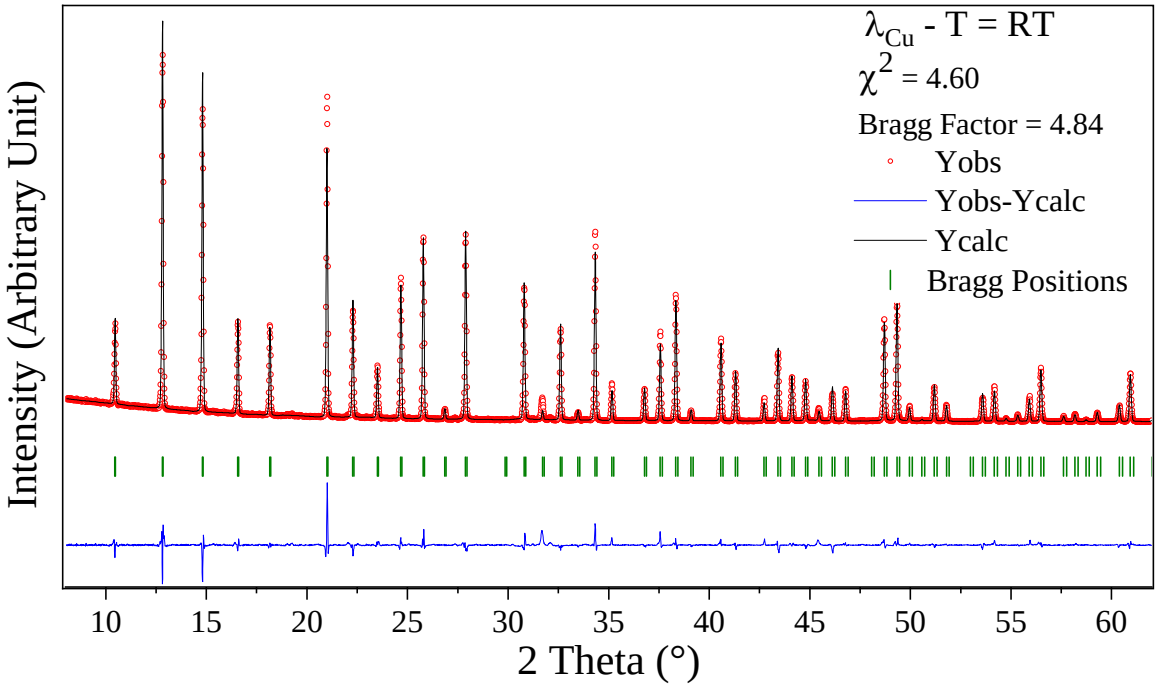

Figure 33: *powder X-Ray diffraction patterns of Schlippe's Salt with D8 ADVANCE.*

Furthermore, analysis through XRD refinement (shown in Figure 33) and EDS (shown in Figure 34) have been performed to assess the purity of the compound. The cell parameters deduced through Rietveld refinement (a = 11.959(2)) are quite similar to those previously reported by Mereiter *et al.* [65] **No unwanted phase is apparent** in the XRD pattern obtained and proportions in atoms found were **coherent with the theory** (on average, it was estimated that experimental composition was of 36%, 14%, and 50% which is rather close compared to the 37.5%, 12.5%, and 50% expected in theory for Na, Sb, and S respectively and the mapping proves that it is a homogeneous and single-phased compound).

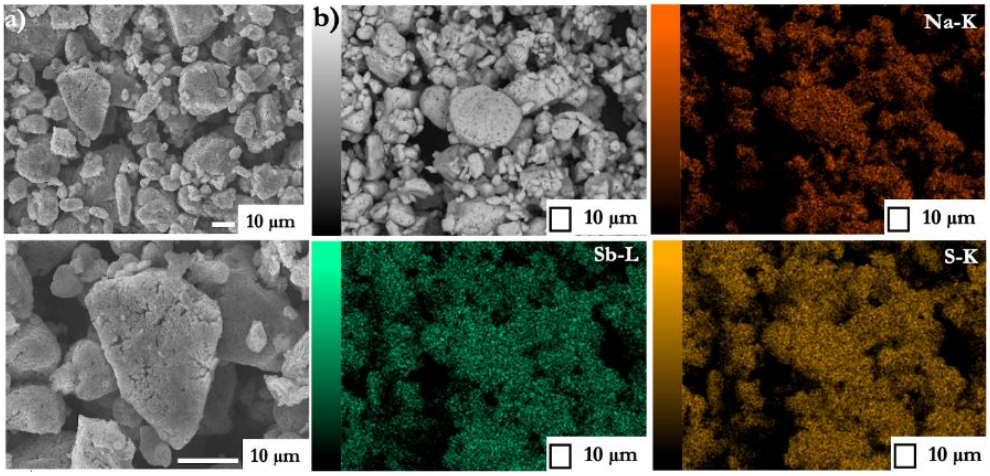

Figure 34: SEM images a) with x1000 and x2500 magnification b) with EDS-Elemental mapping of Na, Sb, and S.

The amount of water present in the compound was also checked through DSC-TGA.

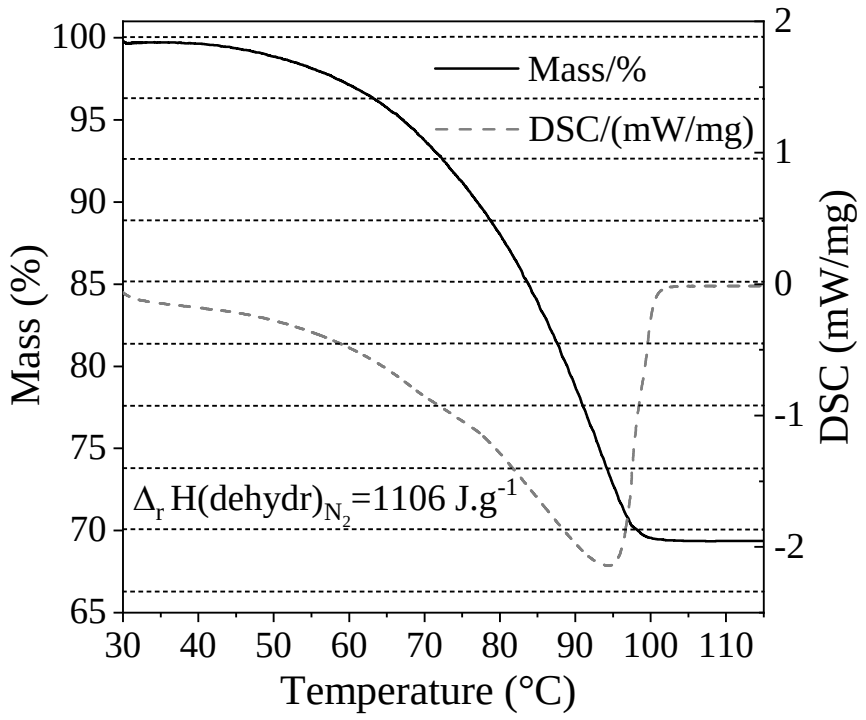

Figure 35: DSC-TGA curves of Schlippe's Salt under nitrogen flux. Heating rate = 3 °C/min. each horizontal line represents the number of water molecules present in the structure (9 at 100%, 0 at 66.16%).

From those results, it can be determined that the water molecules in the structure evaporate as soon as 30 °C up to approximately 100 °C. This dehydrated compound, once left back in ambient temperature and normal atmosphere, **rapidly reabsorbs water** from ambient air and returns to its original $Na_3SbS_4 \cdot 9H_2O$ composition. The experimental value of enthalpy of the dehydration process can be calculated from DSC (1106 J.g^{-1}). However, it can be noticed that not all the water is exactly extracted from the compound. It could be assumed that the leftover water is the last molecule still maintaining Schlippe's Salt structure before a rearrangement into the anhydrous compound[66] ($P\bar{4}2_n$,

a = b = 7.1653 Å, c = 7.2896 Å) as other works already show that the formation of Na_3SbS_4 is more complicated than simple heating of its hydrated form.[67]

More details can be found in *Appendix 2*.

II.C.5. Influence of concentration

As the volume of the vessel in our current setup is rather limited (25 mL or 50 mL), a study of the evolution of the synthesis' efficiency according to the concentration was necessary as any higher amount of product obtained for a fixed volume would be an improvement of the process. Tests were made from an assumed amount of samsonite synthesized compared to the volume of water between 20 to 120 mmol.L^{-1} (or 18.4 g.L^{-1} to 110.6 g.L^{-1}).

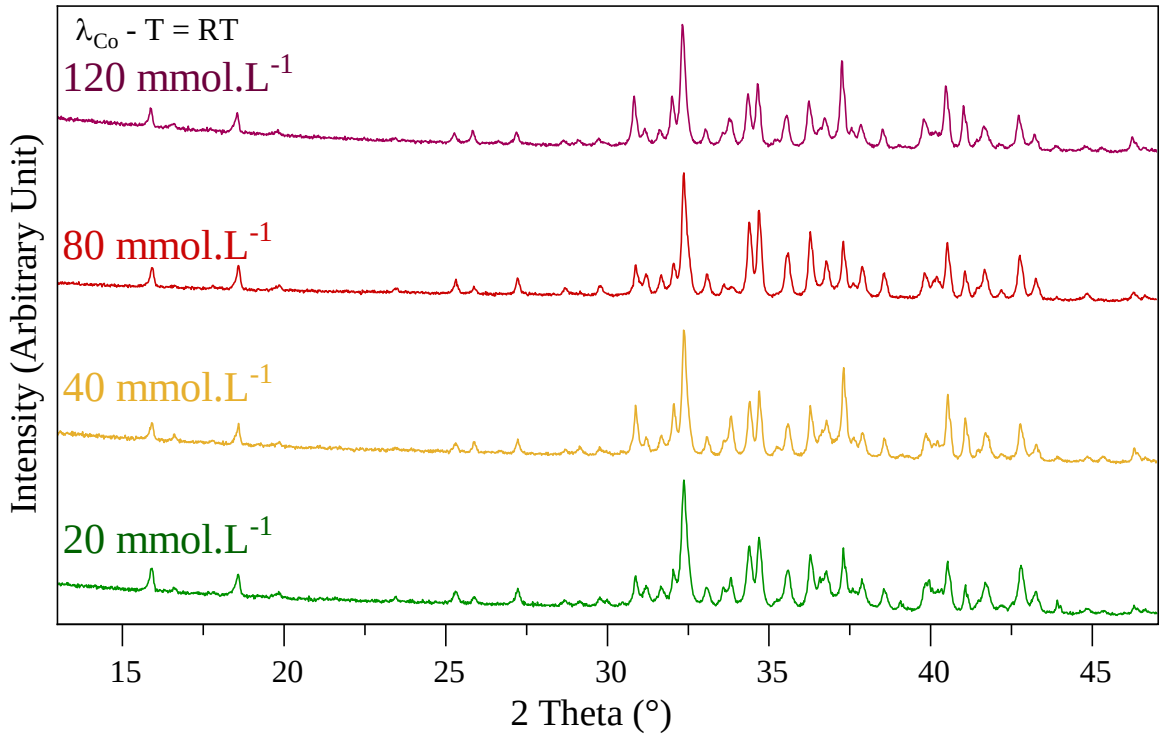

Figure 36: *Room temperature XRD patterns of powders obtained through hydrothermal synthesis according to assumed produced product compared to solvent volume.*

The following values were estimated from Rietveld refinement of the XRD patterns obtained in Figure 36:

Table 6: *Samsonite proportions synthesized according to the assumed amount synthesized.*

Yield (mmol.L^{-1})	*20*	*40*	*80*	*120*
Samsonite Phase (%)	67	73	79	65

From the results obtained, it can be assumed that the optimal value seems to be **close to 80 mmol.L^{-1}.** This means that, with the vessels available at our lab, **1.4 and 2.8 g of powder can be synthesized** with an optimal amount of samsonite purity for this synthesis method.

II.C.6. Influence of heating cycle

While the "heating cycle" is here treated as a single parameter, it needs to be divided into multiple aspects that are focused on separately: the **rising rate** of temperature, the **maximum** temperature set, and the **duration of the plateau** at said temperature and the **lowering rate** of temperature. As for the optimal temperature, experiments were made between 150 and 210 °C in water.

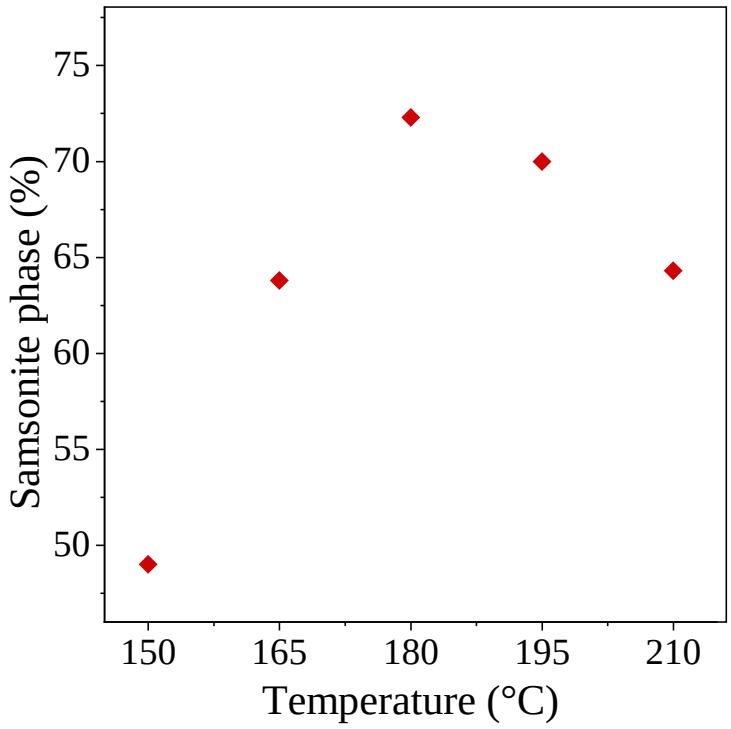

Figure 37: *Evolution of the proportion of the samsonite phase in powder obtained from hydrothermal synthesis according to maximum temperature.*

A summary of the results deduced through Rietveld refinement is shown in Figure 37. As can clearly be noticed, a maximum can be estimated at **around 180 °C**. A particular remark should be added about the value obtained at 150 °C as, while a general refinement was possible and, from the general shape of the patterns, it is clear that the samsonite phase is in much lower quantity than in experiments set at other temperatures, the crystallization of the powder, in general, was rather poor and the value is probably the less precise among the five.

Now that an optimal temperature has been determined, a study of the duration of the experiment was done. Starting with the rise of temperature, tests were made from "instantaneous" heating (placing

the vessel in a pre-heated conventional oven) to a day long. Different heating rates have been tested, 8/3, 2/9, and 1/9 °C.min^{-1}. Results were summarized in the following Table 7:

Table 7: *Samsonite phase synthesized dependent on the duration of rising temperature slope at 180 °C.*

Rising temperature slope duration (rate)	*Samsonite Phase (%)*
"Instantaneous"	55
1 hour (8/3 °C.min^{-1})	93
12 hours (2/9 °C.min^{-1})	89
24 hours (1/9 °C.min^{-1})	91

In this case, it was made evident, **a too-rapid temperature shift is strongly inefficient for the synthesis of this compound**, implying that crucial mechanisms are happening during this specific step of the hydrothermal process, any long duration does not seem to improve significantly the quantity of quaternary sulfide formed. So, the estimation that can be done here is that while rather fast mechanisms are happening in this part of the synthesis, they are important and seemingly cannot (or at least at a much lesser efficiency) happen during the plateau and/or descent of temperature.

In regard to the duration of the temperature plateau, multiple times were attempted. Those attempts were summarized in the following Table 8:

Table 8: *Dependence of the samsonite phase proportion against dwell-time duration at a fixed temperature of 180 °C*

Plateau duration	*Samsonite Phase (%)*
No Plateau	82 (binary sulfides present)
3 hours	93 (but $AgSbS_2$ is also present)
12 hours	92 (but $AgSbS_2$ is also present)
24 hours	93 (only Ag_3SbS_3 present)

In experiments with less than a day dwell time, numerous phases seem to be present, at the 24 h point, however, pyrargyrite seems to be the only unwanted product present. As such, to keep the impurity of the powder to a minimum, a **24 h plateau seems to be the most reliable option**.

Finally, in the case of the lowering rate of temperature at the end of the synthesis process, **no significant change from varying this parameter was witnessed**. As such, for further synthesis, letting the system cool down with its own inertia was decided.

To conclude, the heating cycle that seemed optimal from the data obtained so far was a heating up to **180 °C in an hour**, followed by a **24h plateau** and, finally a **cool down following the system's inertia**.

II.C.7. The eventuality of (sulf)oxide formation

To check the possibility of oxide or sulfoxide formation during synthesis was done without any sulfide-based compound to check if any of those may have been formed and were confused with anything else. To follow the optimal parameters encountered so far, acetate precursors were used.

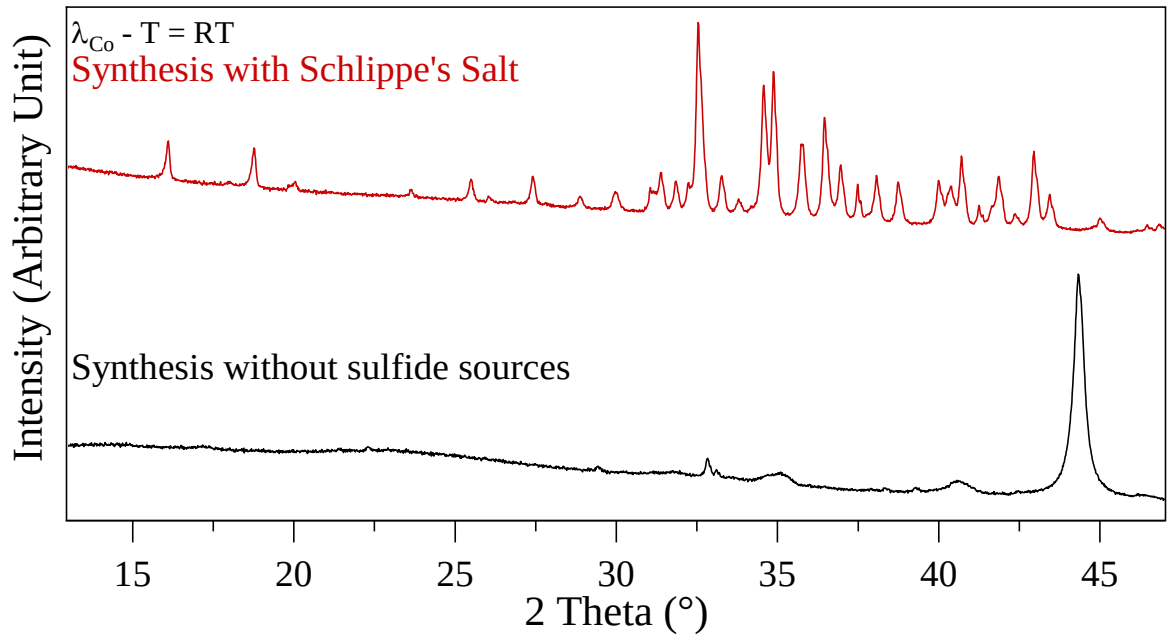

Figure 38: *Comparison of room temperature XRD patterns between powders obtained through hydrothermal synthesis with and without a sulfur source present.*

From Figure 38, it can be seen that the synthesis method with no sulfide compounds **does not lead to any phases** that also appear during the regular processes.

Additionally, the mapping of the powder obtained shows no presence of oxide compounds.

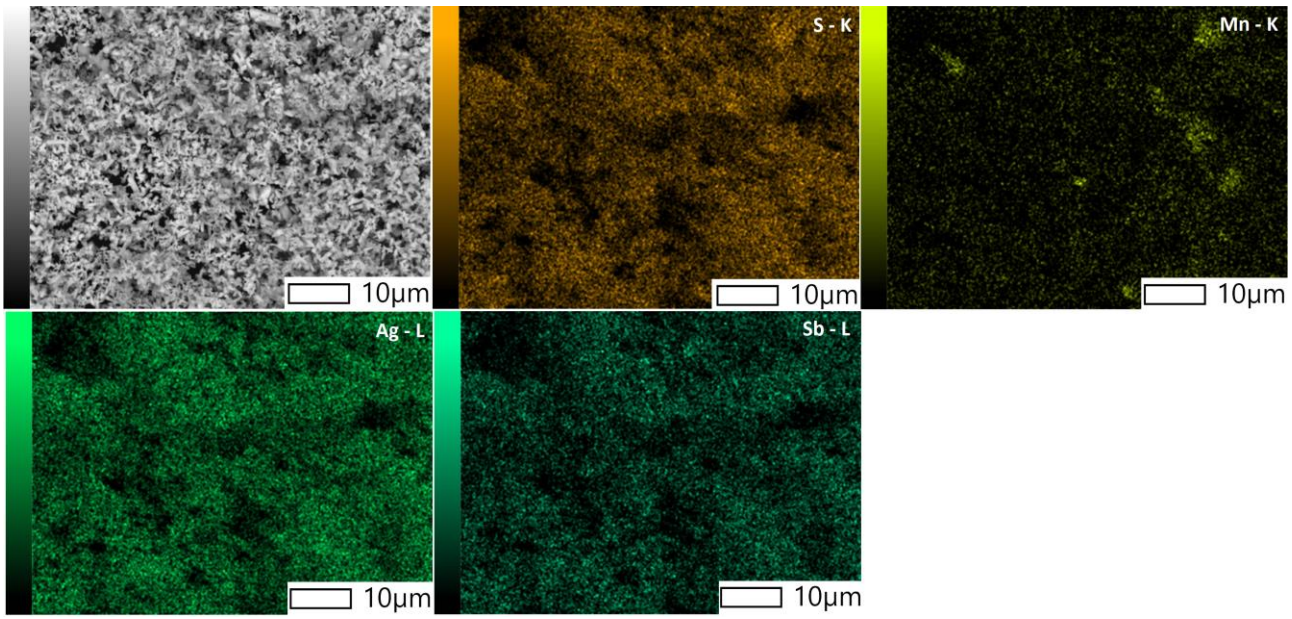

Figure 39: SEM images with EDS-Elemental mapping of Ag, Mn, Sb, and S.

As such, it seems that, in the context of hydrothermal synthesis, the presence of oxygen is not actually an issue as long as sulfur is present in some way in the closed system.

However, during the study of the potential oxygen-based compound creation, the formation of the **yet never reported $Na_3Zn_4(SbO_4)_3 \cdot 6H_2O$** phase has been noted (details about its synthesis are detailed in Appendix 1).

II.C.8. Optimal solvothermal synthesis protocol for samsonite phase and conclusions

Following all the influences discussed previously, it can be summed up that, in the case of the samsonite phase, some parameters are majorly prevalent on the final composition:

- Volume (where a high-volume fill seems to be optimal in this case): **82%**
- Precursors (where Schlippe's Salt was shown to be a key aspect for the successful formation of the samsonite compound and manganese concentration seems to favor the formation of a compound): **Silver acetate, Schlippe's salt, and excess manganese acetate**
- Solvent (water and ethanol are the only solvents functional in this context, water proving to be the most efficient one): **Water**
- Concentration (where a domain of stoichiometric amounts of precursors for 40-80 $mmol.L^{-1}$ of samsonite seemed to be the somewhat optimal quantities): **80 $mmol.L^{-1}$**
- Heating cycle (where the temperature and plateau seemed to have a major effect on the amount of samsonite produced, peaking at 180 °C with at least 24 h of a plateau. The

lowering of temperature is seemingly irrelevant but the rise of temperature seems to at least need to exist for it to be efficient): **8/3 °C.min^{-1} / 180 °C – 24 h / inertia**

Consequently, the experimental protocol that was used to synthesize the **currently optimal amount of samsonite possible** appears to be the following:

Stoichiometric amounts of silver acetate ($Ag(CH_3CO_2)$, Strem Chemicals, 99%, 1.1508 g, 6.8947 mmol) and Schlippe's salt ($(Na_3SbS_4.9H_2O)$, synthesized, 100%, 1.6582 g, 3.4465 mmol) and an excess amount of manganese acetate tetrahydrate ($Mn(CH_3CO_2)_2.4H_2O$, Alfa Aesar, 98%, 2.5226 g, 10.292 mmol) are introduced in 41 mL of distilled water. The solution was agitated with a strong magnetic stir for ten minutes and then transferred to a 50 ml Teflon vessel and locked in a steel case. The vessel is heated up to 180 °C in an hour and the temperature was maintained for 24 hours before letting the system cool down. The powder produced through that process has been then filtrated and washed with distilled water.

While this is an **efficient process with rather high purity**, it still has aspects that could be improved: The synthesis involves a duration of approximately 2 days for the adequate formation of the compound, beforehand, the synthesis of a precursor that is no longer commercially available. Also, no configuration has proven to be efficient enough to get rid of the traces of the pyrargyrite phase completely, a component that, once formed, is not easy to get rid of. [68] As such, a method that has analog properties, but a smaller duration scale was studied: polyol synthesis.

PART III :

POLYOL SYNTHESIS

III. POLYOL SYNTHESIS

A. State of the art

The term "**polyol**" is used since the solvent used also has at least two hydroxyl groups in its composition. During this process, an organic compound is used as a solvent, but **also as a reducing agent.**

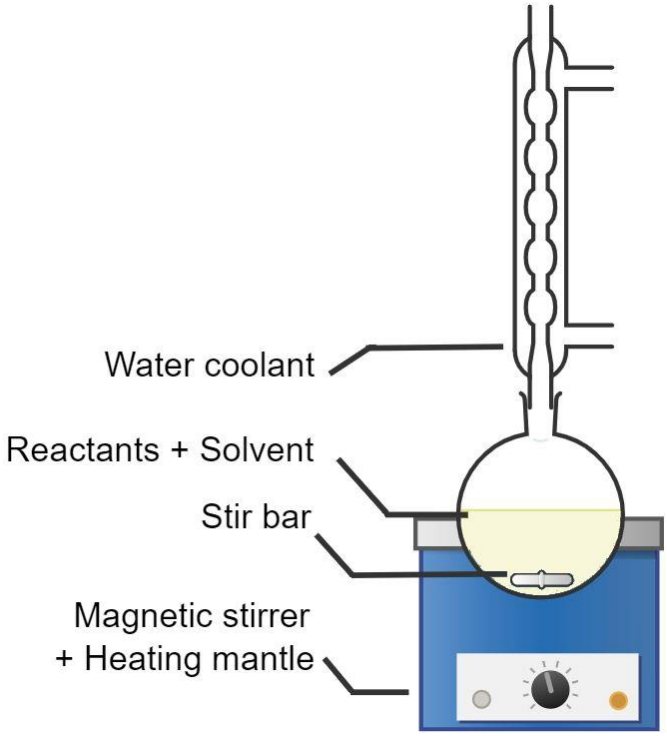

Figure 40: *General presentation of the polyol process*

The process was first defined in the 1980s as a liquid state method that allows obtaining metal nanoparticles from oxides or salts.[69] However, it has been used since to synthesize various oxide or **sulfide compounds**, so its possibilities go beyond its first usage. [70–73]

The nature of the solvent brings many advantages:

- A high boiling point leads to a **high synthesis temperature**. This allows reaching temperatures like "soft" hydrothermal synthesis but without the need for an autoclave.
- The **reducing nature** of the solvent, previously mentioned.
- **Minimal** coalescence.
- The high viscosity and ability of a polyol to adsorb on particle surfaces allow better **control of the morphology and size**, allowing for narrow size distribution.
- This method, unlike many other solvent-based syntheses, such as citrate or sol-gel routes, **does not need a subsequent heating cycle** to obtain the compound needed.

Multiple steps seemingly occur during the polyol process:

At first, the precursors used are **dissolved** into the solvent. This part can occur either straight away, at room temperature, or during the temperature rise. It depends on the solubility of the reactants in the solvent and its variation with temperature. It is then followed by the formation of either **intermediate phases** or a **"stock" of diluted ions**. Followed by the **nucleation** of particles, probably following **similar mechanisms** previously discussed for the solvothermal synthesis. It ends with the **growth and aging** of the particles formed, once again, following similar precipitation rules discussed previously.

Additionally, as this is still a precipitation mechanism, it can also be assumed that the generalities previously mentioned during the chapter about solvothermal synthesis about the LaMer model and Oswalt ripening are **still relevant** in this process as well.[31,36]

The following reaction mechanisms have been reported for the polyol process: [74]

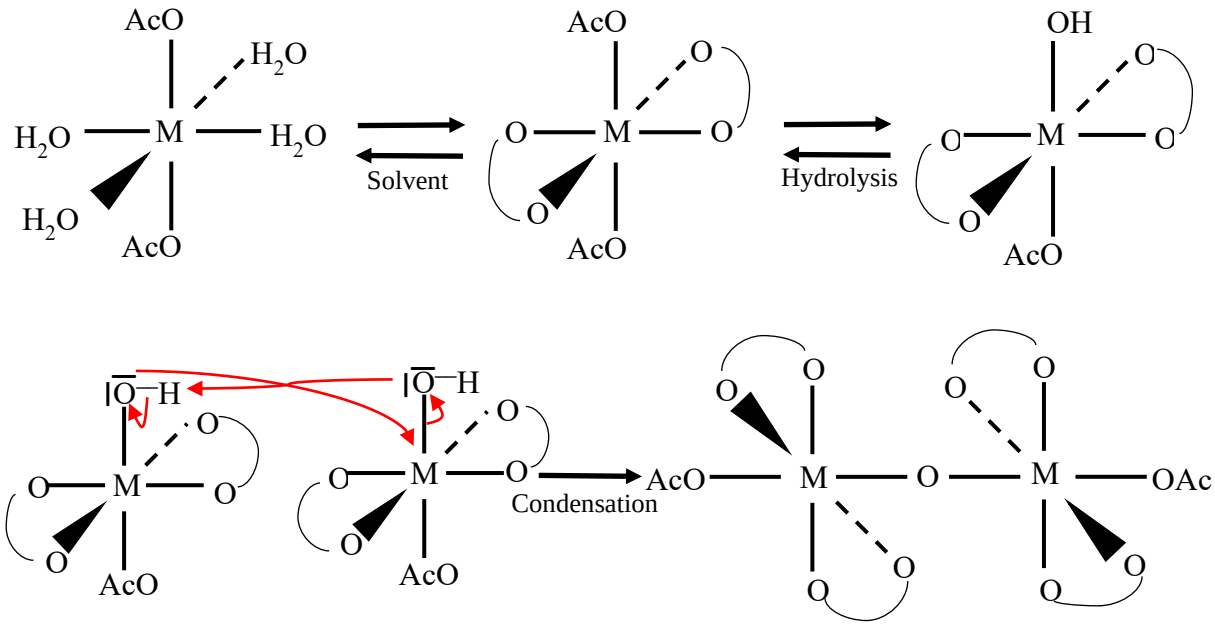

Figure 41: *General synthesis mechanisms during the polyol process where M is the solvated metal and "O—O" is the polyol compound.*

According to literature, the water present during this process is highly influential on the compound that ends up being formed (hydroxide, oxide, or metal), as it forces the hydrolysis of the precursors and favors their decomposition before condensation (as shown in Figure 41). That water can come from the precursors themselves or traces of water present in the solvent. [70] **The hydrolysis ratio** is defined by the value $h = n_{H2O}/n_M$ with n_M the molar amount of metals present in the solution. The presence of the anions in the salts used will also have an effect as they may change the behavior of the previously mentioned water and the cation released.[75]

However, as the objective in this thesis is the synthesis of a sulfide compound, not an oxide, mechanisms that involve the action of sulfide precursors/anions during this process will have to be deduced from the compounds obtained through the various setups.

The solvent that is mostly used in this process is usually ethylene glycol, but other variations can be used to tune the viscosity and the boiling point that may be considered necessary for the synthesis aimed. For example, glycols will have a combined **increase of boiling point and viscosity** while diols could be used to have a similar boiling point to glycols but a **higher viscosity**. The following Table 9 gathers non-exhaustive examples of what one might consider for a choice of solvent:

Table 9: *Non-exhaustive list of properties of various organic solvents*

Properties \ Solvent	*Ethylene Glycol*	*Tetraethylene Glycol*	*Propan-1,3-diol*	*Pentane-1,5-diol*
Chemical Formula	$HOCH_2CH_2OH$	$HO(CH_2CH_2O)_4H$	$HO(CH_2)_3OH$	$HO(CH_2)_5OH$
Molar mass ($g.mol^{-1}$)	62.07[76]	194.23[77]	76.09[78]	104.15[79]
Density at 20 °C ($g.cm^{-3}$)	1.113[76]	1.12[77]	1.053[78]	0.99[79]
Viscosity at 20 °C (mPa.s)	16.06[55]	56.18[77]	52.7[80]	135[79]
Boiling point (°C)	197[76]	327.3[77]	214[78]	241[79]

However, some details must be considered when setting up a polyol process. Indeed, before even the precipitation process, an unwanted reaction such as the possibility for solvents, once heated for at least an hour above 200 °C, to form carbon dots. [81]

The behavior of the metals added to the solvent is also to be considered. For example, it has been shown that, during a polyol process containing silver nitrate used as a precursor, the silver particles formed acted for an autocatalytic reduction of silver, but also catalyzed the self-reaction of ethylene glycol that was being used. [82]

The two previous aspects mentioned alone mean the reuse of the solvent after synthesis would not be a possibility.

Also, while sulfides have been synthesized through this method, **the formation of complex quaternary sulfides is rather seldom**, most of the focus that can be found in literature is on binary (or, at best, ternary) compounds with controlled morphology and at a nanoscale. [70,71,74]

B. Experimental Section

The first experimental protocol to be used in order to synthesize the samsonite phase was based on the modified polyol process suggested by *Weller et al.*[72] where acetates and sulfur, combined

with a reducing agent, are used in tetraethylene glycol to synthesize the tetrahedrite phase. First attempts have thus been made without the reducing agent and then compared to the same process with a reducing agent:

Protocol 1:

Stoichiometric amounts of silver acetate ($Ag(CH_3CO_2)$, Alfa Aesar, 99%, 0.7238 g, 4.337 mmol), antimony acetate ($Sb(CH_3CO_2)_3$, Sigma Aldrich, 99.99%, 0.6479 g, 2.168 mmol), manganese acetate tetrahydrate ($Mn(CH_3CO_2)_2.4H_2O$, Alfa Aesar, 98%, 0.3269 g, 1.094 mmol) and sulfur (S, Alfa Aesar, 99.5%, 0.2085 g, 6.505 mmol) have been introduced in 100 mL of tetraethylene glycol inside a 250mL round flask mounted by a water coolant system. The solution was agitated by magnetic stirring while N_2 is bubbled for 10 minutes. The solution was then heated up to 180 °C and maintained for 1 hour. The solution has then been let cooled down at the system's inertia before filtrating and washing the obtained powder with ethanol.

Protocol 2:

Stoichiometric amounts of silver acetate ($Ag(CH_3CO_2)$, Alfa Aesar, 99%, 0.7238 g, 4.337 mmol), antimony acetate ($Sb(CH_3CO_2)_3$, Sigma Aldrich, 99.99%, 0.6479 g, 2.168 mmol), manganese acetate tetrahydrate ($Mn(CH_3CO_2)_2.4H_2O$, Alfa Aesar, 98%, 0.3269 g, 1.094 mmol) and sulfur (S, Alfa Aesar, 99.5%, 0.2085 g, 6.505 mmol) have been introduced in 66 mL of tetraethylene glycol inside a 250mL round flask mounted by a water coolant system. The solution was agitated by magnetic stirring while N_2 was bubbled for 10 minutes. Meanwhile, an excess amount of sodium borohydride ($NaBH_4$) was dissolved in 33mL of tetratethylene glycol and was then added to the mixture. The solution was then heated up to 180 °C and maintained for 1 hour. The solution has then been let cooled down at the system's inertia before filtrating and washing the obtained powder with ethanol.

Following these attempts, the protocol was modified on specific parameters to see their respective influences on the synthesis. Changes revolved around:

- *The atmosphere used:* to study the influence oxygen might have on the synthesis.
- *Types of solvents:* as this is a parameter with a lot of possible options, it was decided to limit this study to 3 solvents: glycol (with tetraethylene glycol), diol (with propan-1,3-ol), and aminol (with 1-aminopropan-3-ol). The use of 1-aminopropan-3-ol could be considered as unjustified as it does not follow the type of solvent used in a "polyol synthesis", however, we do consider that the still polar nature of the solvent, its properties being in the scale of other diols, the potential effects of the amino group compared to a diol as a better reducing agent makes this solvent worthy of study and discussion in this same part and not as a different synthesis method.

- *Types of precursors:* precursors used in the previous part *(Part II)* are re-used in this part. This includes the use of Schlippe's Salt to study the necessity of an SbS_4^{3-} anion for an appropriate samsonite synthesis like it is in the case of hydrothermal synthesis. This could help us learn if we are facing the exact same mechanisms or if there are important nuances between the two methods.
- *Varying with concentration:* the concentration was progressively increased to study the limitations of the polyol process and the powder quantity that can be produced with it for a fixed volume. The potential for up-scaling will also be discussed.
- *The stirring speed:* more of a circumstantial study of this parameter than with actual intent. An influence of the stirring speed was noticed and has been studied for optimal synthesis.
- *Heating cycle:* This included the temperature reached, the duration of the temperature plateau, the rising temperature slope, and the decreasing temperature slope (while the temperature and the plateau are controlled quantitatively, the control of the slopes will be more qualitative).

The final synthesis method set up according to the effectiveness of the method was the following:

Protocol 3:

Stoichiometric amounts of silver acetate ($Ag(CH_3CO_2)$, Alfa Aesar, 99%, 1.5924 g, 9.5408 mmol), antimony acetate ($Sb(CH_3CO_2)_3$, Sigma Aldrich, 99.99%, 1.4258 g, 4.7704 mmol), manganese acetate tetrahydrate ($Mn(CH_3CO_2)_2.4H_2O$, Alfa Aesar, 98%, 0.5904 g, 2.4090 mmol) and sulfur (S, Alfa Aesar, 99.5%, 0.4588 g, 14.3112 mmol) are introduced in 200 mL of 3-aminoproan-1-ol inside a 500mL round flask mounted by a water coolant system. The solution is vigorously agitated by magnetic stirring while N_2 is bubbled for 10 minutes. The solution is then heated up to 180 °C and maintained for 3 hours and 30 minutes. The solution is then let cooled down at the system's inertia before filtrating and washing the obtained powder with ethanol.

C. Results and discussions

In a similar way to the previous part, the results will be discussed according to what are to be considered important parameters of this synthesis method. Once all of these have been assessed, the aim will be to suggest a reaction mechanism that may explain what is exactly going on during this process with all the empirical information gathered.

III.C.1. Influence of Atmosphere

To assess the influence of the atmosphere during synthesis, two atmospheres were compared, nitrogen and air (where the bubbling process is simply skipped).

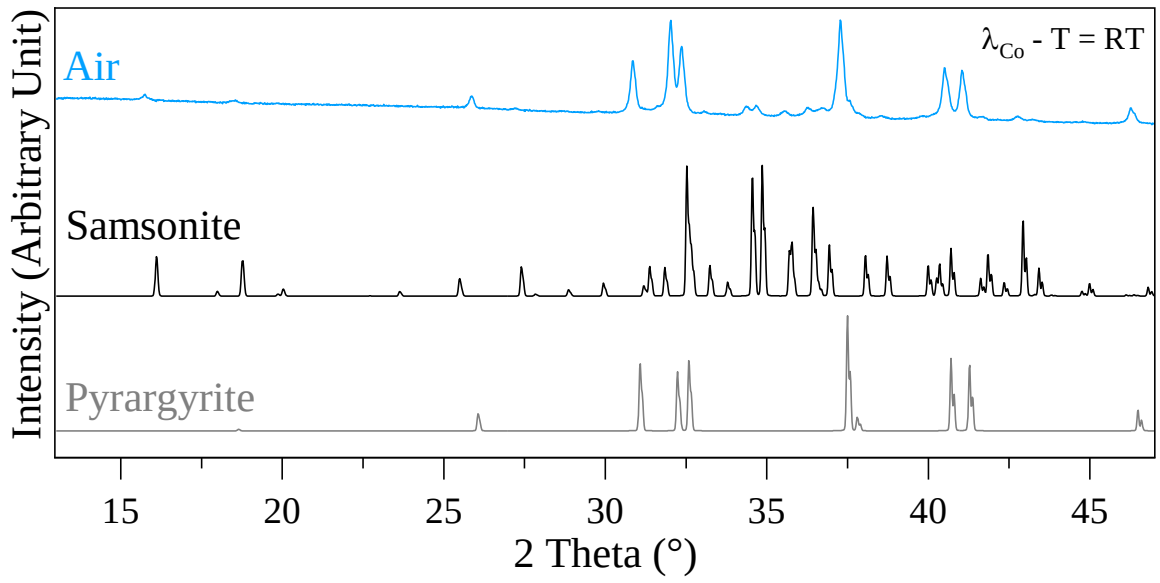

Figure 42: *Room temperature XRD patterns of powder obtained through polyol synthesis without a controlled atmosphere and simulated patterns of pyrargyrite (COD: 1011162) and samsonite (COD: 9010235) phases.*

Oddly enough, while **no oxide compound appears under air**, the samsonite does not appear as the major compound, Ag_3SbS_3 becomes once more the major compound, according to the XRD pattern obtained in Figure 42. As such, an additional test was done with a bubbling of oxygen instead of nitrogen, to learn if it was the bubbling itself influencing the compound obtained or if nitrogen is specifically needed for an efficient synthesis.

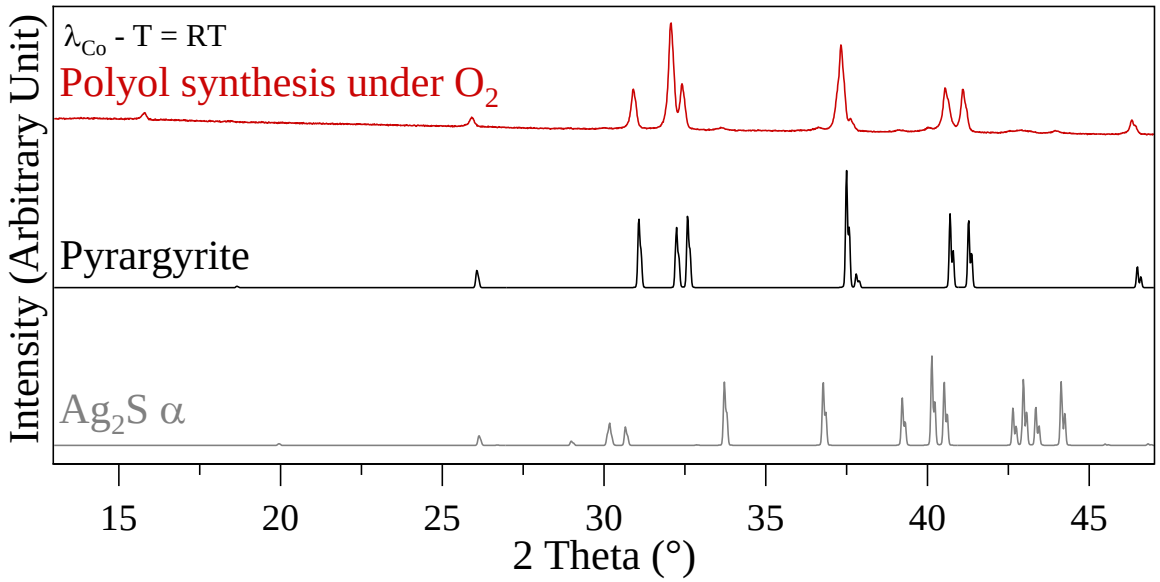

Figure 43: *Room temperature XRD pattern of the powder obtained through polyol synthesis under pure oxygen with simulated patterns of the pyrargyrite phase (COD: 1011162) and the silver sulfide phase (COD: 1544685).*

The samsonite phase **does not seem to be present at all**, as Figure 43 shows, furthermore, it could be noticed that only pyrargyrite and silver sulfide are the compounds present by the end of the process.

As such, it is clear that the presence of **oxygen is hindering the formation of the samsonite phase** without directly provoking the formation of oxides. Multiple hypotheses could be made from this, the oxygen could be somehow blocking the solvated manganese from condensing or the properties of the solvent might be influenced by reactions with the atmosphere. A study of the left-over organic solvent at the end of the process might be necessary to more adequately understand what is exactly happening.

In the case of the samsonite synthesis specifically**, nitrogen** has clearly been shown to be the gas to be used during this process to synthesize properly the compound.

III.C.2. Influence of solvent

III.C.2.a) Strict « polyols »

Two solvents that exactly follow the concept of « polyol » have been tested. Propan-1,3-diol and tetraethylene glycol. Both have also been tested with the reducing $NaBH_4$ agent mentioned in *Protocol 2*.

In the case of tetraethylene glycol, the temperature scope studied was from 160 °C up to 300 °C. The samsonite phase has **successfully been synthesized at 220 °C**. Unfortunately, the XRD patterns obtained in Figure 44, unlike those in solvothermal synthesis, are of rather poor quality when samsonite seems to be present in a major amount, while the higher temperature may be easier to read, but samsonite is only seen as traces or a minor quantity of the powder analyzed. No reheating attempts of the powders synthesized at low temperatures led to any significant change without loss of the samsonite phase.

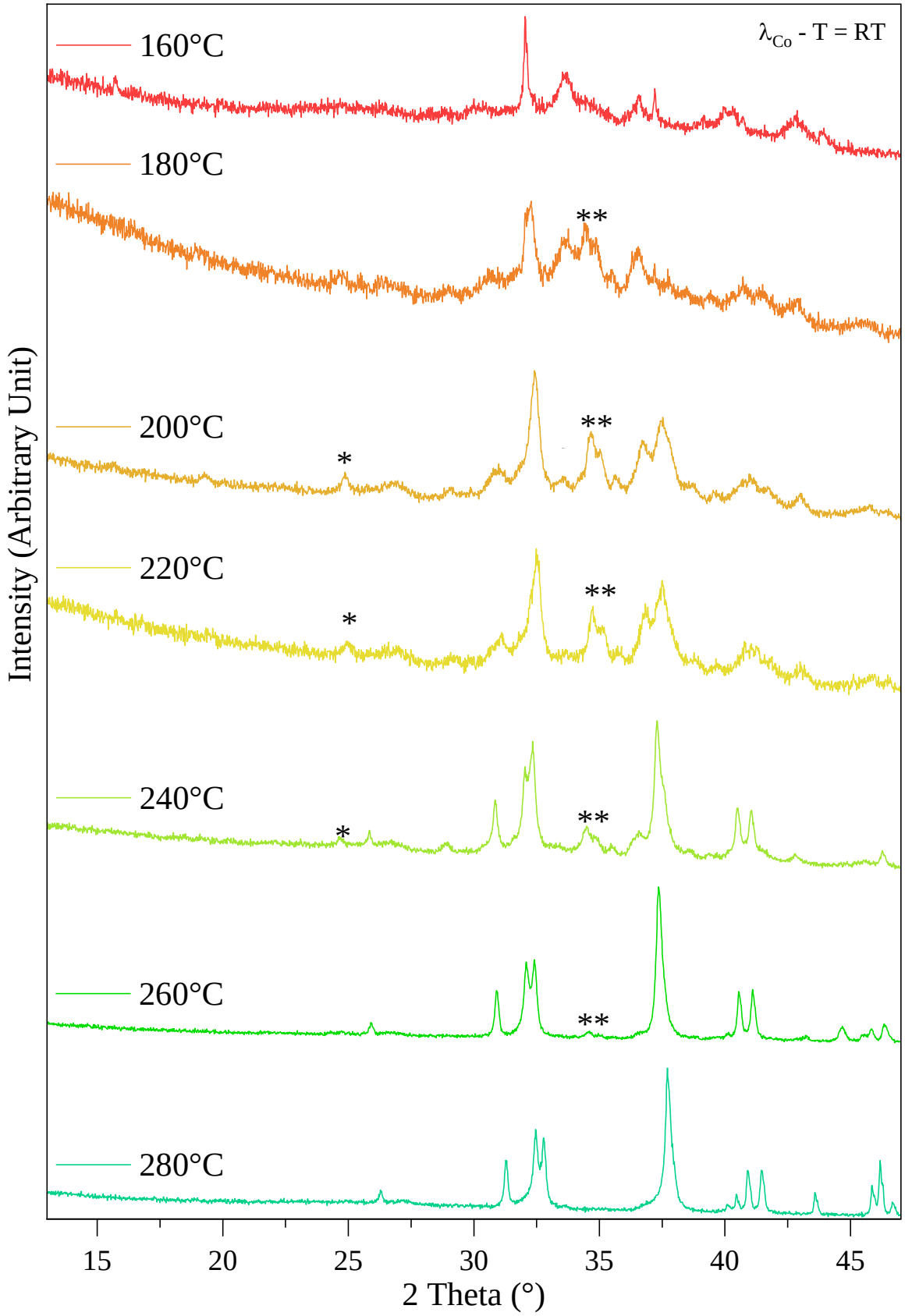

Figure 44: *Room Temperature XRD Patterns of powder obtained through polyol synthesis with tetraethylene glycol according to temperature plateau. * are peaks related to the samsonite phase.*

However, concerning propan-1,3-diol despite various temperatures tested, no samsonite phase could be witnessed.

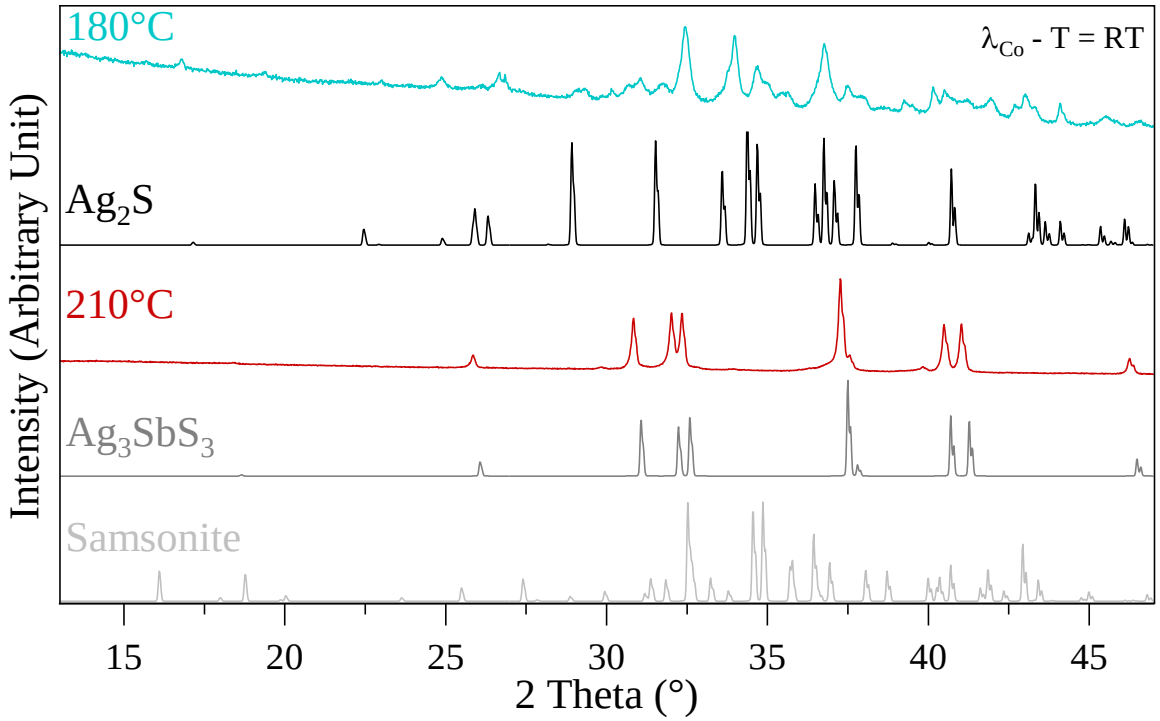

Figure 45: *Room temperature XRD patterns of powders obtained through the polyol synthesis with propan-1,3-diol as a solvent and simulated patterns of silver sulfide (COD: 1544685), pyrargyrite (COD: 1011162), and samsonite (COD: 9010235) phases.*

Additional testing done with the reducing agent led to unsuccessful results as no samsonite traces could be found with either solvent. The reducing power from the saturated agent may be too powerful to let the compound appear or it may allow for parasitic reactions to take place.

III.C.2.b) The strange case of 3-aminopropan-1-ol

Aminopropanol is a solvent that has characteristics with innate potential compared to the other previously used polyols. Indeed, first, thanks to the size, symmetry, and charge distribution of the molecule, it can **easily solvate any precursors and rearrange accordingly**, better than even other organic compounds from the same family. Consequently, this makes it a flexible solvent for many various uses.[83]

Secondly, as a primary amino solvent, it has been shown that the following reaction may occur:

$$RNH_2 + S_n \leftrightarrow RN^+H_2—S_n^-$$

$$RN^+H_2—S_n^- + RNH_2 \leftrightarrow RN^+H_3 + RNH—S_n^-$$

With $RN^{+}H_2—S_n^-$ as a strong acid and $RNH—S_n^-$ as a weak acid. This study also shows that in these conditions, S_n^- and S_n^{2-} are present in the solvent.[84]

These aspects may explain the surprising results obtained, not only in this specific section dedicated to the influence of solvents but also in the potential influence of precursors and also the difference in reaction mechanisms between hydrothermal synthesis and the polyol process.

As can be seen in Figure 46, the amount of samsonite phase is strongly close to the amounts of powder obtained through hydrothermal synthesis, with a minimal amount of parasitic product, **without the presence of pyrargyrite** and below 5 % (dyscrasite ($Ag_{3-x}Sb$) and elemental antimony being the phases present).

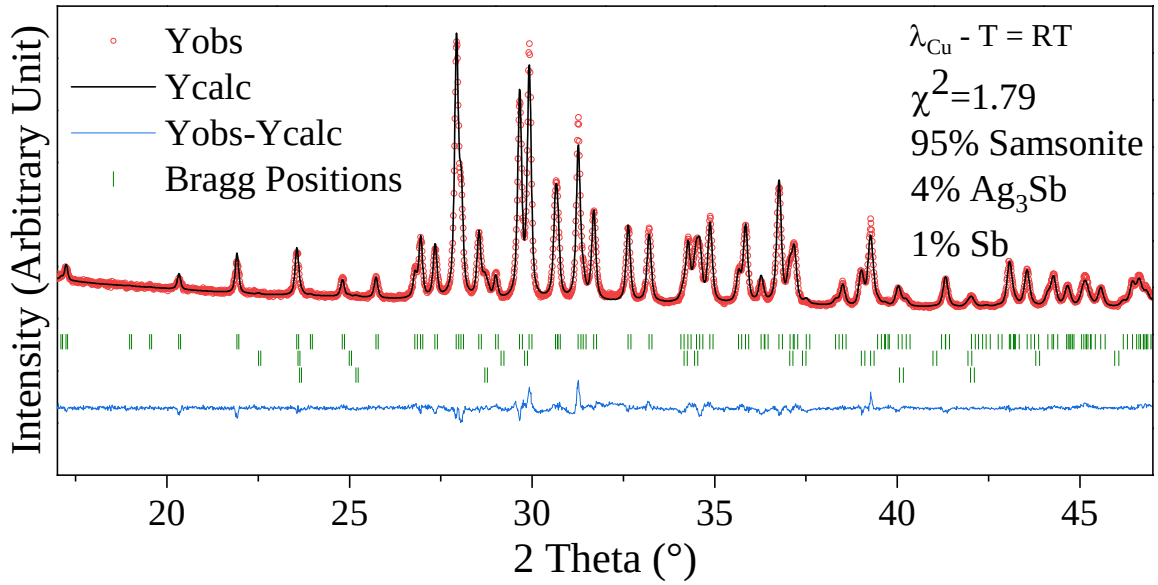

Figure 46: *Room temperature XRD pattern of the powder obtained from polyol synthesis with aminopropanol as a solvent.*

The temperature of **180 °C** was determined as optimal as additional unwanted compounds appear as soon as 170 °C.

If you look back at the mechanisms from the literature in Figure 41, combined with the equations of reactions between sulfur and amino compounds the following variant could be suggested in Figure 47:

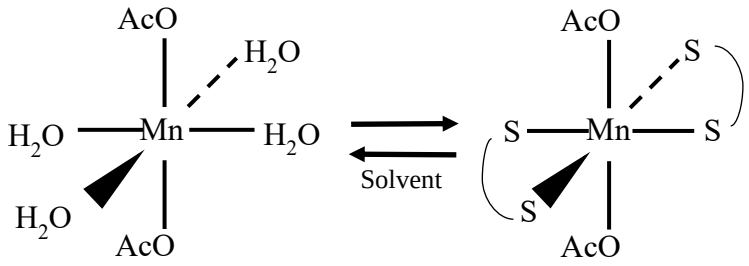

Figure 47: Suggested mechanism during the polyol process for manganese with "S—S" is the aminopropanol combined with the sulfur precursor.

In this case, as only manganese is the only precursor with water present, this is the only metal introduced into the solvent that should be having this specific configuration. Assuming this precise reaction happens and the hydrolysis and condensation involve sulfur rather than oxygen, this would mean that manganese would be in the AX_6 configuration that it has inside the samsonite crystal structure. Supposedly, this could be the push that **allows manganese to be incorporated better during the polyol process** than with more regular solvents.

III.C.3. Influence of precursors

As shown previously in Figure 46, the use of acetate precursors and sulfur has shown to be a strongly efficient combination of precursors as 95% of samsonite was synthesized, with only the addition of unwanted alloys and metallic compounds. However, while these were strongly promising results, deeper research into the precursors used with the possibility of an even purer compound was done.

As **Schlippe's salt** is a compound that was quite successful in the formation of the samsonite phase, it was used here in an attempt to synthesize it potentially more efficiently. However, as XRD patterns in Figure 48 indicate, the results are **catastrophically below** the ones involving the use of sulfur and antimony acetate with no samsonite phase seemingly being synthesized.

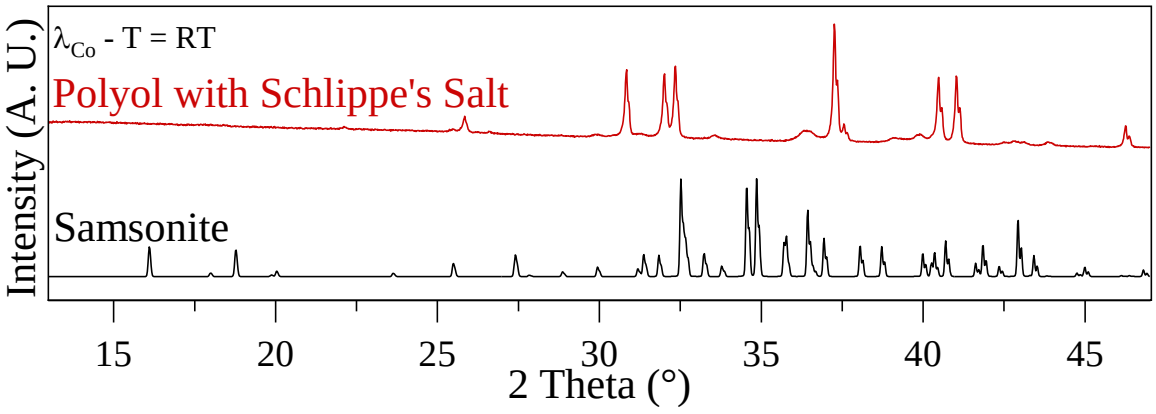

Figure 48: Room temperature XRD pattern from powder obtained through polyol synthesis with Schlippe's salt as a precursor and the simulated pattern of the samsonite phase (COD: 9010235).

But how is it so? While the compound is strongly soluble in water, its behavior might be quite different in a different solvent and the thioantimoniate anions might not be as easily accessible through this process. Another fact to consider is that, unlike antimony acetate and elemental sulfur, Schlippe's salt is a highly hydrated compound. With acetates and sulfur, the hydrolysis ratio can be determined to be $h = 4/7$ as manganese acetate is the only compound introducing water into the system. With Schlippe's salt and its 9 water molecules replacing sulfur, the hydrolysis ratio drastically increases to $h = 13/7$, **more than tripling it**.

An **excess amount of sulfur** has also been experimented with, as an excess amount of it did not seem to hinder the hydrothermal synthesis, an attempt to witness the influence of excess sulfur has been performed here too, with a 133% molar amount of sulfur (to simulate the 8 sulfur equivalents provided by Schlippe's salt during the hydrothermal process). Results were surprising as, while the samsonite phase was still present by the end of the process, instead of pyrargyrite (Ag_3SbS_3) or dyscrasite (Ag_3Sb) phases as unwanted products, **myrargyrite ($AgSbS_2$) was produced instead**.

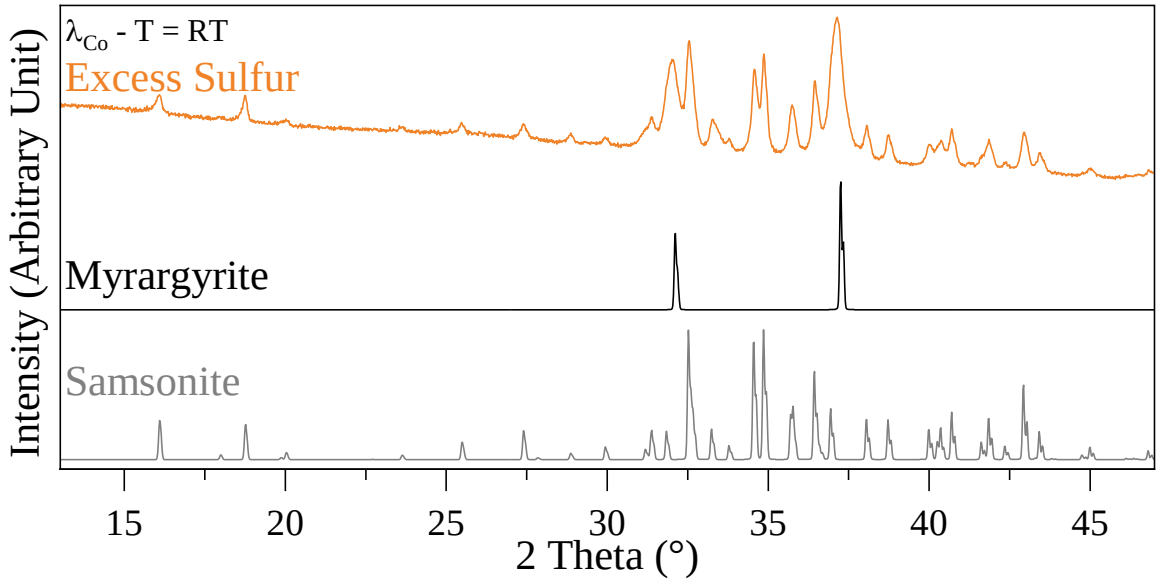

Figure 49: *Room temperature XRD pattern obtained from power synthesized through polyol process with excess sulfur and simulated patterns of myrargyrite (COD: 9002733) and samsonite (COD: 9010235) phases.*

Sulfide precursors also proved to be **lacking in efficiency** compared to the acetate compound. According to the XRD patterns shown in Figure 50, **only Ag_3SbS_3, MnS, and traces of $AgSbS_2$** phases are formed during this process when using Ag_2S, Sb_2S_3, and MnS.

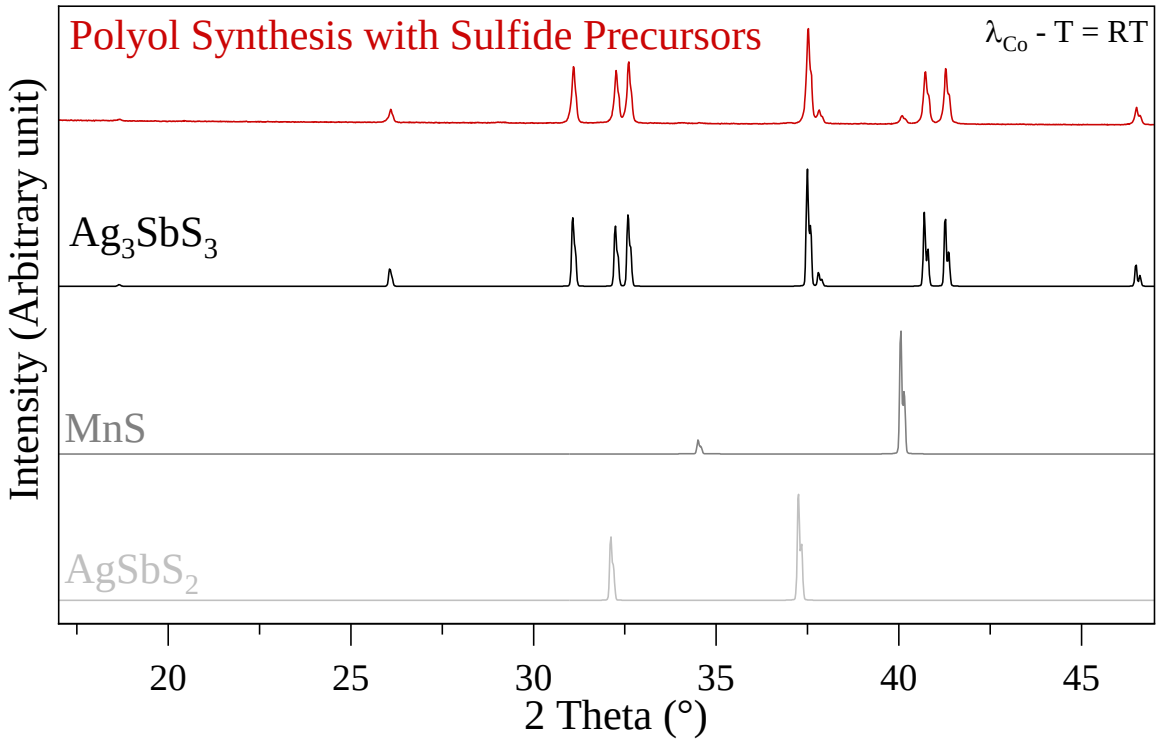

Figure 50: *Room temperature XRD pattern of powder obtained through Polyol synthesis with sulfide precursors with simulated patterns of Ag_3SbS_3, MnS, and $AgSbS_2$.*

The results are **strongly similar to those that were obtained through solid-state synthesis**. The use of these sulfides may have pushed the reaction toward these more thermodynamically stable compounds, with MnS not reacting at all. **An exchange of ions seems to be a necessity for the formation of a samsonite phase.**

III.C.4. Influence of the concentration

This section will be mostly focused on the influence of variations in the concentration of precursors added into the solvent.

Table 10: *Dependence of the samsonite phase proportion against the assumed amount synthesized through the polyol process in 100mL.*

Yield ($g.L^{-1}$)	*11*	*15*	*22*	*35*
Samsonite phase (%)	97	88	86	71

As can be noticed from Table 10, **the higher the concentration, the lesser the synthesis is efficient**, as an additional Ag-Sb-S phase, $AgSbS_2$, appears as another secondary compound. The optimal amount that can be reached seems to be **11 $g.L^{-1}$** which is lesser than the yield that can be reached with the hydrothermal process, however, it does not contain any pyrargyrite phase.

III.C.5. Influence of stirring speed

Surprisingly, stirring speed has a quite heavy influence on the efficiency of the process. While literature about the study of this aspect during coprecipitation-style synthesis is rather sparse, there are some previously existing examples of the Reynolds number, the value that predicts the flow patterns according to the system the fluid is in, influencing reaction rate and speed, as shown in Figure 51.

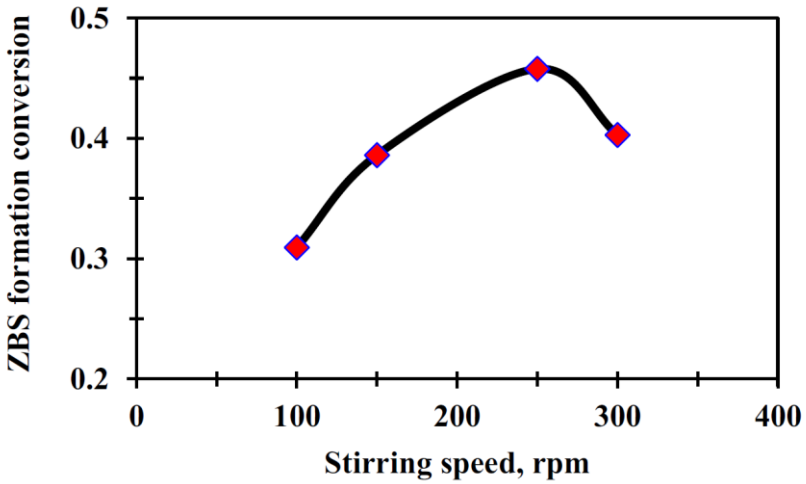

Figure 51: *$Zr_5O_8(SO_4)_2$ synthesis rate according to stirring speed.* [72]

As the Reynolds number can be calculated with the following formula: [85]

$$Re = \frac{\rho D^2 N}{\mu}$$

Where Re is the Reynolds number, ρ is the liquid density (in $kg.m^{-3}$), D is the stirrer width (in m), N is the stirrer rotational speed (in $rad.s^{-1}$) and μ is liquid viscosity (in Pa.s). It can be deduced that the stirring speed is influential in the synthesis of a compound. As the liquid density and viscosity are not known for 3-aminopropan-1-ol at 180 °C, only the stirring speed will be compared here.

As such, a brief study of this aspect of our synthesis is necessary. Three speeds were tried: 750, 1000, and 1250 rotations per minute (rpm) in aminopropanol. The tests have been made with a 3 h long plateau.

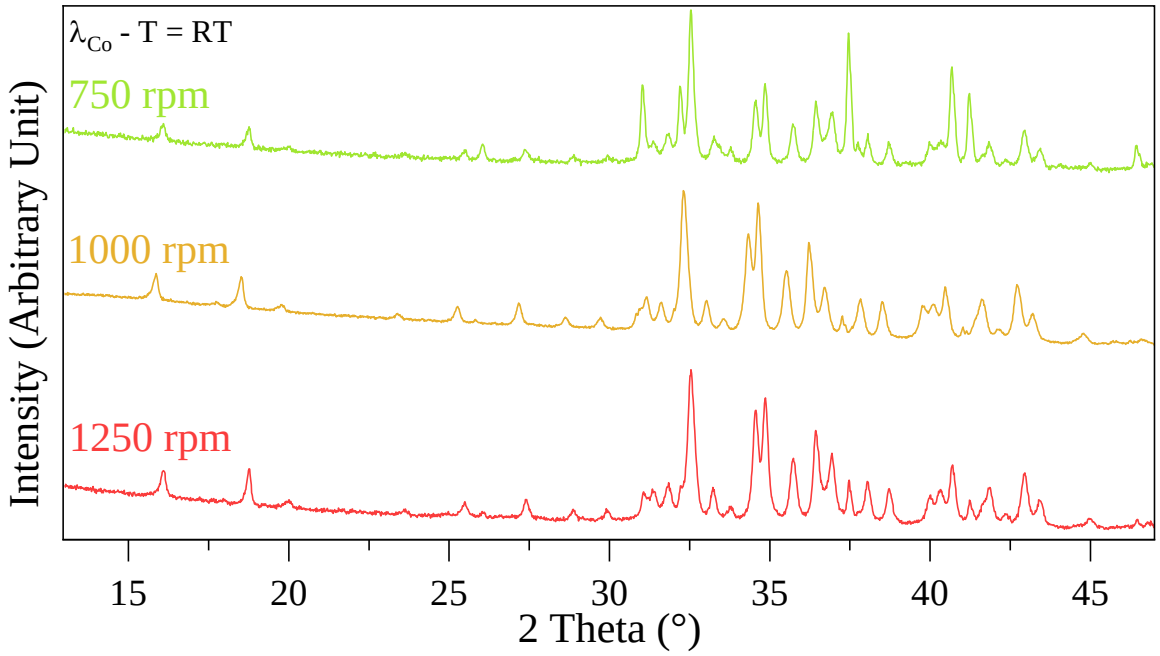

Figure 52: *Room temperature XRD patterns of powders obtained according to their stirring speed during the polyol synthesis process.*

Refinements were made on all three XRD patterns to assess the proportion between the samsonite and pyrargyrite phases and the following results can be compared:

Table 11: *Proportions of samsonite and pyrargyrite phases according to speed.*

Speed (rpm)	*Samsonite (%)*	*Pyrargyrite (%)*
750	67.5	32.5
1000	97.5	2.5
1250	91.9	8.1

Seemingly, **the optimal rotational speed is around 1000 rotations per minute** during the plateau. It has been noticed that during the cooling stage of the experimental protocol, the lack of magnetic stirring, **at any moment,** ended up lowering the amount of samsonite synthesized. As such, it was decided that the stirring speed during the heating process and the plateau would be maintained at 1000 rpm, during the cool-down, the stirring was maintained at a minimal rotational speed of **750 rpm** (the only speed that could be consistently maintained at this step with the experimental setup due to the increasing viscosity).

III.C.6. Influence of the heating cycle

Another capital aspect of the synthesis is the heating cycle the reactive mixture goes through.

With the setup at our disposal, precise control of the rising temperature rate was too difficult to assess correctly. Consequently, a focus was made on the temperature used, the length of the heating, and the method used to cool down the system. The temperature has been discussed previously in section *III.C.2.* as it is strongly dependent on the solvent used. The following experiments were all made with aminopropanol at 180 °C.

Tests with various plateau durations have been performed, from as low as 10 minutes to as long as 5 hours. Then, through the refinement of XRD patterns, the proportions of the samsonite phase have been deduced. The results were then aggregated in Figure 53:

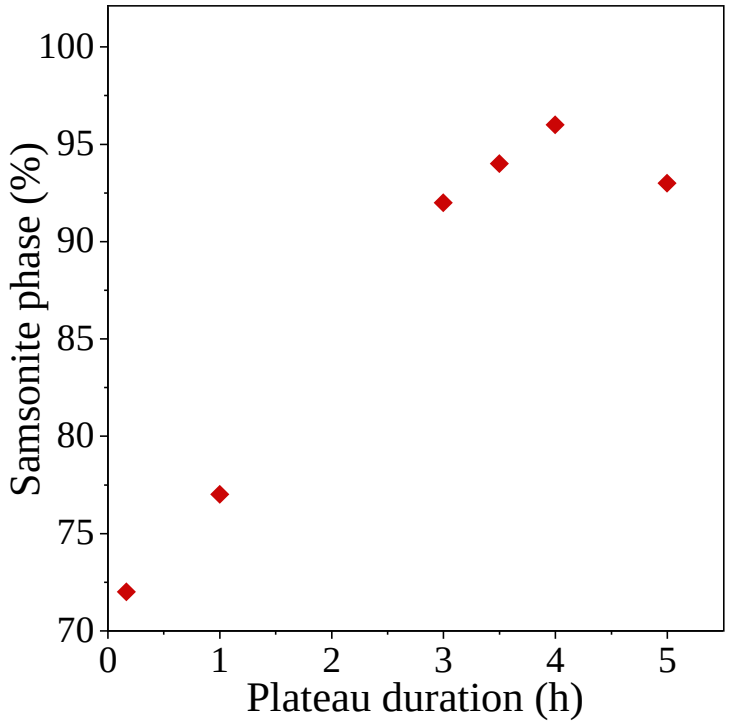

Figure 53: *Samsonite phase present in powder obtained from polyol process according to plateau duration.*

A clear tendency is visible from these results, showing that **the optimal duration is around 4 hours**. First, it is worth noticing that even without any plateau, the samsonite phase has been synthesized. Unfortunately, as an in-situ study of the compounds during the process was not an option, **two main possibilities can be happening here**:

- One option may be that, as we know from *III.C.2.*, processes at temperatures below 180 °C do still produce samsonite, even if it is less efficient, it may still be that there is a threshold of temperature where there is enough energy in the system to trigger the formation of samsonite and the time spent above this temperature is equivalent to the time of a “theoretical plateau”.

- Another possibility could be that the process started once the peak is reached and only during the cooling phase if the temperature was above the set temperature.

One critical aspect of the heating cycle that has an influence on the polyol process is the decreasing temperature rate. It was noticed during the upscale of the process that the **pyrargyrite phase had returned at an alarming rate.** After eliminating one eventuality after another, only one remained: the cooling speed of the system. Because of the setup, the round-bottom flask was still partially submerged in the silicon oil at the end of the process, that slower cooling seems to be the origin of the return of larger amounts of Ag_3SbS_3. However, as soon as the setup was modified to allow continuous stirring and complete separation from the bath and flask at the end of the process, XRD revealed a similar result to previous experiences at a smaller scale, even though, unfortunately, the pyrargyrite phase was not completely suppressed. This may be due to the larger amount of liquid that needs to cool down.

In the case of 100mL synthesis, the control of the decrease in temperature has a noticeable effect, but not as major as the 250mL as only approximately a 5% decrease could be noticed.

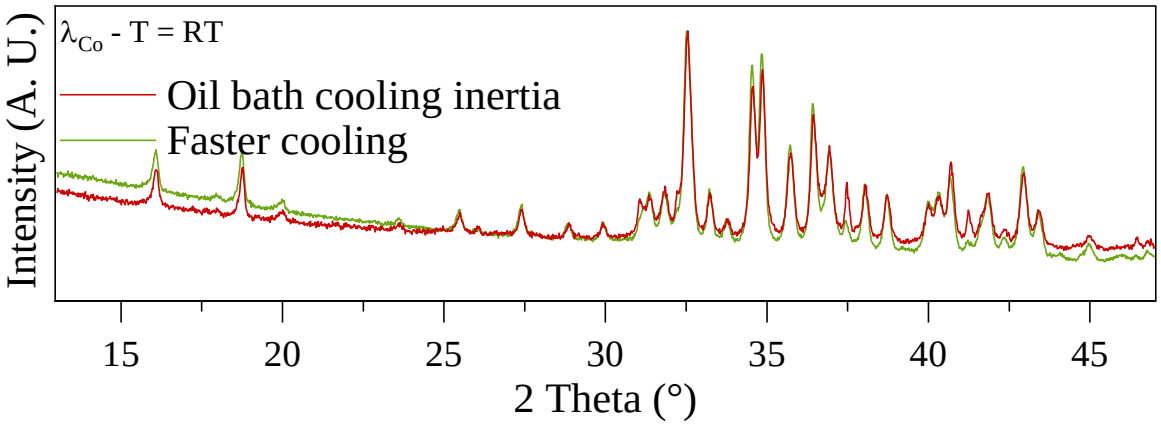

Figure 54: *Room temperature XRD patterns of powders obtained by polyol process depending on the cooling method.*

These two observations at both scales are important when trying to understand the mechanics behind polyol synthesis. If (additional) pyrargyrite appears during the cooling process, that means there is a temperature where the samsonite phase is **no longer being synthesized** while pyrargyrite starts being formed from the other compounds and there is also another temperature where Ag_3SbS_3 is not being formed either.

As it is now known that synthesis with a 4-hour-long plateau has no apparent pyrargyrite. Additionally, a slower cool down allows samsonite and dyscrasite to be consumed while pyrargyrite appears. This indicates a **critical piece of information**: pyrargyrite seems to be synthesized either during the heating-up process at the soonest, or partially during the plateau at the latest. That

pyrargyrite is then decomposed during said plateau and, if not cooled fast enough, another reaction will allow for the ternary sulfide to be reformed.

III.C.7. Mechanisms behind the polyol synthesis

From the synthesis steps described in the State-of-the-Art *section III.A* and the results obtained from the multiple experiments in *III.B.*, an estimation of the reactions and mechanisms which may occur during the polyol process that may be established:

The first reaction may be the dissolution of the precursors used (with the mechanisms shown in *III.A.* in general, and in the case of manganese more specifically, described in *III.C.2.b.*) that should be happening during the stirring and the rising slope of temperature:

$$8\ Ag(CH_3CO_2) + 2\ Mn(CH_3CO_2)_2 + 4\ Sb(CH_3CO_2)_3 + 12\ S \rightarrow "8\ Ag^+ + 2\ Mn^{2+} + 4\ Sb^{3+} + 12\ S^{2-}"$$

The following reaction would be the simultaneous synthesis of the samsonite and pyrargyrite phases:

$$8\ Ag^+ + 2\ Mn^{2+} + 4\ Sb^{3+} + 12\ S^{2-} \rightarrow Ag_4MnSb_2S_6 + Ag_3SbS_3 + Ag^+ + Mn^{2+} + Sb^{3+} + 3\ S^{2-}$$

The following reaction is the reduction of Ag_3SbS_3 into Ag_3Sb. Unlike hydrothermal synthesis, this reaction happens thanks to the reductive power of the 3-aminopropan-1-ol. As the pyrargyrite phase diminishes during the temperature plateau, it can be assumed this is the slowest reaction during the process:

$$Ag_3SbS_3 \rightarrow Ag_3Sb + 3\ S$$

However, it can be noticed with XRD patterns that the pyrargyrite phase (Ag_3SbS_3) and dyscrasite one (Ag_3Sb) are never present simultaneously. It can be assumed this reaction is a fast one and all the Ag_3Sb phase gets instantly consumed to form additional pyrargyrite:

$$Ag_4MnSb_2S_6 + Ag_3Sb + Ag^+ + Mn^{2+} + Sb^{3+} + 3\ S^{2-} \leftrightarrow 2\ Ag_4MnSb_2S_6$$

The leftover Ag_3Sb can be due to either ion staying dissolved in the organic solvent and/or the impurities already present in precursors.

With two strongly efficient methods of synthesis, it is now possible to study the physical properties of the samsonite phase and compare the potential differences induced by both methods.

PART IV: PHYSICAL PROPERTIES OF SAMSONITE

IV. PHYSICAL PROPERTIES OF SAMSONITE

A. State of the art

Due to its only natural nature, little is known about the physical properties of the samsonite phase. The crystal structure has been thoroughly studied from 100 to 400 K by L. Bindi and M. Evan, using the Gram-Charlier development to identify atomic displacements.[10] The aim of the study was more about proving the efficiency of the method with unknown mineral structures rather than about the samsonite mineral specifically.[10] This study shows **the strong anisotropic displacement of the silver atoms** while indicating that **no ionic conductivity** is actually witnessed in the structure.[10]

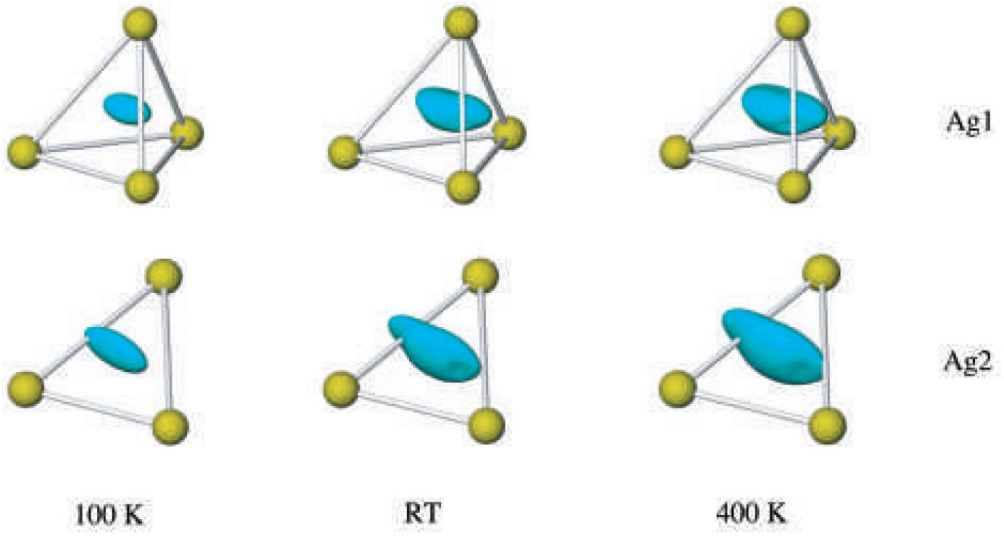

Figure 55: *Non-harmonic probability density isosurfaces of Ag1 and Ag2 for samsonite at 100 K, RT, and 400 K.*[4]

In regards to the physical properties that have been studied for the samsonite phase, resources are sparse and quite old (between the 1910s to the 1940s) so what is referenced can be citations of citations and the information might be rather vague:

- While under heat inside an open tube, samsonite supposedly becomes liquid while emitting antimony gases, then the mineral would decompose into gaseous sulfur dioxide, antimony oxide, antimony, silver, and a manganese-based compound.[86]
- Samsonite dissolves in nitric acid.[86]
- Crystal form and size have been assessed: Their shape is represented in Figure 56 and their size averages around the millimeter scale.[86]
- The samsonite's scratch hardness on the Mohs scale is 2.5. A value that is between Gypsum (2) and Calcite (3) on a scale of 1(a talc crystal) to 10 (a diamond).[87]
- The samsonite's indention hardness of 187-212VHN100 (where 187-212 is the hardness number (in $kg.mm^{-2}$), VH is the Vickers Scale and N100 is the force applied (in N)).[87]

- The mineral is an opaque black, translucent if thin enough. Red-brown in transmitted light. Polished sections may transmit a bluish-white with red reflections.[87]

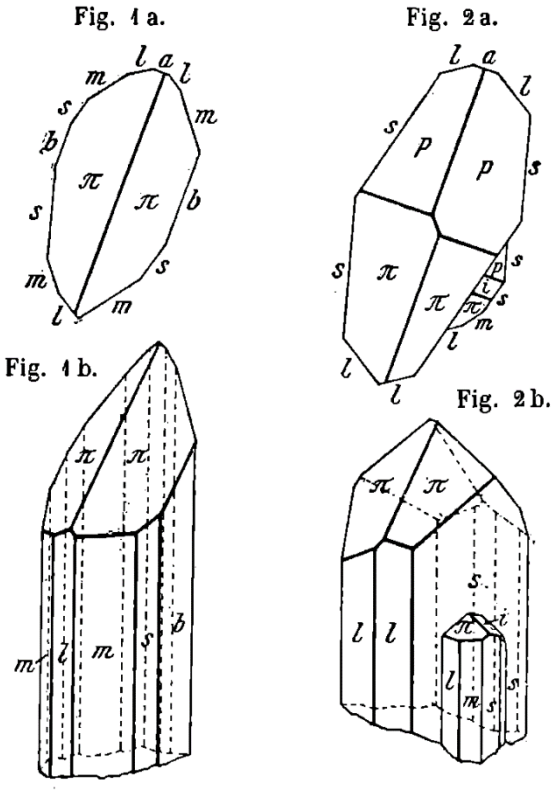

Figure 56: Representation of two crystals -a) and b)- representative of samsonite shape. The same letter means the faces are of the same crystal shape.

As samsonite has such **little and/or outdated information**, probably due to the lack of interest originating from its rarity and lack of a synthetic method to form it, many properties can be studied here. Also, as two methods have been previously proven to be efficient enough to form the wanted compound, the influence of shape and size can be additionally assessed. Thanks to the precise crystallographic parameters obtained by Bindi and Evan, it will also be possible to check if the structure is changed in any way between the synthetic and natural formation.[10]

B. Characterization and sintering techniques

The crystallographic parameters were determined through high-resolution powder X-Ray Diffraction (XRD). The data were collected at room temperature with two different devices. First, through a Bruker D8 ADVANCE diffractometer [copper anode λ = 1.54059 Å, monochromatic Ge 111, Lynx Eye detector], in reflection configuration. Data were collected from 8 up to 100° with a step size of 0.009198°, and a step time of 1.7 s. A diffraction pattern of a standard LaB_6 powder was also registered under the same conditions to obtain the instrumental broadening of the diffractometer. The peak shape was then corrected from the instrumental broadening using the aforementioned

calibration acquisition. Those data were then refined using the FullProf and WinPlotr software package. [26,27]

Regarding the structure refinement, systematic error correction (zero-point shift and asymmetry) was applied, and the background was adjusted using a polynomial function. With respect to the crystallographic structure, the lattice parameters, atomic positions, and isothermal temperature factor (B_{iso}) were also refined.

Secondly, X-ray scattering data suitable for Pair Distribution Function (PDF) analysis were collected using a Rigaku SmartLab (rotating anode Mo $\lambda = 0.71146$ Å) diffractometer. The powdered sample was loaded into a quartz capillary (0.4 mm in diameter) and measured in transmission mode using a HyPix3000 detector. Data were collected from 3 to 112° using four different speed-time, depending on the angular range (3° to 35°: 0.5 °/min; 34° to 65°: 0.2 °/min; 64° to 95°: 0.1 °/min, and 94° to 112°: 0.1 °/min). The experimental PDF was extracted using the program PDFgetX3 [88] and analyzed using the program Diffpy-CMI.[89] The total scattering structure function, S(Q), was produced in PDFgetX3 by subtracting the quartz container scattering and utilizing the appropriate sample composition. The pair distribution function pattern, G(r), was calculated via the Fourier transformation of the total scattering data utilizing a maximum $Q_{MaxInst} = 14.6431$ Å^{-1}. Values of $Q_{damp} = 0.02$ Å^{-1} and $Q_{broad} = 0.08$ Å^{-1} have been extracted from the refinement of a LaB_6 standard in Diffpy-CMI and were used for further refinement.

The study of the behavior of samsonite under varying temperatures was performed through Thermo-Gravimetric Analysis (TGA). The data was collected on a Netzsch TGA apparatus (STA 449 F3 Jupiter) over the temperature range of 200 °C with 3 °C/min. An N2 flux (100mL/min) and air (N2 80mL/min - O2 20mL/min) were used during the acquisition.

Imaging, mapping, and elemental analysis were performed using a Scanning Electron Microscope (SEM; JEOL - JCM7000) equipped with an Energy Dispersive Spectrometer (EDS). The samples were measured at an operating voltage of 15 kV. The image processing program ImageJ was then used to correctly assess the size distribution in the pictures obtained.[90–92]

The granulometry was determined with a Malvern laser diffraction particle sizer (Mastersizer 2000, Hydro200S sample disperser), and the powder was dispersed in ethylene glycol under constant ultrasonic stirring. The refractive index and absorbance were assumed to be close enough to the ternary sulfide Ag_3AsS_3 for the samsonite particles and the refractive index of ethylene glycol was used during this process. The dispersion was studied from 0.01 to 10 000 µm.

In-Situ XRD was performed through a Bruker Rigaku SmartLab diffractometer [copper anode $\lambda = 1.54059$ Å, monochromatic, HyPix3000 detector], in reflection configuration. It allows analysis under

a controlled temperature (from 12 K to 1400 K) and atmosphere (vacuum, Air, N_2, Ar_2, O_2… pressure up to 10 bars). Data were collected from 5 up to 80° with a step size of 0.001°, and a step time of 1.0 s. A diffraction pattern of a standard LaB_6 powder was also registered under the same conditions to obtain the instrumental broadening of the diffractometer. The peak shape was then corrected from the instrumental broadening using the aforementioned calibration acquisition. Those data were then refined using the FullProf and WinPlotr software package. [26,27]

Magnetic properties were assessed with the magnetometer MPMS 3 SQUID, 7T (options VSM, DC, AC). Data were collected from 2.5 to 350 K under a constant magnetic field of 100 Oe and from -50000 to 50000 Oe under a constant temperature of 5 K and 20 K.

The SPS system (FCT - Type HP D 25) reaches up to 2200 °C with a heating speed of up to 700 °C.min^{-1} and pressure between 5 and 250 kN while under a controlled atmosphere. Dimensions of components can reach up to 80mm in diameter. Molds of graphite and tungsten carbide are used depending on the pressure applied. Details of the cycles used are detailed more in *IV.C.4*.

C. Results and discussion

IV.C.1. X-Ray Diffraction and Pair Distribution Function

The synthesized powder from the polyol and hydrothermal process has been thoroughly characterized through X-Ray patterns in two different methods: The first one is the same used previously for the characterization of the powders formed, but more accurate and shown in Figure 57 and 58 respectively. In this section, a more thorough overview of the results obtained through the Rietveld refinement will be given. The other method used is the **pair distribution function (PDF)**. This technique allows ignoring some parameters that can influence the information obtained, such as the morphology of the powder studied, and the characteristics of the instrument used. It involves the use of a high-energy X-Ray at a short wavelength and a wide angular range. The data obtained must be then treated with a Fourier Transformation that leads to a G(r) function defined by the following equation:

$$G(r) = \frac{2}{\pi}\int_0^{\infty} F(Q)\sin(Qr)dQ = \frac{2}{\pi}\int_{Q_{min}}^{Q_{max}} [Q(S(Q)-1)]\sin(Qr)dQ$$

With Q the magnitude of the scattering momentum (Å^{-1}) (calculated with $Q = \frac{4\,\pi \sin(\theta)}{\lambda}$ with θ the scattering angle (°) and λ the wavelength (Å)), F the Fourier function, S the structure function, and r the distance between atoms (Å).

From both methods, there is a summary of the general results obtained and compared to those previously found in literature before going into more detail for both of them:

Table 12: *General crystal data of the synthetic samsonite phase via polyol process compared to litterature[10].*

Chemical Formula	$Ag_4MnSb_2S_6$		
Molecular weight (g/mol)	922.28		
Space Group	P 1 $2_{1/n}$ 1		
Refinement	Rietveld (D8 ADVANCE)	PDF (Rigaku Smartlab)	Gram-Charlier Development (Bruker-Nonius KappaCCD)
Radiation	Cu 1.54059 Å	Mo 0.71146 Å	Mo 0.71073 Å
Cell Parameters			
a (Å)	10.3737(9)	10.4(8)	10.3702(8)
b (Å)	8.1047(3)	8.0(4)	8.0647(7)
c (Å)	6.6569(4)	6.5(9)	6.6400(7)
α (°)	90	90	90
β (°)	92.6269(8)	92.91(9)	92.676(12)
V (Å³)	559.10(6)	555.3(0)	554.71(9)
Calculated density (g/cm³)	5.478	5.5191	5.5199

Table 13: *General crystal data of the synthetic samsonite phase via hydrothermal process compared to litterature[10].*

Chemical Formula	$Ag_4MnSb_2S_6$		
Molecular weight (g/mol)	922.28		
Space Group	P 1 $2_{1/n}$ 1		
Refinement	Rietveld (D8 ADVANCE)	PDF (Rigaku Smartlab)	Gram-Charlier Development (Bruker-Nonius KappaCCD)
Radiation	Cu 1.54059 Å	Mo 0.71146 Å	Mo 0.71073 Å
Cell Parameters			
a (Å)	10.374(2)	10.4(2)	10.3702(8)
b (Å)	8.105(4)	8.1(5)	8.0647(7)
c (Å)	6.657(3)	6.6(2)	6.6400(7)
α (°)	90	90	90
β (°)	92.62(0)	92.6(7)	92.676(12)
V (Å³)	560.71(2)	562.4(3)	554.71(9)
Calculated density (g/cm³)	5.477	5.446	5.5199

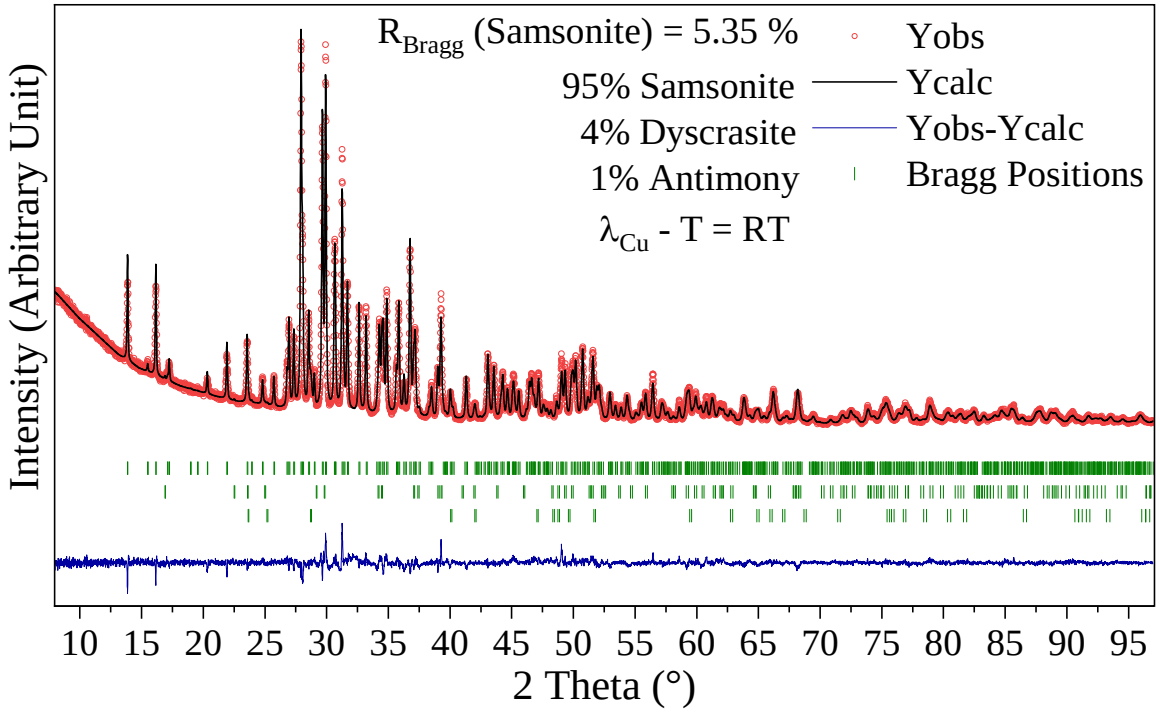

Figure 57: *Full Room Temperature XRD pattern of powder obtained polyol synthesis and its refinement, done through the Rietveld Model.*

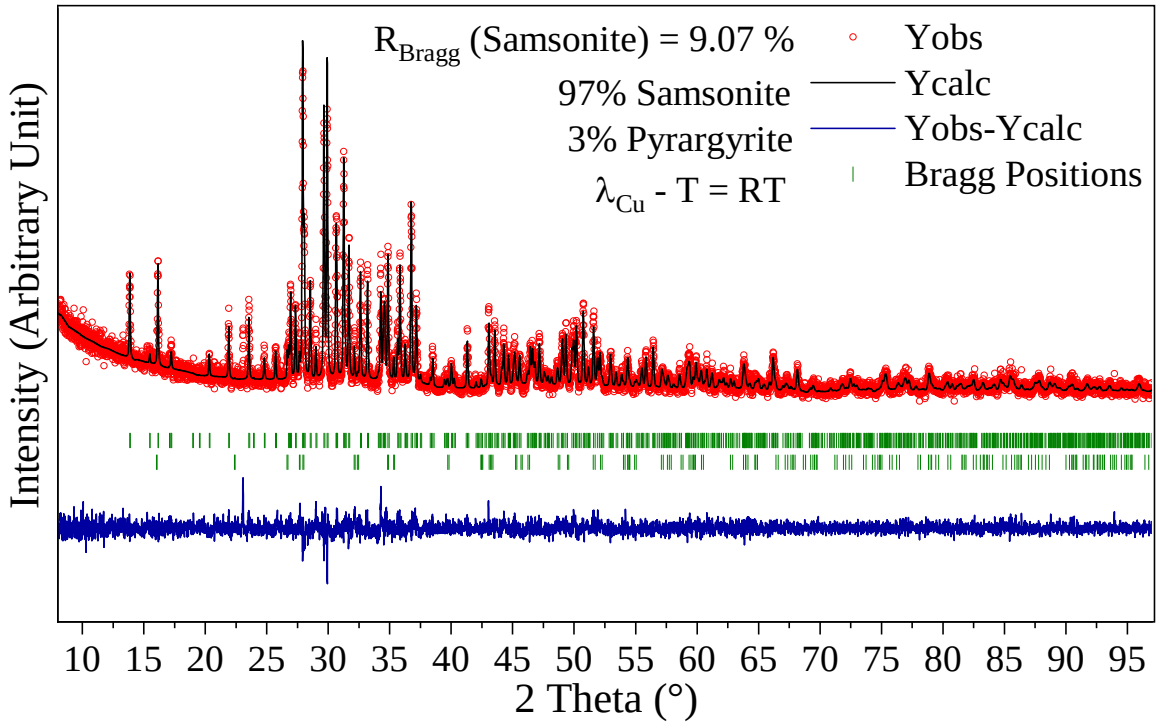

Figure 58: *Full Room Temperature XRD pattern of powder obtained hydrothermal synthesis and its refinement, done through the Rietveld Model.*

Atomic positions and isotropic displacement parameters, obtained from the refinement of the D8 ADVANCE pattern, are reported in Tables 14 and 15. It should be noted that, due to only negative B_{iso} values being estimated during refinement of atom S2 in both powders, they were specifically removed.

Table 14: *Atomic coordinates processes, isotropic displacement parameters (B_{iso}) and occupation of samsonite phase synthesized through polyol process obtained from D8 diffractometer.*

Atoms	*x*	*y*	*z*	B_{Iso} (Å²)	*Occ.*
Ag1	0.3070(0)	0.2466(4)	0.5719(2)	2.85(4)	1.000
Ag2	0.4942(6)	0.9696(0)	0.7627(0)	4.29(2)	1.000
Mn	0.00000	0.00000	0.50000	0.55(6)	0.500
Sb	0.1834(9)	0.1646(3)	0.0384(6)	0.63(1)	1.000
S1	0.0936(7)	0.2701(4)	0.3487(4)	0.61(2)	1.000
S2	0.5186(0)	0.6733(3)	0.6694(3)	N/A	1.000
S3	0.2633(6)	0.4229(6)	-0.1090(5)	0.33(5)	1.000

Table 15: *Atomic coordinates processes, isotropic displacement parameters (B_{iso}) and occupation of samsonite phase synthesized through hydrothermal process obtained from D8 diffractometer.*

Atoms	*x*	*y*	*z*	B_{Iso} (Å²)	*Occ.*
Ag1	0.30873(4)	0.24684(5)	0.57290(6)	3.343(1)	1.000
Ag2	0.49370(4)	0.96882(6)	0.76194(7)	4.227(1)	1.000
Mn	0.000000	0.000000	0.500000	2.188(3)	0.500
Sb	0.18266(3)	0.16471(4)	0.03922(5)	0.898(0)	1.000
S1	0.09342(1)	0.26805(1)	0.34696(1)	0.614(3)	1.000
S2	0.51356(1)	0.67553(1)	0.66696(1)	N/A	1.000
S3	0.26209(1)	0.42725(1)	-0.10456(1)	1.100(3)	1.000

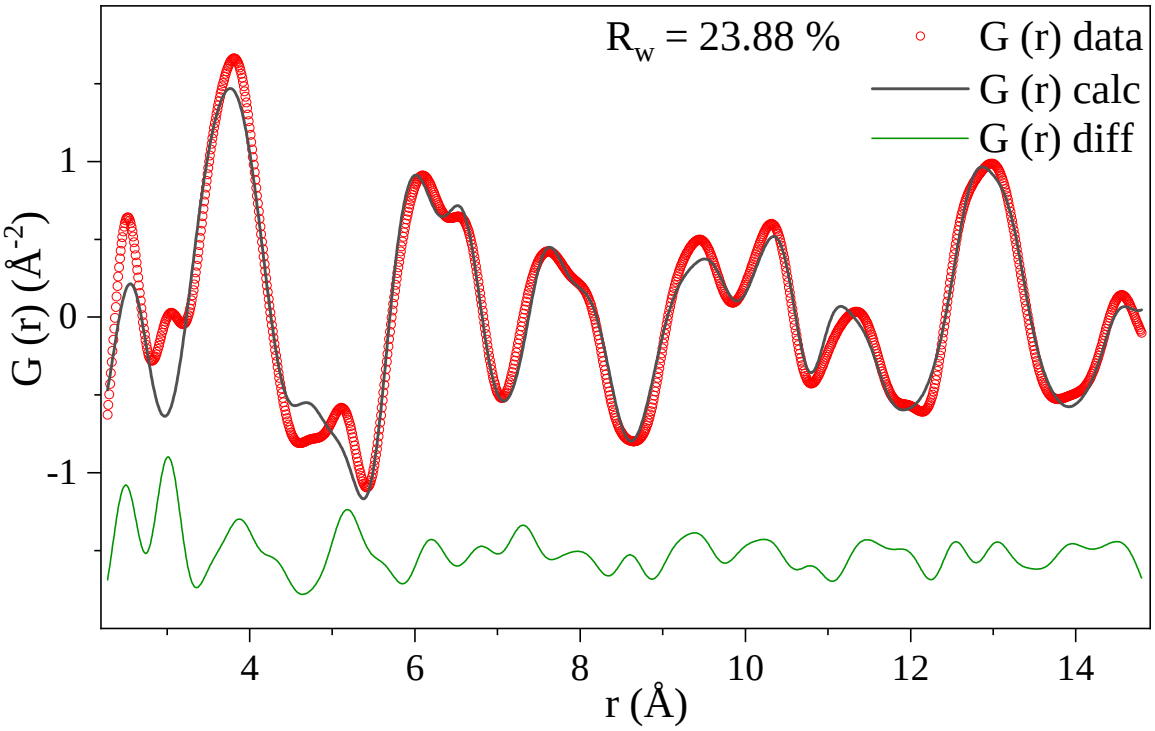

Figure 59: *Diagram of samsonite phase synthesized through polyol process obtained through the Pair Function Distribution*

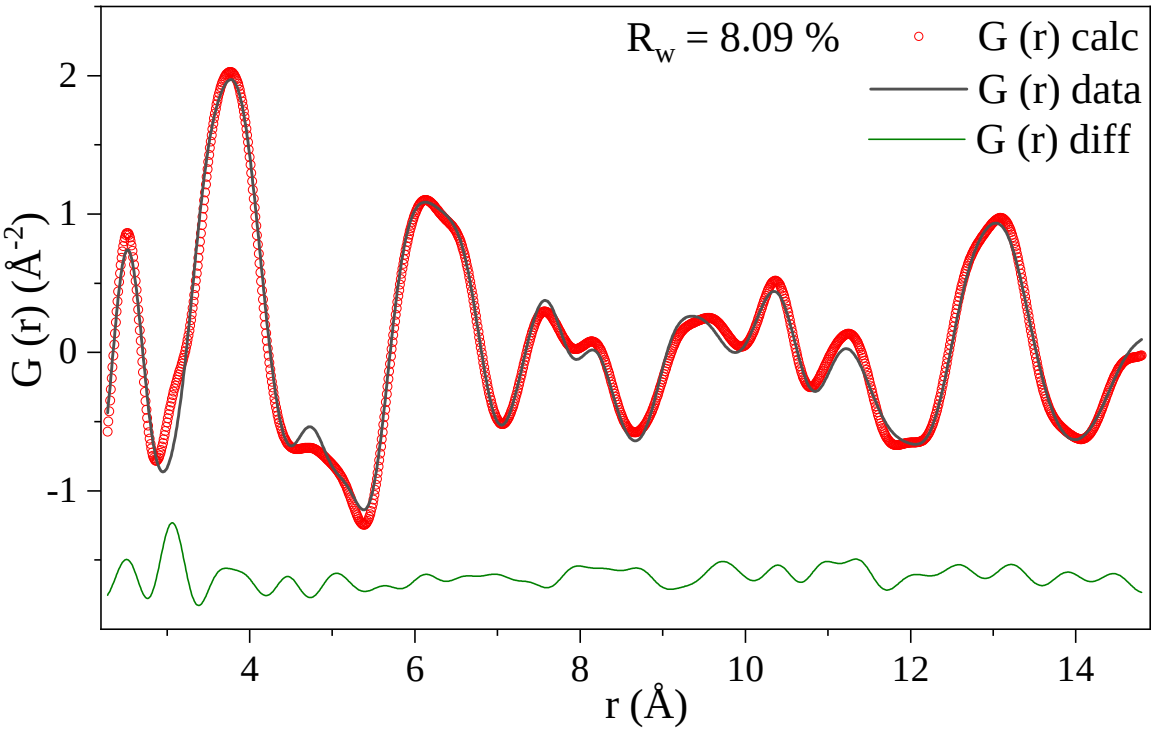

Figure 60: *Diagram of samsonite phase synthesized through hydrothermal process obtained through the Pair Function Distribution*

Atomic positions and isotropic displacement parameters, obtained from the refinement of the PDF pattern, are reported in Table 16.

Table 16: *Atomic coordinates of samsonite phase synthesized through both processes and isotropic displacement parameters (B_{iso}) according to the synthesis process used obtained from the Rigaku Smartlab diffractometer*

Atoms	*x*	*y*	*z*	B_{Iso} *(Å²)(polyol)*	B_{Iso} *(Å²)(hydrothermal)*
Ag1	0.3068(0)	0.2459(9)	0.5714(4)	1.(8)	(2)
Ag2	0.4946(1)	0.9692(3)	0.7622(9)	5.000(0)	(3)
Mn	0.000000	0.000000	0.500000	0.(3)	(0)
Sb	0.1833(9)	0.1647(4)	0.0387(2)	1.(2)	1.(4)
S1	0.0936(8)	0.2716(1)	0.3490(4)	(4)	(1)
S2	0.5186(5)	0.6745(9)	0.6690(0)	0.(1)	(0)
S3	0.2626(2)	0.4220(4)	-0.1094(0)	(1)	5.000(2)

Results seem coherent from method to method, regardless of the characterization processes used, though data obtained from the PDF refinement seems to be rather lacking in precision. A study with instruments of a higher $Q_{MaxInst}$ would allow for a more precise refinement.

IV.C.2. Decomposition study (ATG-DSC and in-situ XRD)

As the previously mentioned decomposition study leave quite a bit to be desired, an ATG-DSC was performed on the synthesized samsonite phase. Tests were made both under air and then nitrogen. Unfortunately, **the reaction under air provoked a reaction with the platinum crucible**. The behavior under nitrogen was different. The crucible had no unwanted reaction but, while the XRD pattern obtained from the powder following the heating showed the decomposition of the samsonite phase into the formation of a pyrargyrite phase, the ATG-DSC (Figure 61) shows intriguing data. **Neither the mass nor the energy has any significant variation** showing at what moment the decomposition starts.

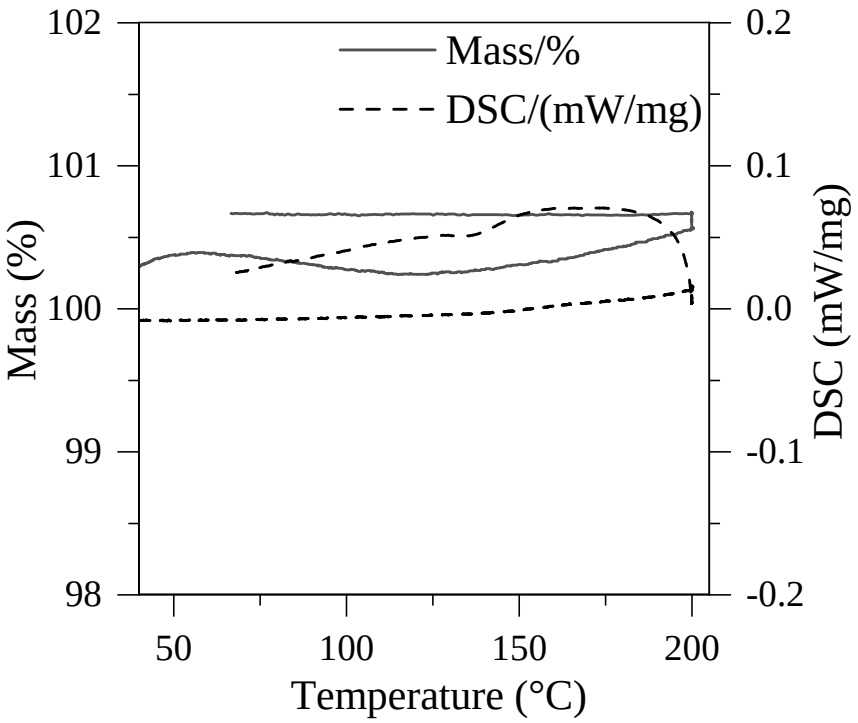

Figure 61: *DSC–TGA curves of samsonite in Nitrogen. Heating rate = 3 °C.min^{-1}.*

Consequently, it was decided to do an in-situ XRD during a heating cycle. The first attempt was another surprising result as absolutely nothing happened. The heating rate was made higher (to match the rate used during the ATG) and the temperature range observed was made wider to witness the formation of the pyrargyrite phase. This resulted in the XRD patterns shown in Figure 60. Peaks related to the **pyrargyrite phase start to appear at 175 °C**. It can consequently be assumed that this is approximately the temperature of decomposition. The ratio continues to shift in the favor of pyrargyrite during the rest of the process, even if this is not long enough for it to become most of the powder.

Rietveld refinement allows us to properly assess many aspects of this in-situ XRD: The ratio of phases but also the evolution of the crystal parameters of the samsonite phase during the heating. All of the information was collected in Tables 17 and 18 and Figure 62.

Table 17: *Evolution of the proportion of the samsonite and pyrargyrite phase according to temperature. PT is an abbreviation of "Post Treatment"*

Temperature (°C)	*150*	*175*	*200*	*225*	*250*	*30 (PT)*
Samsonite (%)	97	95.4	92.8	91.9	90.7	88.3
Pyrargyrite (%)	0	1.8	4.6	5.7	7.3	9.85

Table 18: *Evolution of the samsonite phase's cell parameters according to temperature.*

Temperature (°C)	*a (Å)*	*b (Å)*	*c (Å)*	*β (°)*	*Volume (Å^{-3})*
30	10.380(61)	8.111(58)	6.662(24)	92.60(944)	560.3(99)
65	10.3792(24)	8.120(00)	6.665(54)	92.60(313)	561.1(87)
100	10.376(77)	8.128(27)	6.668(60)	92.59(442)	561.8(88)
130	10.383(17)	8.141(51)	6.676(31)	92.59(176)	563.7(96)
150	10.383(40)	8.146(94)	6.678(79)	92.59(216)	564.4(00)
175	10.384(47)	8.155(13)	6.683(03)	92.58(733)	565.3(87)
200	10.383(79)	8.161(97)	6.686(41)	92.58(840)	566.1(09)
225	10.381(68)	8.168(92)	6.689(70)	92.58(550)	566.7(56)
250	10.378(68)	8.175(21)	6.692(78)	92.57(996)	567.2(93)
30 (Post-treatment)	10.381(33)	8.114(97)	6.664(74)	92.61(549)	560.8(80)

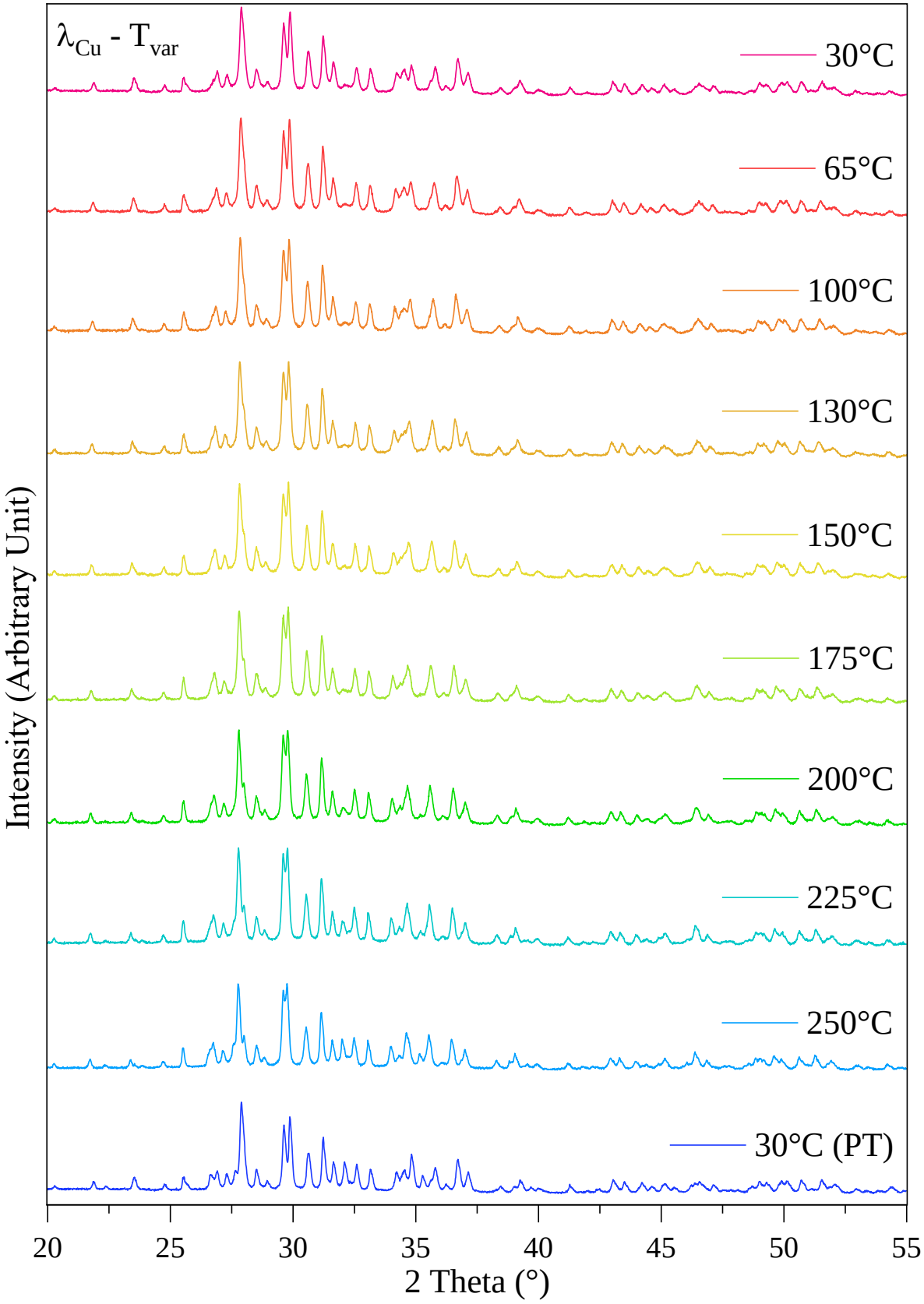

Figure 62: *In-Situ XRD patterns of Polyol synthesized samsonite powder according to temperature.*

Interesting information can be extracted from the data: First, regarding the decomposition of samsonite, it seems like the phase appears **between 150 and 175 °C** and continually increases while above those temperatures. However, if you look back at Figure 59 (and the zoomed-in section in Figure 63), absolutely no variation of energy or mass can be particularly noticed in that temperature range.

This information poses an additional question: If the samsonite phase is unstable above 150 °C and all synthesis processes tested through this study are only efficient at 180 °C, is a pure synthesis ever possible? Ag_3SbS_3 is already present in hydrothermal synthesis and, despite a seemingly promising appearance of the dyscrasite phase (Ag_3Sb), it is in the end, only part of the Ag-Sb-S system that pyrargyrite is already a part of.

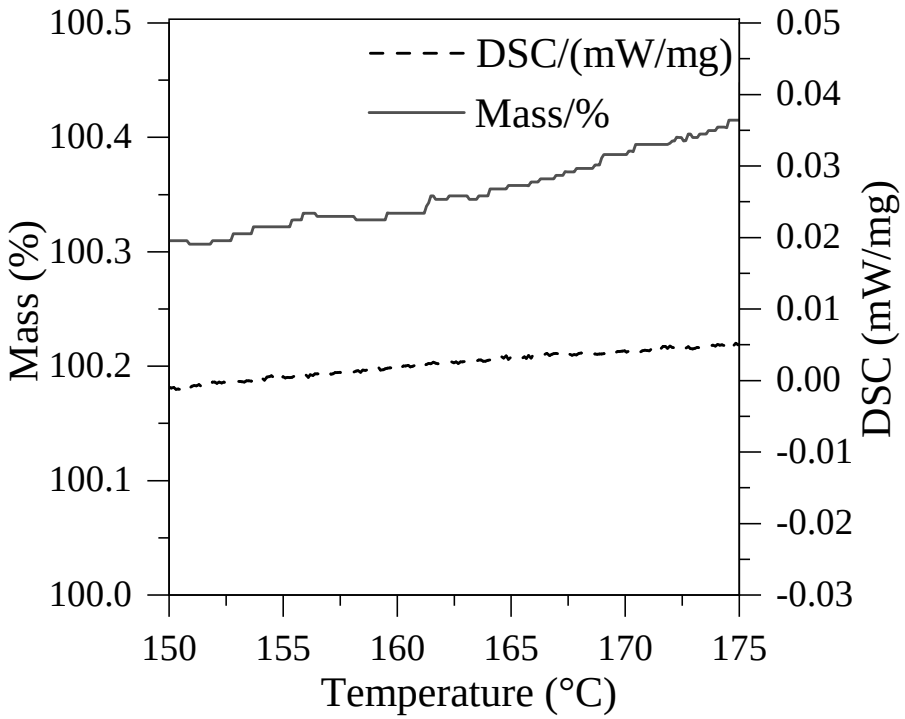

Figure 63: *DSC–TGA curves of samsonite in Nitrogen from Figure 52, zoomed in on the 150-175 °C domain. Heating rate = 3 °C.min^{-1}.*

Justifying precisely what is going on is rather complicated. What could be assumed from such results is that bonds are being broken and created with equal amounts of energy.

As such, a deeper look into the possibilities of the assumed decomposition reaction should be done. Two reactions could be considered with a simple view of things:

$$Ag_4MnSb_2S_6 \rightarrow Ag_3SbS_3 + MnS + AgSbS_2$$

or

$$Ag_4MnSb_2S_6 \rightarrow 2\,Ag_2S + MnS + Sb_2S_3$$

The issue however is, if either (or both) reactions would be happening, there would be only a release of energy (and in the case of the second reaction, we would be seeing binary compounds appearing, which is not the case). There is also the fact that no binary compound is seemingly appearing during the decomposition process. With that info, another option could be offered:

$$Ag_4MnSb_2S_6 \rightarrow 2\,Ag_2S + MnS + Sb_2S_3$$

and

$$3\,Ag_2S + Sb_2S_3 \rightarrow 2\,Ag_3SbS_3$$

This configuration might resolve a few issues. Because from a brief look at the structure, there is no "easy" way to just extract MnS_6 sites and let ternary compounds present. However, if we take into consideration that samsonite seemingly decomposes in the temperature range where pyrargyrite is known to easily be formed then the combination of these two reactions happening simultaneously is a possibility. Samsonite decomposes into binary compounds, releasing energy and, simultaneously, silver sulfide and antimony sulfide are reacting with each other, consuming energy to create these bonds.

With the Ag-Sb-S system and binary sulfides being thoroughly studied in the literature, a theoretical calculation of the reaction at the assumed temperature can be done: [93,94]

$$\Delta_fH_{295}(Ag_2S) = \text{-}31\ \text{kJ.mol}^{\text{-}1}\ \Delta_fH_{295}\ (Sb_2S_3) = \text{-}141.8\ \&\ \Delta_fH_{295}(Ag_3SbS_3) = \text{-}202.2$$

$$\Delta_rH(Ag_3SbS_3) = \Delta_fH(Ag_3SbS_3) - \frac{1}{2}\left(3\,\Delta_fH(Ag_2S) + \Delta_fH(Sb_2S_3)\right)$$

$$\Delta_rH_{295}(Ag_3SbS_3) = -84.8\ \text{kJ.mol}^{-1}$$

$$S°_{295}(Ag_2S) = 144\ \text{J.mol}^{\text{-}1}\text{.K}^{\text{-}1}\ S°_{295}(Sb_2S_3) = \text{-}4.4\ \text{J.mol}^{\text{-}1}\text{.K}^{\text{-}1}\ \&\ S°_{295}(Ag_3SbS_3) = 301.9\ \text{J.mol}^{\text{-}1}\text{.K}^{\text{-}1}$$

$$\Delta_rS(Ag_3SbS_3) = S°(Ag_3SbS_3) - \frac{1}{2}\left(3\,S°(Ag_2S) + S°(Sb_2S_3)\right)$$

$$\Delta_rS_{295}(Ag_3SbS_3) = 519.2\ \text{J.mol}^{-1}$$

While assuming that Δ_rH and S° are constant under varying temperatures the following estimate of the free Gibbs energy can be found:

$$\Delta_rG_T(Ag_3SbS_3) = \Delta_rH_{295}(Ag_3SbS_3) - T\Delta_rS_{295}(Ag_3SbS_3)$$

$$\Delta_rG_{433K}(Ag_3SbS_3) = -226\ \text{kJ.mol}^{-1}$$

This shows that the reaction should be possible under these conditions. However, this would imply that the exact energy taken (~ -84.8 kJ.mol^{-1}) is also somehow exactly the energy released when the samsonite phase is decomposing.

Another way to check the possibility of this reaction is to study the evolution of silver disulfide and antimony trisulfide during a DSC-TGA cycle. If a formation of the ternary compound happens, from it could be deduced the energy of the reaction, the enthalpy of formation of Ag_3SbS_3, and potentially the enthalpy of formation of $Ag_4MnSb_2S_6$.

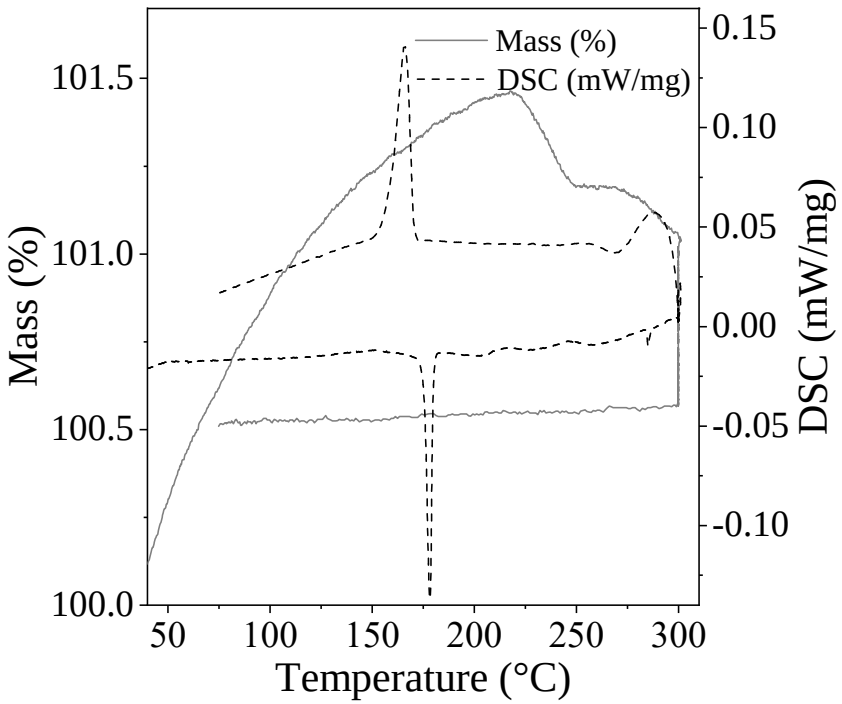

Figure 64: *DSC–TGA curves of silver sulfide and antimony sulfide mix up to 300 °C. Heating rate = 3 °C.min^{-1}.*

Such a study has been set up and the results obtained in Figure 61 shows clear variations of energy during the process. The peaks witnessed around 180 °C are the structural transitions of Ag_2S. Another additional peak can be noticed at around 280 °C.

The results are somewhat coherent with those obtained in literature, as shown in Figure 63, with variations possibly dependent on the formation of pyrargyrite and the formation and destruction of pyrostilpnite (an allotropic form of Ag_3SbS_3) and myrargyrite ($AgSbS_2$):

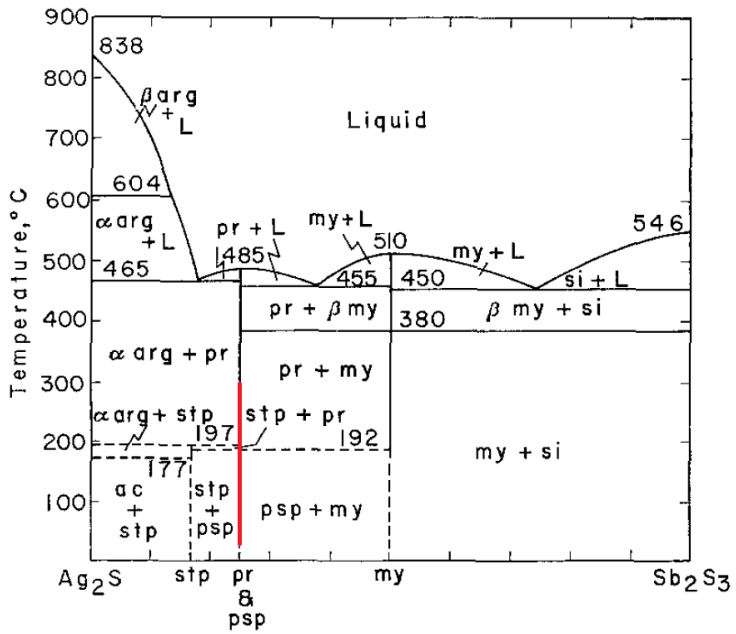

Figure 65: *The pseudobinary system Ag_2S-Sb_2S_3. All assemblages are in equilibrium with vapor. Phase relations involving the stephanite phase (Ag_5SbS_4) and pyrostilpnite (Ag_3SbS_3) are inferred from the behavior of minerals.* [95] *All compositions are in atomic percent. The red line represents the domain studied through DSC-TGA.*

Additionally, XRD patterns obtained after the process allow us to see that some precursors were still present, justifying the presence of an Ag_2S form change peak during the cool-down. However, from up to 175 °C, nothing is still noticeable as a significant reaction that could be attributed to the odd "no energy released" seen on the DSC of the samsonite phase.

Consequently, with the current information available, it is impossible to correctly assess the mechanisms involved in the decomposition of the samsonite phase.

IV.C.3. Magnetic properties

The magnetic properties of the samsonite powder synthesized through the polyol process have been carried out. The magnetic moment was thus determined according to temperature for a fixed magnetic field of 100 Oe and according to the magnetic field for a fixed temperature of 5 K.

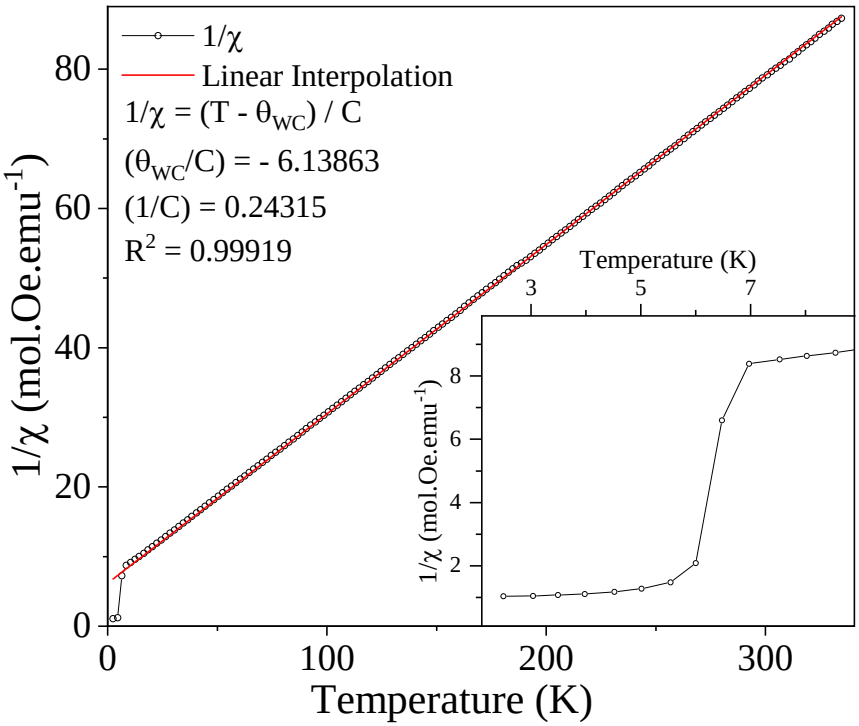

Figure 66: *Magnetic susceptibility of the samsonite phase according to temperature with a constant field of 100 Oe.*

From the evolution of the properties assessed in Figure 66, it could be assumed that the compound is a **paramagnetic phase** with a transition at approximately 7 K. Consequently, it can be assumed that the powder follows the according equation:

$$\chi = \frac{C}{T - \theta_{WC}}$$

with C being the Curie constant (in $m^3.mol^{-1}.K$), T the temperature (in K), and θ_{WC} the Weiss-Curie Temperature (in K).

The θ_{WC} could be determined as -25.24 K, proving the **antiferromagnetic fluctuations**. Additionally, through the Curie constant, the magnetic moment of the compound could also be found according to the following equation:

$$\mu_{eff} = \sqrt{\frac{8C}{N}}\,\mu_B$$

With N being the number of magnetic atoms in the unit cell and C being the Curie constant. The curie constant has previously been determined as C = 4.1126 $m^3.mol^{-1}.K$ and N = 1 as only the manganese atoms in the structure can be considered magnetic. This leads to a magnetic moment of 5.68 μ_B. The theoretical value of the magnetic moment of Mn^{2+} is 5.92 μ_B which **confirms the oxidation state of the manganese atoms** in the structure of the samsonite phase.

Additionally, the study of the magnetic moment according to the magnetic field gives additional information about the magnetic properties. As can be noticed in Figure 67, the magnetic moment is globally **proportional** to the magnetic field and **no saturation** could be reached as, at 5 Tesla, the magnetic moment is only slightly above 1 $\mu_B.Mn^{-1}$, meaning a quite heavy magnetic field would be necessary to witness it at 5 $\mu_B.Mn^{-1}$. A slight hysteresis is seemingly appearing between -10 000 to 10 000 Oe.

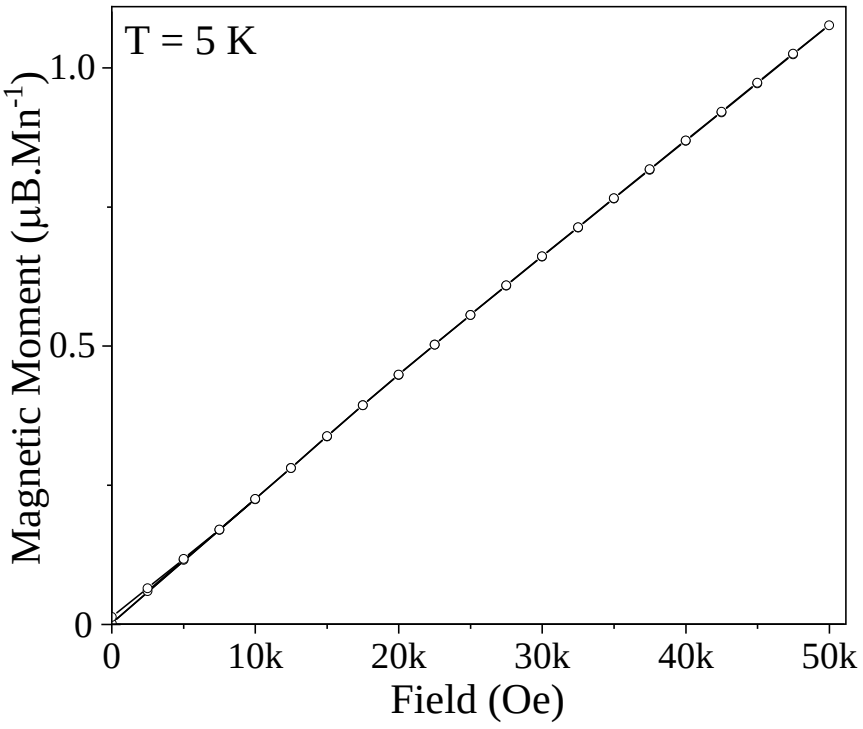

Figure 67: *Magnetic moment of the samsonite phase according to the magnetic field from 0 Oe to 50 000 Oe with a constant temperature of 5 K.*

A closer study of it allows for a confirmation of its presence and a more precise study so said hysteresis, as shown in Figure 68.

From it, the coercivity field of the compound can be determined to be approximately 600 Oe, and its remnant magnetization of $1.25 \cdot 10^{-2}$ $\mu_B.Mn^{-1}$.

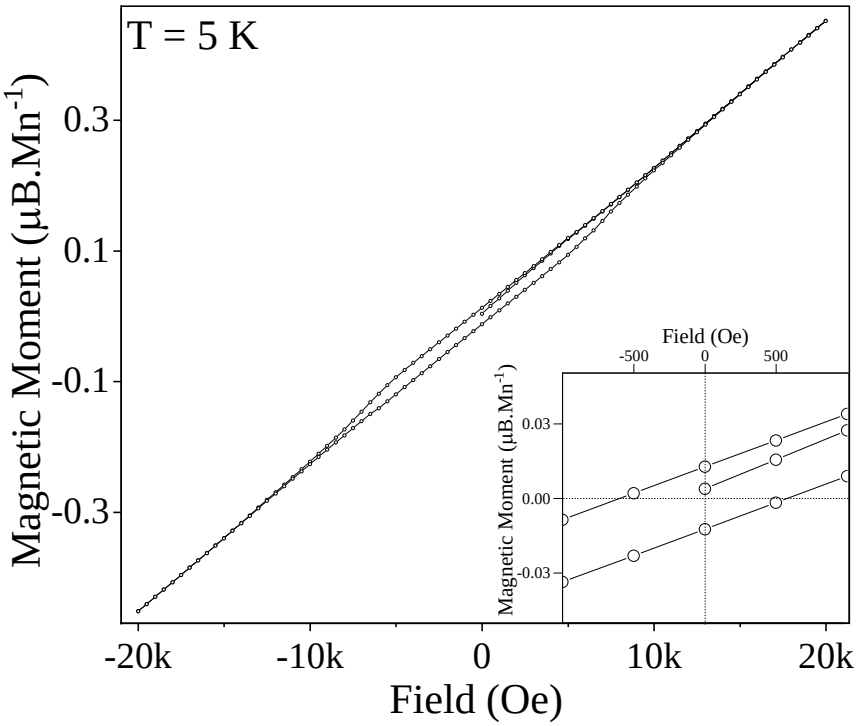

Figure 68: *Magnetic moment of the samsonite phase according to the magnetic field from -20 000 Oe to 20 000 Oe with a constant temperature of 5 K.*

Paramagnetic behavior was also confirmed for temperatures above 8 K, as shown in Figure 69, no hysteresis could be observed.

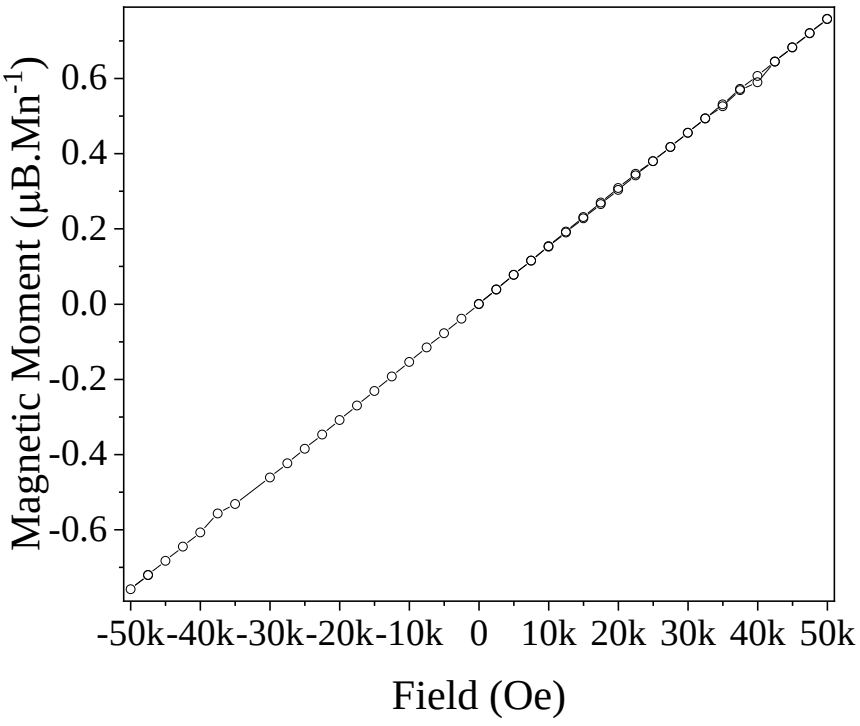

Figure 69: *Magnetic moment of the samsonite phase according to the magnetic field from -50 000 Oe to 50 000 Oe with a constant temperature of 20 K.*

IV.C.1. Grain morphologies

As two viable synthesis methods have been found to form the samsonite phase, besides the purity that has been thoroughly discussed in the previous sections, a comparison of the morphology of the powders synthesized to better understand any additional differences might be noted between both methods.

Two techniques have consequently been used to correctly assess these characteristics: Granulometry and Scanning Electron Microscopy.

While granulometry was not completely adequate to obtain the precise results for the size distribution of both powders obtained through the hydrothermal and polyol methods, a general notion of the grains of polyol synthesis being mostly below the ones of hydrothermal synthesis.

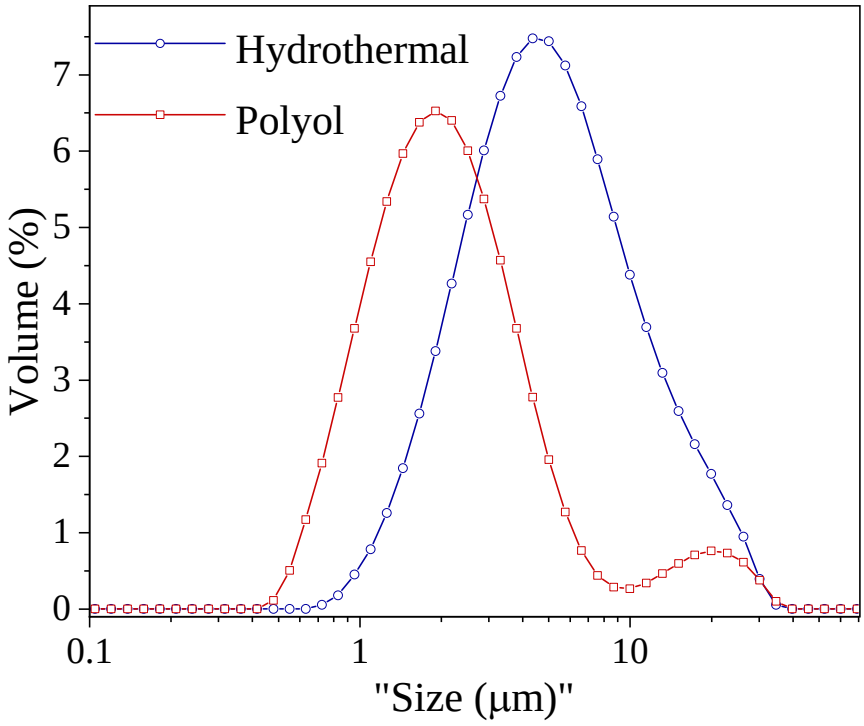

Figure 70: Distribution of size according to the volume of the powder present in the solvent.

The SEM pictures alone that are gathered in Figure 71, show evidence that the granulometry is rather lacking in precision. What could be assumed is that the results are not of the grains themselves but rather from clusters that may have formed.

Globally, both methods lead to compounds around the **sub-micrometer scale**, with a 790 nm average and a 745 nm median for the powder obtained through polyol synthesis while an average of 893 nm and a 772 nm median for the powder obtained through the hydrothermal process could be found. However, what is noticeable at a first glance, is the shape of the grains. While polyol synthesis

produces **scale-shaped particles,** grains produced through hydrothermal synthesis seem mostly **cylindrically shaped,** while other shapes seem to also be present.

From these data, it can be gathered that to have a more homogeneous compound in this regard specifically, the better solution will be to use the polyol process.

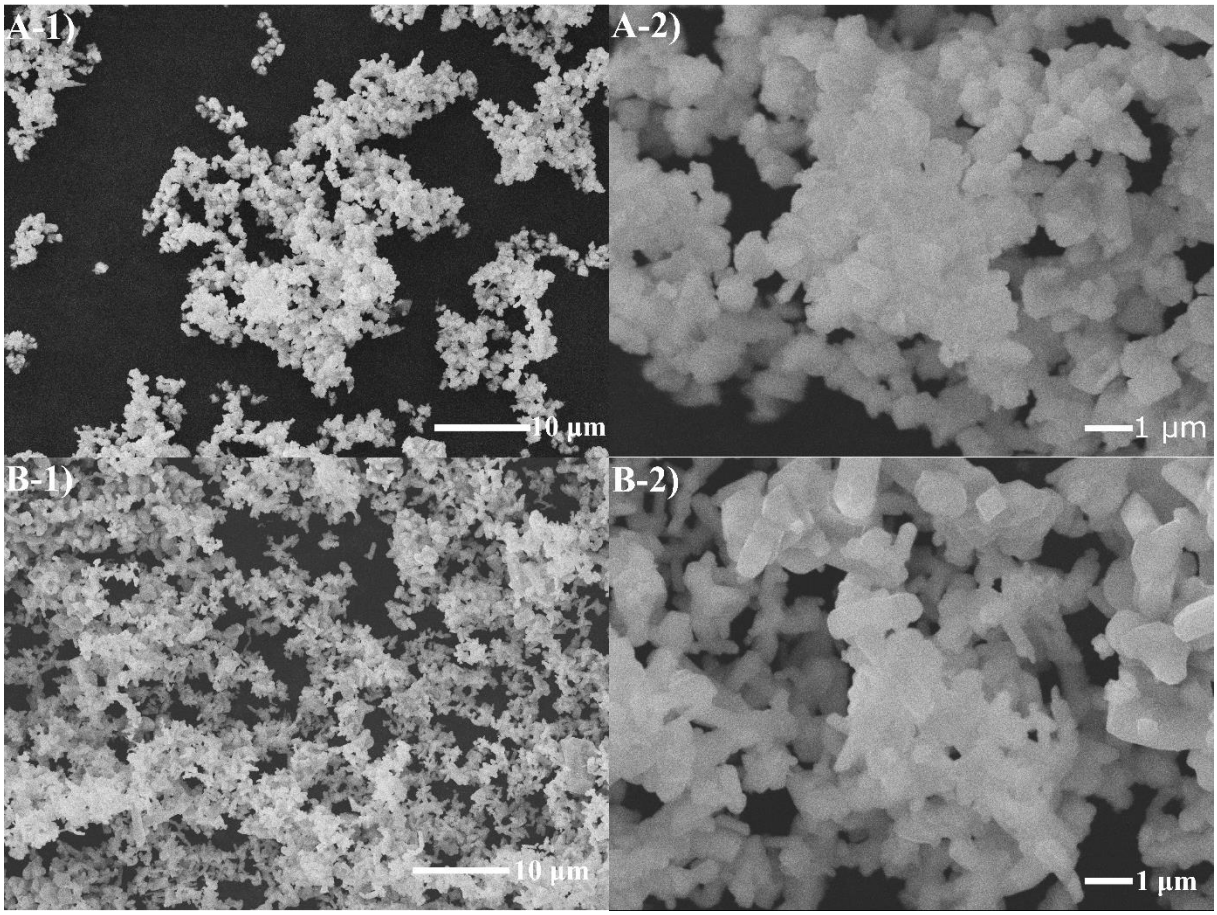

Figure 71: *SEM images of powders obtained from A) Polyol Synthesis and B) Hydrothermal Synthesis. Pictures were both taken at a 1) x2 000 and 2) x10 000 magnification.*

Comparing the mapping of both methods in Figure 72, it can also be noticed that element-wise, **the polyol process is also really homogeneous** in that regard. The points of apparent excesses of manganese in the case of hydrothermal synthesis could be traces of manganese sulfide, which would be difficult to notice through XRD patterns, as peaks of samsonite and pyrargyrite tend to be in strongly similar positions to the binary compound.

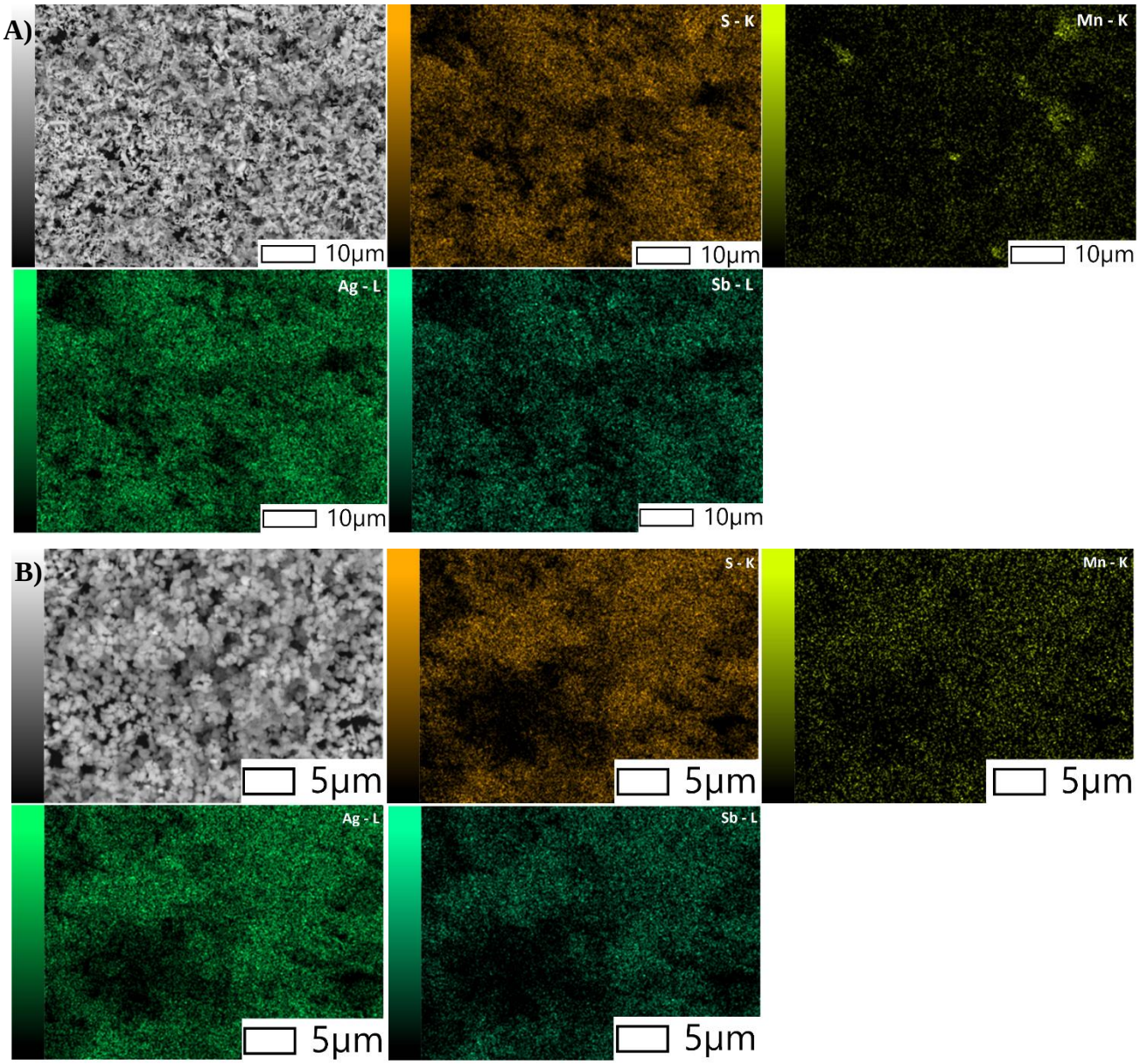

Figure 72: SEM images with EDS-Elemental mapping of Ag, Mn, Sb, and S for A) Hydrothermal and B) Polyol Synthesis.

IV.C.2. Sintering

For further characterization of the synthetic samsonite compounds, multiple attempts at sintering were made to assess the transport properties, solid-state sintering, Spark Plasma Sintering (SPS), High-Pressure SPS, and isostatic pressing.

At first, following the results obtained in *IV.C.2*, the compound was pelleted, sealed under a vacuum in a silica tube, and heated up at 160 °C for a month as a setup for solid-state sintering. Unfortunately, the pellet did not densify and seemingly had partially decomposed into pyrargyrite according to the XRD patterns obtained from it.

As such, it seemed like the low temperature alone is not enough to force joints between grains to form which might increase the whole density of the pellet.

The following attempts were through **Spark Plasma Sintering** has been on various heat and pressure cycles. The first one used the following:

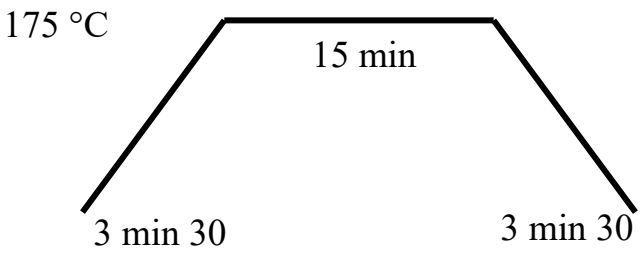

Figure 73: The heating cycle of the Spark Plasma Sintering process with a constant 5kN Force.

Unfortunately, this time the 175 °C was too high in this situation as the compound seemed to have heavily degraded into Ag_3SbS_3 and the pellet was not densified (~70 %).

Another attempt was performed, this time, with information obtained from decompositions, the temperature was thus lowered and a bigger focus was put on the pressure applied to the powder.

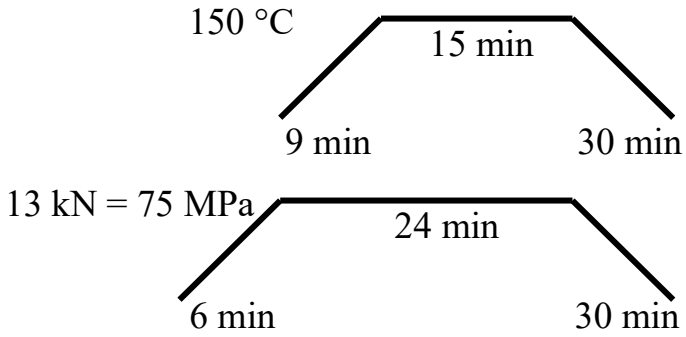

Figure 74: Heating and pressure cycle of the Spark Plasma Sintering process.

The compound was not efficiently densified (~ 70%) but the phases were at least maintained stable according to what could be found through XRD patterns, as shown in Figure 75. The modification of peak intensities may be due to slight shifts in occupations or atomic positions.

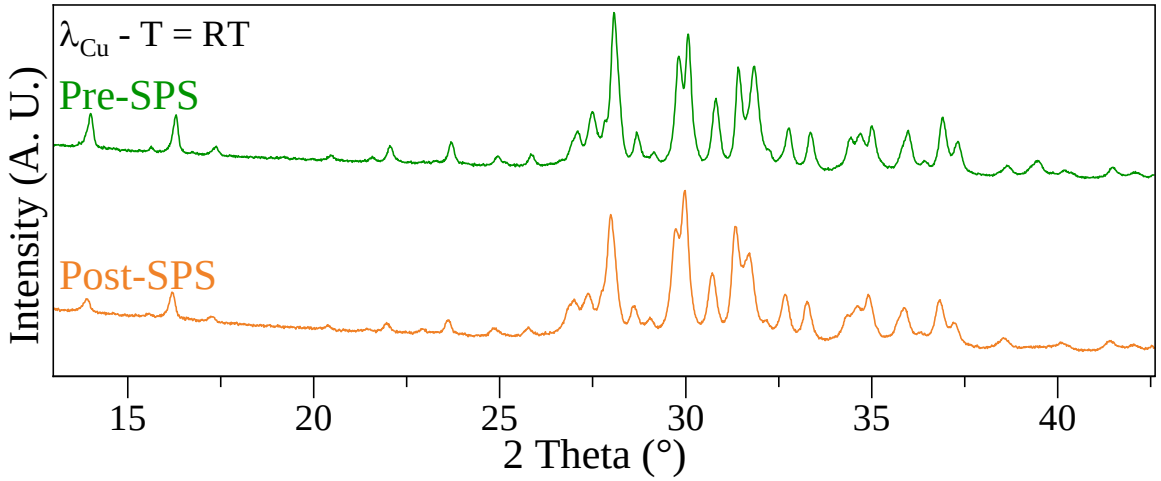

Figure 75: Room Temperature XRD patterns of samsonite synthesized through polyol synthesis before and after SPS treatment following Figure 74's heat and pressure cycle.

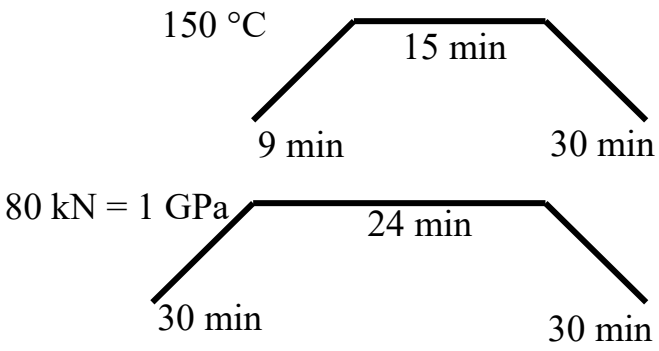

Figure 76: Heating and pressure cycle of the Spark Plasma Sintering process.

Results are similar to the previous one, with a much higher density (~90 %) however, as soon as the pellet formed was taken out of the mold, it progressively started to break down into multiple uneven layers.

As the pellets breaking down may be due to a too rapid lowering of pressure during the last segment, a new attempt was made, but this time with a much longer time to ease the last segment:

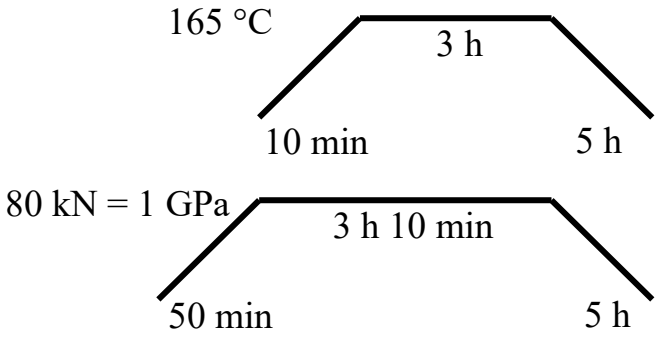

Figure 77: Heating and pressure cycle of the Spark Plasma Sintering process.

Unfortunately, the same effect was the same as seen previously with the pellet progressively breaking after the process. As such, SPS did not seem to be an efficient method for sintering the samsonite phase.

An obvious issue with this compound is that, due to its low temperature of decomposition, both processes do not seem to be efficient enough to allow for proper sintering. What pressure does in these conditions, at best, is just rearranging the grains to make layers, but nothing binds them together so they escape this configuration as soon as they can.

Consequently, the last attempt has been made, as pressure seems to at least have some sort of effect on the density of the powder, through **isostatic pressing**.

A bar of pelleted samsonite was put under an isostatic press with a pressure of 9 tons (maximum available at the CRISMAT laboratory) applied to it. A **density of 80%** was achieved through this method and, according to XRD, the compound does **not appear to have decomposed** in any way, as XRD patterns in Figure 78 show.

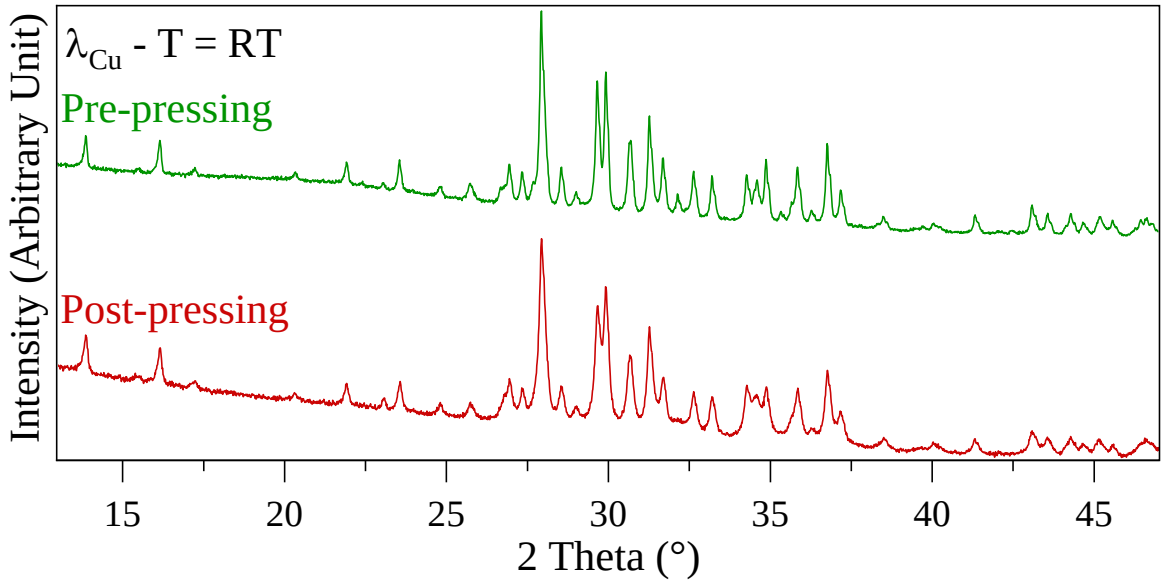

Figure 78: Room Temperature XRD patterns of the samsonite powder before and after sintering through isostatic pressing.

In the end, the isostatic press has appeared to be, so far, the **most efficient sintering method** to handle the samsonite phase. The focus for optimal sintering would need to focus on an application of powerful pressure to force the rearrangement of samsonite grains, as the rise in temperature does not seem consistently reliable.

IV.C.3. Thermoelectric properties

As mentioned previously during the introduction, the thermoelectric properties can be determined through the figure of merit ZT, defined as such:

$$ZT = \frac{\sigma S^2 T}{\kappa}$$

Where T is the temperature (in Kelvin (K)), S is the Seebeck coefficient (in Volt per Kelvin ($V.K^{-1}$)) representing the voltage generated by the difference in temperature, σ is the electrical conductivity (in Siemens per Meter ($S.m^{-1}$)) and κ is the thermal conductivity (Watt per Meter per Kelvin ($W.m^{-1}.K^{-1}$)). As such, to correctly assess these properties, the focus will be on determining the Seebeck coefficient and both conductivities. As shown in Figure 79, these parameters are connected:

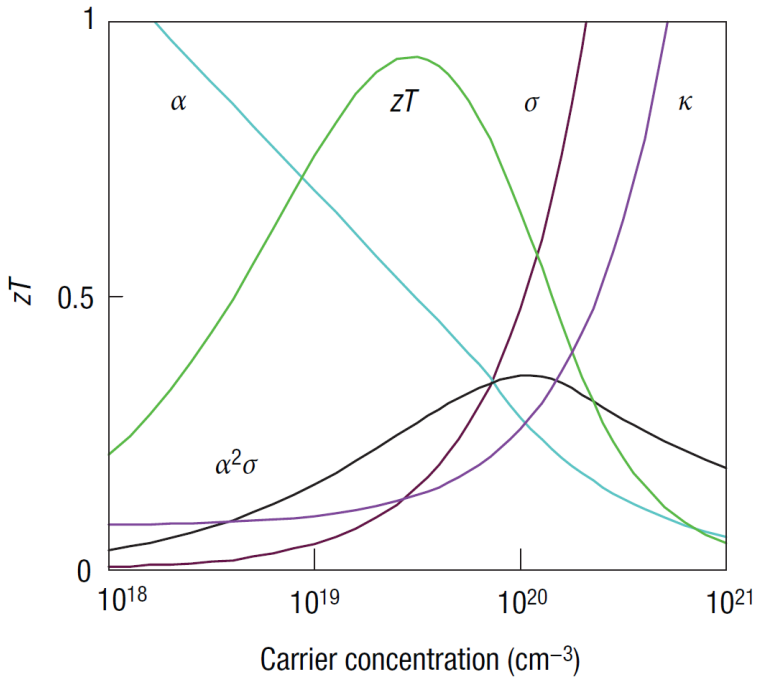

Figure 79: *Evolution of the Seebeck Coefficient, electrical conductivity, and thermal conductivity according to carrier concentration.*[96]

As thermal resistivity could not be correctly assessed due to the imperfect sintering of the powder, attempts were made to measure the electrical resistivity. Unfortunately, as none of the systems available on site were able to estimate it within limits, this means that the samsonite phase has an electrical resistivity beyond 60 MΩ, making it insulating.

CONCLUSION

CONCLUSION

To conclude on the results obtained from the synthesis of the samsonite phase in this manuscript, multiple valuable pieces of information have been obtained:

In the case of **high-temperature synthesis,** the samsonite phase seemingly cannot be reached. From the properties later obtained, it can be assumed that methods that go beyond 250°C would not manage to reach the wanted quaternary sulfide as they would be well beyond the decomposition of the compound, which was estimated between 150 and 175 °C. However, in these conditions, other compounds, such as $MnSb_2S_4$, TiS, and variants of tetrahedrite, doped with silver and manganese, have been uncovered. While processes may not be optimal, they can be the first steps for a deeper study (which is already the case for $MnSb_2S_4$).

With processes of lower temperature, the results were much more optimistic as the samsonite compound could be successfully formed. Both **hydrothermal and polyol processes** were functional at 180°C. Both methods are of different scales of time (hydrothermal synthesis being 2 days long and the polyol process being 6-7 hours long), and while they provide an equivalent purity, the grain shapes formed are different. They are quite similar in scale (790 nm for hydrothermal synthesis and 890 nm for the polyol process) but the polyol synthesis has a much more cohesive shape and size compared to the water-based method. Additionally, the optimization of the processes led to the setup of a **fast and efficient synthesis process** for a thioantimoniate compound **$Na_3SbS_4 \cdot 9H_2O$**, also known as Schlippe's salt.

Both methods have proven to be quite sensitive to the many parameters involved during the experiment. Which one is the most efficient? the answer relies heavily on what is the focus behind the synthesis process.

Hydrothermal synthesis uses water as a solvent and is more efficient than polyol synthesis in unique regard to the yield compared to the volume used (73.76 $g.L^{-1}$ versus 11 $g.L^{-1}$) and upscale seems to have no influence on the purity of the compound formed. However, this method also relies on heavy use of manganese precursors (6 times the stoichiometric amount necessary), and the ternary compound, Ag_3SbS_3 seems impossible to completely remove from the final product formed.

The polyol process is faster than the hydrothermal process and the powder formed is of the nano-scale, it also does not necessitate a preliminary synthesis of precursors any longer available for commercial use. The downsides are that the method relies on the use of 3-aminopropan-1-ol, which is an organic solvent that cannot be reused, also, the heavy influence of the stirring speed and the cooling down of the system in the efficient formation of the compound implies that upscaling may

prove to be more difficult as a deeper study of the Reynold number, the viscosity of the solvent and ways to induce a fast cooldown of the process.

As a characterization of the samsonite compound was sparse, most being made only around the time of the first discovery of the mineral and, consequently, none existing so far for a synthetic version of the compound, the possibilities of a thorough study of it.

Crystal parameters of the synthesized samsonite powder were assessed through the use of a monochromatic XRD and the technique of pair function distribution. The data were compared to those obtained with the mineral using the probability density function and Gram-Charlier development. A study of the decomposition of the compound, done through DSC-TGA and in-situ XRD, shows that the **compound decomposes between 150 and 175 °C**, while the exact mechanisms behind the decomposition cannot be exactly pinpointed, the samsonite phase seemingly decomposes and reforms into pyrargyrite during the heating. This information is not optimistic for a completely pure synthesis of the quaternary sulfide as, if the synthesis of the compound is also only possible above 175 °C, a trace of unwanted products may be inevitable.

Following these results, multiple prospects could be studied: as previously mentioned, unstudied compounds have been found through high-temperature synthesis and could be studied further. Additionally, with the successful use of Schlippe's salt in the formation of a quaternary thioantimoniate with Sb^{3+} atoms in an AX_3E_1 configuration, if this is indeed a worth configuration for better thermoelectric properties, broader research of the potential compounds could be carried out with this precursor.

With a bigger focus on the samsonite phase specifically, further study of supplementary physical and chemical properties could be done. Despite the **poor thermoelectrical properties** assessed in this manuscript, the possibility of **doping** for the compound to modify these properties may make it a more viable option for this purpose. With an already mostly optimized process, substitution may not be out of reach.

However, in any case, either the sintering of the samsonite phase would need to be optimized further or another way to use the compound (such as deposition?) should be found to get full use of its potential properties. The results, so far, of densification of only 80% in a stable state is subpar for a proper study and/or use, however, it was at least assessed that the main way to reach higher densification should be through pressure, rather than temperature.

BIBLIOGRAPHY

(1) Goldsmid, H. J. *Introduction to Thermoelectricity*; Springer Series in Materials Science; Springer: Berlin, Heidelberg, 2016; Vol. 121. https://doi.org/10.1007/978-3-662-49256-7.

(2) Vining, C. B. An Inconvenient Truth about Thermoelectrics. *Nat. Mater.* **2009**, *8* (2), 83–85. https://doi.org/10.1038/nmat2361.

(3) Pichanusakorn, P.; Bandaru, P. Nanostructured Thermoelectrics. *Mater. Sci. Eng. R Rep.* **2010**, *67* (2), 19–63. https://doi.org/10.1016/j.mser.2009.10.001.

(4) Manzano, C. V.; Abad, B.; Muñoz Rojo, M.; Koh, Y. R.; Hodson, S. L.; Lopez Martinez, A. M.; Xu, X.; Shakouri, A.; Sands, T. D.; Borca-Tasciuc, T.; Martin-Gonzalez, M. Anisotropic Effects on the Thermoelectric Properties of Highly Oriented Electrodeposited Bi2Te3 Films. *Sci. Rep.* **2016**, *6* (1), 19129. https://doi.org/10.1038/srep19129.

(5) Zhu, T.; Hu, L.; Zhao, X.; He, J. New Insights into Intrinsic Point Defects in V_2VI_3 Thermoelectric Materials. *Adv. Sci.* **2016**, *3* (7), 1600004. https://doi.org/10.1002/advs.201600004.

(6) Snyder, G. J.; Toberer, E. S. Complex Thermoelectric Materials. In *Materials for Sustainable Energy*; Co-Published with Macmillan Publishers Ltd, UK, 2010; pp 101–110. https://doi.org/10.1142/9789814317665_0016.

(7) Telkes, M. Thermoelectric Power and Electrical Resistivity of Minerals*. *Am. Mineral.* **1950**, *35* (7–8), 536–555.

(8) Werner; Fraatz. Samsonit, ein manganhaltiges Silbermineral von St. Andreasberg im Harz. *Cent. Für Mineral. Geol. Paläontol.* **1910**, 331–335.

(9) *Samsonite*. mindat.org. https://www.mindat.org/photo-656898.html (accessed 2022-03-23).

(10) Bindi, L.; Evain, M. Gram-Charlier Development of the Atomic Displacement Factors into Mineral Structures: The Case of Samsonite, $Ag_4MnSb_2S_6$. *Am. Mineral.* **2007**, *92* (5–6), 886–891. https://doi.org/10.2138/am.2007.2364.

(11) Lai, W.; Wang, Y.; Morelli, D. T.; Lu, X. From Bonding Asymmetry to Anharmonic Rattling in $Cu_{12}Sb_4S_{13}$ Tetrahedrites: When Lone-Pair Electrons Are Not So Lonely. *Adv. Funct. Mater.* **2015**, *25* (24), 3648–3657. https://doi.org/10.1002/adfm.201500766.

(12) Su, H.; Xie, Y.; Wan, S.; Li, B.; Qian, Y. A Novel One-Step Solvothermal Route to Nanocrystalline $CuSbS_2$ and Ag_3SbS_3. *Solid State Ion.* **1999**, *123* (1), 319–324. https://doi.org/10.1016/S0167-2738(99)00094-6.

(13) *Les céramiques industrielles - Propriétés, mise en forme et applications*; 2022.

(14) Riejen, P. *Solid-State Reaction in "Concise Encyclopedia of Advanced Ceramic Materials,"* 1. ed.; Brook, R. J., Ed.; Advances in materials science and engineering; Pergamon Press [u.a.]: Oxford, 1991.

(15) Zestrea, V.; Kodash, V. Y.; Felea, V.; Petrenco, P.; Quach, D. V.; Groza, J. R.; Tsurkan, V. Structural and Magnetic Properties of $FeCr_2S_4$ Spinel Prepared by Field-Activated Sintering and Conventional Solid-State Synthesis. *J. Mater. Sci.* **2008**, *43* (2), 660–664. https://doi.org/10.1007/s10853-007-2168-7.

(16) Kumari, A.; Vidyasagar, K. Solid-State Synthesis, Structural Variants and Transformation of Three-Dimensional Sulfides, $AGaSnS_4$ (A=Na, K, Rb, Cs, Tl) and $Na_{1.263}Ga_{1.263}Sn_{0.737}S_4$. *J. Solid State Chem.* **2007**, *180* (7), 2013–2019. https://doi.org/10.1016/j.jssc.2007.04.017.

(17) Chen, F.; Cao, Y.; Jia, D.; Liu, A. Solid-State Synthesis of ZnS/Graphene Nanocomposites with Enhanced Photocatalytic Activity. *Dyes Pigments* **2015**, *120*, 8–14. https://doi.org/10.1016/j.dyepig.2015.03.030.

(18) Fan, J.; Ekspong, J.; Ashok, A.; Koroidov, S.; Gracia-Espino, E. Solid-State Synthesis of Few-Layer Cobalt-Doped MoS_2 with CoMoS Phase on Nitrogen-Doped Graphene Driven by Microwave Irradiation for Hydrogen Electrocatalysis. *RSC Adv.* **2020**, *10* (56), 34323–34332. https://doi.org/10.1039/D0RA05560C.

(19) Halacoglu, S.; Chertmanova, S.; Chen, Y.; Li, Y.; Rajapakse, M.; Sumanasekera, G.; Narayanan, B.; Wang, H. Visualization of Solid-State Synthesis for Chalcogenide Na Superionic Conductors by in-Situ Neutron Diffraction. *ChemSusChem* **2021**, *14* (23), 5161–5166. https://doi.org/10.1002/cssc.202101839.

(20) Schreiner, S.; Aleandri, L. E.; Kang, D.; Ibers, J. A. Solid-State Chalcogenide Anions of Tantalum and Niobium: Synthesis and Structures of the $Ta_2S_{11}^{4-}$ and $Nb_4Se_{22}^{6-}$ Anions. *Inorg. Chem.* **1989**, *28* (3), 392–393. https://doi.org/10.1021/ic00302a003.

(21) Raju, Ch.; Falmbigl, M.; Rogl, P.; Yan, X.; Bauer, E.; Horky, J.; Zehetbauer, M.; Chandra Mallik, R. Thermoelectric Properties of Chalcogenide Based $Cu_{2+x}ZnSn_{1-x}Se_4$. *AIP Adv.* **2013**, *3* (3), 032106. https://doi.org/10.1063/1.4794733.

(22) Kimura, T. Molten Salt Synthesis of Ceramic Powders. In *Advances in Ceramics - Synthesis and Characterization, Processing and Specific Applications*; Sikalidis, C., Ed.; InTech, 2011. https://doi.org/10.5772/20472.

(23) Deloume, J.-P.; Scharff, J.-P.; Marote, P.; Durand, B.; Abou-Jalil, A. Molten Alkali Metal Oxonitrates, a Liquid State for Nanosized Perovskite Phase Elaboration. *J. Mater. Chem.* **1999**, *9* (1), 107–110. https://doi.org/10.1039/A805309J.

(24) *FACT salt database - list of systems and phases*. http://www.factsage.cn/fact/documentation/FTsalt/FTsalt_list.htm (accessed 2022-06-01).

(25) Ghisani, F.; Timmo, K.; Altosaar, M.; Raudoja, J.; Mikli, V.; Pilvet, M.; Kauk-Kuusik, M.; Grossberg, M. Synthesis and Characterization of Tetrahedrite $Cu_{10}Cd_2Sb_4S_{13}$ Monograin Material for Photovoltaic Application. *Mater. Sci. Semicond. Process.* **2020**, *110*, 104973. https://doi.org/10.1016/j.mssp.2020.104973.

(26) Rodríguez-Carvajal, J. Recent Advances in Magnetic Structure Determination by Neutron Powder Diffraction. *Phys. B Condens. Matter* **1993**, *192* (1–2), 55–69. https://doi.org/10.1016/0921-4526(93)90108-I.

(27) Roisnel, T.; Rodríquez-Carvajal, J. WinPLOTR: A Windows Tool for Powder Diffraction Pattern Analysis. *Mater. Sci. Forum* **2001**, *378–381*, 118–123. https://doi.org/10.4028/www.scientific.net/MSF.378-381.118.

(28) Henry, M.; Jolivet, J.-P.; Livage, J. *De la solution à l'oxyde: condensation des cations en solution aqueuse, chimie de surface des oxydes (Savoirs actuels)*; EDP Sciences, 1994.

(29) Rabenau, A. The Role of Hydrothermal Synthesis in Preparative Chemistry. *Angew. Chem. Int. Ed. Engl.* **1985**, *24* (12), 1026–1040. https://doi.org/10.1002/anie.198510261.

(30) Seward, T. M. Metal Complex Formation in Aqueous Solutions at Elevated Temperatures and Pressures. *Phys. Chem. Earth* **1981**, *13–14*, 113–132. https://doi.org/10.1016/0079-1946(81)90008-2.

(31) LaMer, V. K.; Dinegar, R. H. Theory, Production and Mechanism of Formation of Monodispersed Hydrosols. *J. Am. Chem. Soc.* **1950**, *72* (11), 4847–4854. https://doi.org/10.1021/ja01167a001.

(32) Poupon, M. Synthèse d'oxydes à Base d'éléments à Paire Libre (Se^{IV} et Te^{IV}) Dans Le but d'obtenir Des Structures Cristallines Non-Centrosymétriques Originales. These de doctorat, Caen, 2015.

(33) Nguyen, T. B.; Ermolenko, L.; Retailleau, P.; Al-Mourabit, A. Elemental Sulfur Disproportionation in the Redox Condensation Reaction between *o* -Halonitrobenzenes and Benzylamines. *Angew. Chem.* **2014**, *126* (50), 14028–14032. https://doi.org/10.1002/ange.201408397.

(34) Takeda, N.; Tokitoh, N.; Okazaki, R. Polysulfido Complexes of Main Group and Transition Metals. In *Elemental Sulfur und Sulfur-Rich Compounds II*; Steudel, R., Ed.; Topics in Current Chemistry; Springer: Berlin, Heidelberg, 2003; pp 153–202. https://doi.org/10.1007/b13184.

(35) Cloke, P. L. The Geologic Role of Polysulfides—Part I The Distribution of Ionic Species in Aqueous Sodium Polysulfide Solutions. *Geochim. Cosmochim. Acta* **1963**, *27* (12), 1265–1298. https://doi.org/10.1016/0016-7037(63)90050-4.

(36) Ostwald, W. Studien über die Bildung und Umwandlung fester Körper: 1. Abhandlung: Übersättigung und Überkaltung. *Z. Für Phys. Chem.* **1897**, *22U* (1), 289–330. https://doi.org/10.1515/zpch-1897-2233.
(37) Lv, L.; Wang, H. Ag_2S Nanorice: Hydrothermal Synthesis and Characterization Study. *Mater. Lett.* **2014**, *121*, 105–108. https://doi.org/10.1016/j.matlet.2014.01.121.
(38) Biswas, S.; Kar, S.; Chaudhuri, S. Solvothermal Synthesis of α-MnS Single Crystals. *J. Cryst. Growth* **2005**, *284* (1–2), 129–135. https://doi.org/10.1016/j.jcrysgro.2005.06.043.
(39) *A Single-Source Approach to Bi_2S_3 and Sb_2S_3 Nanorods via a Hydrothermal Treatment | Crystal Growth & Design*. https://pubs.acs.org/doi/full/10.1021/cg0341813 (accessed 2022-07-20).
(40) Byrappa, K.; Yoshimura, M. *Handbook of Hydrothermal Technology: A Technology for Crystal Growth and Materials Processing*; Noyes Publications: Norwich, N.Y, 2001.
(41) James, D. J.; Lu, X.; Morelli, D. T.; Brock, S. L. Solvothermal Synthesis of Tetrahedrite: Speeding Up the Process of Thermoelectric Material Generation. *ACS Appl. Mater. Interfaces* **2015**, *7* (42), 23623–23632. https://doi.org/10.1021/acsami.5b07141.
(42) Liu, Y.; Song, X.; Guo, Y.; Zhong, Y.; Li, Y.; Sun, Y.; Ji, M.; You, Z.; An, Y. Mild Solvothermal Syntheses and Characterizations of Two Layered Sulfides $Ba_2Cu_2Cd_2S_5$ and $Ba_3Cu_4Hg_4S_9$. *J. Alloys Compd.* **2020**, *829*, 154586. https://doi.org/10.1016/j.jallcom.2020.154586.
(43) Yao, H.-G.; Ji, M.; Ji, S.-H.; Zhang, R.-C.; An, Y.-L.; Ning, G. Solvothermal Syntheses of Two Novel Layered Quaternary Silver−Antimony(III) Sulfides with Different Strategies. *Cryst. Growth Des.* **2009**, *9* (9), 3821–3824. https://doi.org/10.1021/cg9000335.
(44) Li, J.; Chen, Z.; Wang, R. J.; Proserpio, D. Low Temperature Route towards New Materials: Solvothermal Synthesis of Metal Chalcogenides in Ethylenediamine. **1999**. https://doi.org/10.1016/S0010-8545(99)00107-1.
(45) Zhang, C.; Wang, K.-N.; Ji, M.; An, Y.-L. Mild Solvothermal Syntheses of Thioargentates A–Ag–S (A = K, Rb, Cs) and A–Ag–Ge–S (A = Na, Rb): Crucial Role of Excess Sulfur. *Inorg. Chem.* **2013**, *52* (21), 12367–12371. https://doi.org/10.1021/ic402092r.
(46) Liu, Y.; Li, Y.; Zhao, J.; Zhang, R.; Ji, M.; You, Z.; An, Y. Solvothermal Syntheses, Characterizations and Semiconducting Properties of Four Quaternary Thioargentates Ba_2AgInS_4, $Ba_3Ag_2Sn_2S_8$, $BaAg_2MS_4$ (M = Sn, Ge). *J. Alloys Compd.* **2020**, *815*, 152413. https://doi.org/10.1016/j.jallcom.2019.152413.
(47) van Almsick, T.; Loose, A.; Sheldrick, W. S. Solvothermal Synthesis and Structure of the $[Ge_2Se_7]^{4-}$ Anion in $(enH_2)[\{Mn(en)_2(enH)\}_2(\mu\text{-}en)](Ge_2Se_7)_2$ and $[Mn(dien)_2]_2Ge_2Se_7$. *Z. Für Anorg. Allg. Chem.* **2005**, *631* (1), 21–23. https://doi.org/10.1002/zaac.200400409.
(48) Kolis, J. W.; Korzenski, M. B. The Synthesis of Transition Metal Sulfides and Sulfo-Salt Crystals in Hydrothermal Brines. *MRS Online Proc. Libr. OPL* **1996**, *453*. https://doi.org/10.1557/PROC-453-35.
(49) Gabriel, C.; Gabriel, S.; Grant, E. H.; Grant, E. H.; Halstead, B. S. J.; Mingos, D. M. P. Dielectric Parameters Relevant to Microwave Dielectric Heating. *Chem. Soc. Rev.* **1998**, *27* (3), 213–224. https://doi.org/10.1039/A827213Z.
(50) *digestec DAB – Berghof Products + Instruments GmbH*. https://www.berghof-instruments.com/en/products/digestec-dab/ (accessed 2022-06-15).
(51) Walters, L. N.; Zhang, C.; Dravid, V. P.; Poeppelmeier, K. R.; Rondinelli, J. M. First-Principles Hydrothermal Synthesis Design to Optimize Conditions and Increase the Yield of Quaternary Heteroanionic Oxychalcogenides. *Chem. Mater.* **2021**, *33* (8), 2726–2741. https://doi.org/10.1021/acs.chemmater.0c02682.
(52) Spetzler, V.; Näther, C.; Bensch, W. The New Silver(I)Thioantimonate(III) $[C_4N_2H_{14}][Ag_3Sb_3S_7]$ and a New Structural Variant of the Silver(I)Thioantimonate(III) $[C_2N_2H_9]_2[Ag_5Sb_3S_8]$ Both Synthesized under Solvothermal Conditions. *J. Solid State Chem.* **2006**, *179* (11), 3541–3549. https://doi.org/10.1016/j.jssc.2006.07.022.
(53) Anderer, C.; Delwa de Alarcón, N.; Näther, C.; Bensch, W. A Strategy for the Preparation of Thioantimonates Based on the Concept of Weak Acids and Corresponding Strong Bases. *Chem. - Eur. J.* **2014**, *20* (51), 16953–16959. https://doi.org/10.1002/chem.201404396.

(54) Feng, S.; Xu, R. New Materials in Hydrothermal Synthesis. *Acc. Chem. Res.* **2001**, *34* (3), 239–247. https://doi.org/10.1021/ar0000105.
(55) Lide, D. R. *CRC Handbook of Chemistry and Physics*, 88th ed.; CRC Press: Boca Raton, FL, 2007.
(56) *Xylenes reagent grade 1330-20-7*. http://www.sigmaaldrich.com/ (accessed 2022-08-24).
(57) *2,2-Dimethoxypropane | Sigma-Aldrich*. http://www.sigmaaldrich.com/ (accessed 2022-08-24).
(58) Vaqueiro, P.; Chippindale, A. M.; Cowley, A. R.; Powell, A. V. Templated Synthesis of the Novel Layered Silver−Antimony Sulfides $[H_3NCH_2CH_2NH_2][Ag_2SbS_3]$ and $[H_3NCH_2CH_2NH_2]_2[Ag_5Sb_3S_8]$. *Inorg. Chem.* **2003**, *42* (24), 7846–7851. https://doi.org/10.1021/ic034926u.
(59) Sherman, D. M.; Ragnarsdottir, K. V.; Oelkers, E. H. Antimony Transport in Hydrothermal Solutions: An EXAFS Study of Antimony(V) Complexation in Alkaline Sulfide and Sulfide–Chloride Brines at Temperatures from 25°C to 300°C at Psat. *Chem. Geol.* **2000**, *167* (1), 161–167. https://doi.org/10.1016/S0009-2541(99)00207-7.
(60) Gammons, C. H.; Seward, T. M. Stability of Manganese (II) Chloride Complexes from 25 to 300°C. *Geochim. Cosmochim. Acta* **1996**, *60* (22), 4295–4311. https://doi.org/10.1016/S0016-7037(96)00275-X.
(61) Danker, F.; Engesser, T. A.; Broich, D.; Näther, C.; Bensch, W. The Cation and Anion Bonding Modes Make a Difference: An Unprecedented Layered Structure and a Tri(Hetero)Nuclear Moiety in Thioantimonates(V). *Dalton Trans.* **2021**, *50* (48), 18107–18117. https://doi.org/10.1039/D1DT03014K.
(62) Danker, F.; Anderer, C.; Poschmann, M.; Terraschke, H.; Näther, C.; van Leusen, J.; Bensch, W.; Kögerler, P. $[Mn(Terpy)Sb_2S_4]_n$, a 1D Network of $MnSb_4S_5$ Rings Exhibiting a Pronounced Magnetocaloric Effect and Luminescence. *Eur. J. Inorg. Chem.* **2020**, *2020* (18), 1751–1758. https://doi.org/10.1002/ejic.202000225.
(63) Planer-Friedrich, B.; Wilson, N. The Stability of Tetrathioantimonate in the Presence of Oxygen, Light, High Temperature and Arsenic. *Chem. Geol.* **2012**, *322–323*, 1–10. https://doi.org/10.1016/j.chemgeo.2012.06.010.
(64) Bertrand, A.; Paecklar, A.; Barbier, T.; Gascoin, F. Rapid Synthesis Process and Characterization for High Purity Sodium Thioantimoniate Nonahydrate. *Dalton Trans.* **2022**, *51* (30), 11340–11345. https://doi.org/10.1039/D2DT01520J.
(65) Mereiter, K.; Preisinger, A.; Guth, H. Hydrogen Bonds in Schlippe's Salt: Refinement of the Crystal Structures of $Na_3SbS_4.9H_2O$ by X-Ray Diffraction and $Na_3SbS_4.9D_2O$ by Neutron Diffraction at Room Temperature. *Acta Crystallogr. B* **1979**, *35* (1), 19–25. https://doi.org/10.1107/S0567740879002442.
(66) Gamo, H.; Phuc, N. H. H.; Muto, H.; Matsuda, A. Effects of Substituting S with Cl on the Structural and Electrochemical Characteristics of Na_3SbS_4 Solid Electrolytes. *ACS Appl. Energy Mater.* **2021**, *4* (6), 6125–6134. https://doi.org/10.1021/acsaem.1c00927.
(67) Banerjee, A.; Park, K. H.; Heo, J. W.; Nam, Y. J.; Moon, C. K.; Oh, S. M.; Hong, S.-T.; Jung, Y. S. Na_3SbS_4 : A Solution Processable Sodium Superionic Conductor for All-Solid-State Sodium-Ion Batteries. *Angew. Chem. Int. Ed.* **2016**, *55* (33), 9634–9638. https://doi.org/10.1002/anie.201604158.
(68) Rodríguez-Rodríguez, C.; Nava-Alonso, F.; Uribe-Salas, A.; Viñals, J. Pyrargyrite (Ag 3 SbS 3): Silver and Antimony Dissolution by Ozone Oxidation in Acid Media. *Hydrometallurgy* **2016**, *164*, 15–23. https://doi.org/10.1016/j.hydromet.2016.04.014.
(69) Fiévet, F.; Ammar-Merah, S.; Brayner, R.; Chau, F.; Giraud, M.; Mammeri, F.; Peron, J.; Piquemal, J.-Y.; Sicard, L.; Viau, G. The Polyol Process: A Unique Method for Easy Access to Metal Nanoparticles with Tailored Sizes, Shapes and Compositions. *Chem. Soc. Rev.* **2018**, *47* (14), 5187–5233. https://doi.org/10.1039/C7CS00777A.
(70) Jézéquel, D.; Guenot, J.; Jouini, N.; Fiévet, F. Submicrometer Zinc Oxide Particles: Elaboration in Polyol Medium and Morphological Characteristics. *J. Mater. Res.* **1995**, *10* (1), 77–83. https://doi.org/10.1557/JMR.1995.0077.

(71) Poul, L.; Ammar, S.; Jouini, N.; Fievet, F.; Villain, F. Synthesis of Inorganic Compounds (Metal, Oxide and Hydroxide) in Polyol Medium: A Versatile Route Related to the Sol-Gel Process. *J. Sol-Gel Sci. Technol.* **2003**, *26* (1), 261–265. https://doi.org/10.1023/A:1020763402390.
(72) Weller, D. P.; Stevens, D. L.; Kunkel, G. E.; Ochs, A. M.; Holder, C. F.; Morelli, D. T.; Anderson, M. E. Thermoelectric Performance of Tetrahedrite Synthesized by a Modified Polyol Process. *Chem. Mater.* **2017**, *29* (4), 1656–1664. https://doi.org/10.1021/acs.chemmater.6b04950.
(73) Poul, L.; Ammar, S.; Jouini, N.; Fiévet, F.; Villain, F. Metastable Solid Solutions in the System ZnO□CoO: Synthesis by Hydrolysis in Polyol Medium and Study of the Morphological Characteristics. *Solid State Sci.* **2001**, *3* (1), 31–42. https://doi.org/10.1016/S1293-2558(00)01129-8.
(74) Préaud, S. Oxydes thermoélectriques à structures complexes. phdthesis, Université Paris-Saclay, 2020.
(75) Poul, L.; Jouini, N.; Fiévet, F. Layered Hydroxide Metal Acetates (Metal = Zinc, Cobalt, and Nickel): Elaboration via Hydrolysis in Polyol Medium and Comparative Study. *Chem. Mater.* **2000**, *12* (10), 3123–3132. https://doi.org/10.1021/cm991179j.
(76) *Ethylene glycol anhydrous, 99.8 107-21-1*. http://www.sigmaaldrich.com/ (accessed 2022-07-28).
(77) *Tetraethylene glycol for synthesis 112-60-7*. http://www.sigmaaldrich.com/ (accessed 2022-07-28).
(78) *1,3-Propanediol 98 504-63-2*. http://www.sigmaaldrich.com/ (accessed 2022-07-28).
(79) *1,5-Pentanediol for synthesis 111-29-5*. http://www.sigmaaldrich.com/ (accessed 2022-07-28).
(80) *504-63-2 - 1,3-Propanediol, 99% - 1,3-Dihydroxypropane - Trimethylene glycol - A10829 - Alfa Aesar*. https://www.alfa.com/fr/catalog/A10829/ (accessed 2022-07-28).
(81) Dong, H.; Kuzmanoski, A.; Gößl, D. M.; Popescu, R.; Gerthsen, D.; Feldmann, C. Polyol-Mediated C-Dot Formation Showing Efficient Tb^{3+}/Eu^{3+} Emission. *Chem. Commun.* **2014**, *50* (56), 7503–7506. https://doi.org/10.1039/C4CC01715C.
(82) Skrabalak, S. E.; Wiley, B. J.; Kim, M.; Formo, E. V.; Xia, Y. On the Polyol Synthesis of Silver Nanostructures: Glycolaldehyde as a Reducing Agent. *Nano Lett.* **2008**, *8* (7), 2077–2081. https://doi.org/10.1021/nl800910d.
(83) Novakovskaya, Y. V. 3-Aminopropanol: Polymolecular Structures That Determine Unique Solvation Motifs. arXiv September 4, 2021. https://doi.org/10.48550/arXiv.2109.01870.
(84) Daly, F. P.; Brown, C. W. Raman Spectra of Sodium Tetrasulfide in Primary Amines. Evidence for Sulfide (S_4^{2-} and S_8^{n-}) Ions in Rhombic Sulfur-Amine Solutions. *J. Phys. Chem.* **1975**, *79* (4), 350–354. https://doi.org/10.1021/j100571a013.
(85) Poernomo, H.; Kundari, N. A.; Nafiah. The Effect of Stirring Speed and Reactant Residence Time in the Bench Scales CSTR on the Reaction Conversion of ZBS. *Alex. Eng. J.* **2022**, *61* (2), 1309–1317. https://doi.org/10.1016/j.aej.2021.06.012.
(86) Kolbeck, F.; Goldsohmidt, V. XXXIV. Über Samsonit von Andreasberg. *Z. Für Krist. - Cryst. Mater.* **1912**, *50* (1–6), 455–458. https://doi.org/10.1524/zkri.1912.50.1.455.
(87) Anthony, J.; Bideaux, R.; Bladh, K.; Nichols, M. *Handbook of Mineralogy*; Mineralogical Society of America: Chantilly, VA 20151-1110, USA, 2003; Vol. 1.
(88) Juhás, P.; Davis, T.; Farrow, C. L.; Billinge, S. J. L. *PDFgetX3*: A Rapid and Highly Automatable Program for Processing Powder Diffraction Data into Total Scattering Pair Distribution Functions. *J. Appl. Crystallogr.* **2013**, *46* (2), 560–566. https://doi.org/10.1107/S0021889813005190.
(89) Juhás, P.; Farrow, C.; Yang, X.; Knox, K.; Billinge, S. Complex Modeling: A Strategy and Software Program for Combining Multiple Information Sources to Solve Ill Posed Structure and Nanostructure Inverse Problems. *Acta Crystallogr. Sect. Found. Adv.* **2015**, *71* (6), 562–568. https://doi.org/10.1107/S2053273315014473.

(90) Abramoff, M. D.; Magalhães, P. J.; Ram, S. J. Image Processing with ImageJ. *Biophotonics Int.* **2004**, *11* (7), 36–42.
(91) Schneider, C. A.; Rasband, W. S.; Eliceiri, K. W. NIH Image to ImageJ: 25 Years of Image Analysis. *Nat. Methods* **2012**, *9* (7), 671–675. https://doi.org/10.1038/nmeth.2089.
(92) *ImageJ*. https://imagej.nih.gov/ij/ (accessed 2022-09-23).
(93) Aspiala, M.; Tesfaye, F.; Taskinen, P. Thermodynamic Study in the Ag–Sb–S System by the EMF Method. *J. Chem. Thermodyn.* **2016**, *98*, 361–366. https://doi.org/10.1016/j.jct.2016.03.009.
(94) Johnson, G. K.; Papatheodorou, G. N.; Johnson, C. E. The Enthalpies of Formation of SbF_5(l) and Sb_2S_3(c) and the High-Temperature Thermodynamic Functions of Sb_2S_3(c) and Sb_2S_3(l). *J. Chem. Thermodyn.* **1981**, *13* (8), 745–754. https://doi.org/10.1016/0021-9614(81)90063-X.
(95) Keighin, C. W.; Honea, R. M. The System Ag-Sb-S from 600°C to 200°C. *Miner. Deposita* **1969**, *4* (2), 153–171. https://doi.org/10.1007/BF00208050.
(96) Snyder, G. J.; Toberer, E. S. Complex Thermoelectric Materials. *Nat. Mater.* **2008**, *7* (2), 105–114. https://doi.org/10.1038/nmat2090.
(97) Djokić, S. Synthesis and Antimicrobial Activity of Silver Citrate Complexes. *Bioinorg. Chem. Appl.* **2008**, *2008*, 1–7. https://doi.org/10.1155/2008/436458.
(98) Zhang, G.; Yang, G.; Ma, J. S. Versatile Framework Solids Constructed from Divalent Transition Metals and Citric Acid: Syntheses, Crystal Structures, and Thermal Behaviors. *Cryst. Growth Des.* **2006**, *6* (2), 375–381. https://doi.org/10.1021/cg0503245.
(99) Yeates, R. M.; Harrison, W. T. A. Synthesis, Crystal Structure and Properties of $Na_3Zn_4O(AsO_4)_3 \cdot 6H_2O$, a New Framework Zincoarsenate. *J. Mater. Chem.* **2002**, *12* (4), 1103–1106. https://doi.org/10.1039/b110288e.

APPENDIX

A-1: Hydrothermal Synthesis of $Na_3Zn_4O(SbO_4)_3 \cdot 6H_2O$

Through the research of the perfect synthesis of the samsonite phase, multiple aspects of the process were either a little too irrelevant or complicated to properly assess. In this context, the following protocol may seem rather stark in contrast to the rest of the manuscript as the steps that led to this attempt were not mentioned.

For this synthesis, citrates, sodium chloride, and antimony acetate were used in the experimental protocol. In the case of antimony acetate, the same precursor bought and used in the main manuscript was used here. For silver citrate and zinc citrate, the compounds were synthesized following the experimental processes that can be found in the literature. [97,98]

Equivalent amount metal-wise of silver citrate ($Ag_3(C_6H_5O_7)$, synthesized, 0.1281 g, $2.5 \cdot 10^{-4}$ mol), zinc citrate ($Zn_3(C_6H_5O_7)_2(H_2O)_2$, synthesized, 0.1531 g, $2.5 \cdot 10^{-4}$ mol), antimony acetate ($Sb(CH_3CO_2)_3$, Sigma Aldrich, 99.99%, 0.2241 g, $7.5 \cdot 10^{-4}$ mol) and are introduced in 15 mL of distilled water. The solution is agitated with a strong magnetic stir for ten minutes and then transferred to a 25 ml Teflon vessel and locked in a steel case. The vessel is heated up to 100°C in 3 hours and the temperature is maintained for 12 hours then is heated up to 170°C in 24 hours and the temperature is maintained for 24 hours before letting the system cool down. The powder produced through that process is filtrated and washed with distilled water.

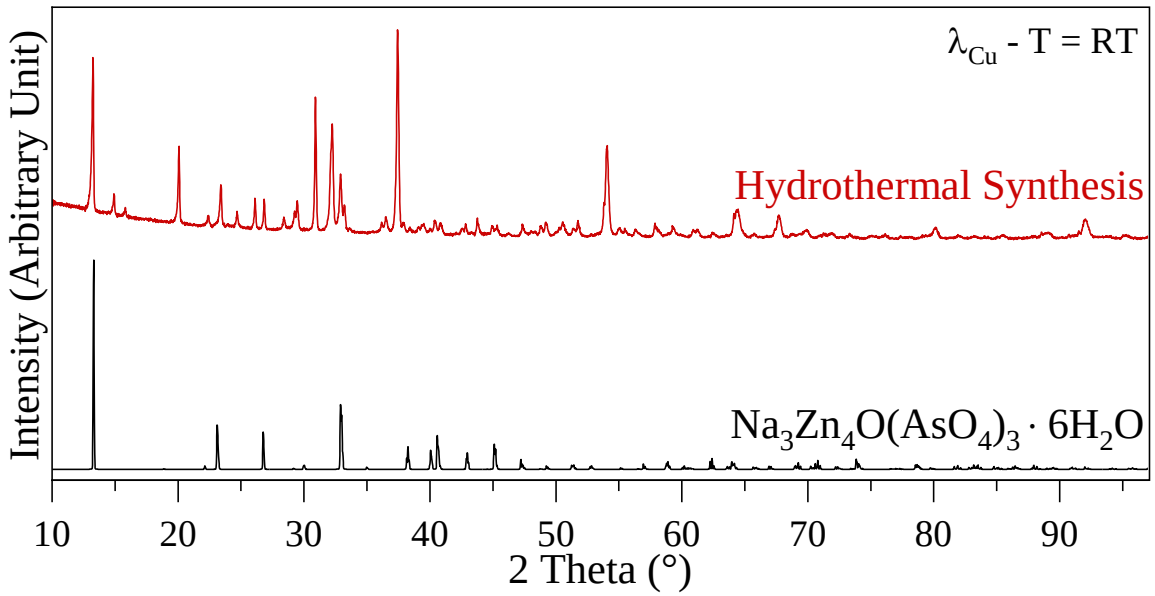

Figure 80: *Room Temperature XRD pattern from powder obtained through hydrothermal synthesis and the simulated pattern of $Na_3Zn_4O(AsO_4)_3 \cdot 6H_2O$*

Surprisingly, **this exact composition has never actually been reported**, only variants with phosphorus and arsenic are the elements present in $M_3Zn_4O(XO_4)_3 \cdot nH_2O$, with M a univalent anion and X either being phosphorus or arsenic.[99]

However, despite multiple attempts, by reproducing the protocol or by changing multiple parameters (precursors, heating cycle, concentration…) in hopes of having a more reliable process, the structure could unfortunately not be reached again.

A-2: Rapid Synthesis process and characterization for high purity sodium thioantimoniate nonahydrate

ARTICLE

Rapid Synthesis Process and Characterization for High Purity Sodium Thioantimoniate Nonahydrate

Received 00th January 20xx,
Accepted 00th January 20xx

DOI: 10.1039/x0xx00000x

A. Bertrand, [a] A. Paecklar, [a] T. Barbier,*[a] and F. Gascoin [a]

For the first time, $Na_3SbS_4.9H_2O$, also known as Schlippe's salt, has been synthesized through high-energy ball milling. This innovative synthesis way allows for obtaining high purity thioantimonate nonahydrate with around 90% yield in only approximately four hours. To validate the synthesis route described herein, the crystal structure has been refined, at room temperature, through high-resolution X-Ray diffraction, pair distribution function analysis and Energy Dispersive Spectrometry. Dehydration and rehydration of the compound have also been studied by thermogravimetric analysis and differential scanning calorimetry.

Introduction

The limited Li resources in the Earth's crust, together with recent rapid rises in the price of the Li precursors, as well as its geologically uneven distribution are criteria that have to be taken into account for large-scale energy-storage applications.(1–3) Therefore, the replacement of Li^+ ions with Na^+ as charge carriers would be an ideal solution.

Thus, following that trend, sodium thioantimonates (Na_3SbS_4) and its conjugated nonahydrate ($Na_3SbS_4.9H_2O$), also known as Schlippe's salt, were highly studied for room-temperature-operable all-solid-state Na-ion batteries.(4–10) Indeed, sulfide Na-ion solid electrolytes are promising because of their potential for greater safety, lower cost, and performance compared to flammable organic liquid electrolytes used in Li-ion batteries.(11)

More recently, Schlippe's salt was used as antimony and sulfur precursors for hydrothermal synthesis of hybrid compounds.(12–14) The latter precursor, freely soluble in water compared to other classic antimony precursors, offers the great benefit of not using amine solvents, such as ethylenediamine, commonly used for dissolving sulfur compounds.(15) Therefore, such precursors allow obtaining of ternary and quaternary sulfide compounds by eliminating the use of toxic solvents and the production of hazardous waste. However, the salt is no longer available for commercial purchase, which means it is now necessary to synthesize it efficiently and quickly for it to not become too much of a time cost on processes where this compound is needed. Unfortunately, most synthesis methods reported recently are multiple days long due to the slow recrystallization process and have a low yield of approximately 30%.(13)

Herein, a new rapid and scalable synthesis method, using high-energy ball-milling, is described for the first time. This process, which allows obtaining single-phase compounds in only four hours possesses the great benefits of no concerns about the generation of toxic H_2S gas or other noxious process intermediates.

To attest to the innovative method used for synthesizing single-phase sodium thioantimoniate nonahydrate, structural characterization performed through X-Ray diffraction and pair distribution function analysis have been performed. The crystallographic parameters have then been compared and discussed with the ones previously reported.(16)

Experimental section

A mixture of binary Na_2S (Alpha Aesar, 97%, 1.93 g, 24.7 mmol), Sb_2S_3 (Sigma-Aldrich, 98%, 2.82 g, 8.26 mmol), and elemental S (Alpha Aesar, 99,5%, 0.533 g, 16.6 mmol) was introduced, into 9 mL of distilled water inside a 45 mL tungsten carbide jar containing 48 tungsten carbide balls with a diameter of 5 mm (49.7 g). The mixture was then milled at 450 rpm for 2 hours (divided into 8 cycles of 15 minutes, each separated with a minute-long break to let the system cool down). The resulting solution was washed and filtered with deionized water. The dark brown powder obtained of unwanted products (Na_2SO_4 and Sb_2O_3) was discarded. The filtrate was dried through rotary

[a] CRISMAT, UMR6508 CNRS ENSICAEN, 6 bd Maréchal Juin, 14050 CAEN cedex 4, France. Email : Tristan.barbier@ensicaen.fr

† Footnotes relating to the title and/or authors should appear here.

Electronic Supplementary Information (ESI) available: [details of any supplementary information available should be included here]. See DOI: 10.1039/x0xx00000x

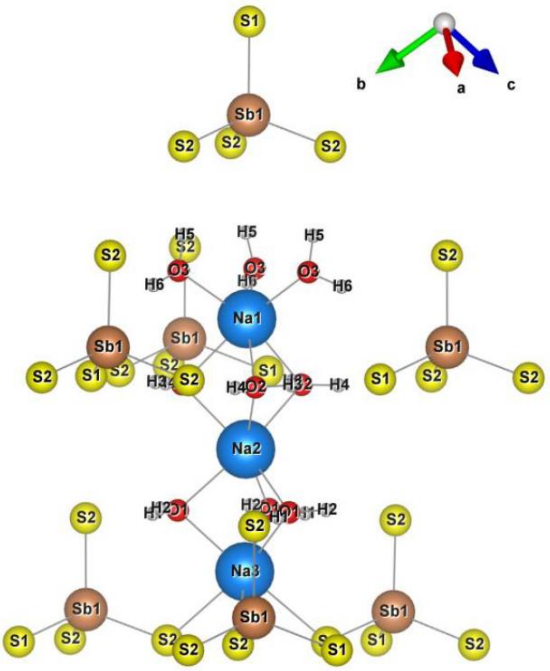

Figure 1: Schlippe's salt structure along a Na1-Na2-Na3 axis.

evaporation to force the salt's precipitation. The powder obtained was then recovered and characterized.

The crystallographic parameters were determined through high-resolution powder X-Ray Diffraction (XRD). The data were collected at room temperature with two different devices. First, through a Bruker D8 ADVANCE diffractometer [copper anode λ = 1.54059 Å, monochromatic Ge 111, Lynx Eye detector], in reflection configuration. Data were collected from 8 up to 100° with a step size of 0.009198°, and a step time of 1.7 s. A diffraction pattern of a standard LaB_6 powder was also registered under the same conditions to obtain the instrumental broadening of the diffractometer. The peak shape was then corrected from the instrumental broadening using the aforementioned calibration acquisition. Those data were then refined using the FullProf and WinPlotr software package.(17,18)

Regarding the structure refinement, the systematic error correction (zero-point shift and asymmetry) was applied, and the background was adjusted using a polynomial function. With respect to the crystallographic structure, the lattice parameters, atomic positions, and isothermal temperature factor (B_{iso}) were also refined. Hydrogen atoms, however, have been set with the parameters that were already determined by K. Mereiter *et al.* (16) through neutron diffraction. Indeed, the fact that hydrogen atoms only have one electron makes them very hard to detect with X-Rays accurately due to X-Rays' scatter from the electron density. (19,20)

Secondly, X-Ray scattering data suitable for Pair Distribution Function (PDF) analysis were collected using a Rigaku SmartLab (rotating anode Mo λ = 0.71146 Å) diffractometer. The

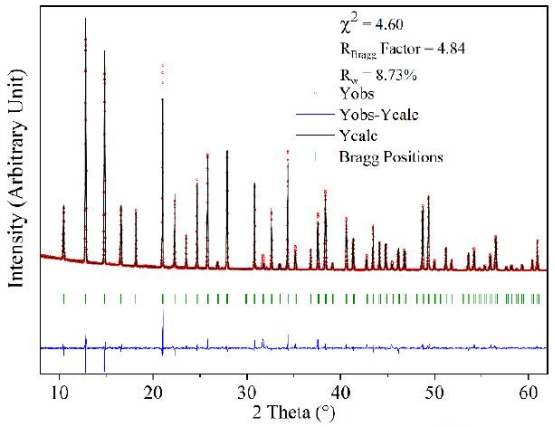

Figure 2: powder X-Ray diffraction patterns of Schlippe's Salt with D8 ADVANCE.

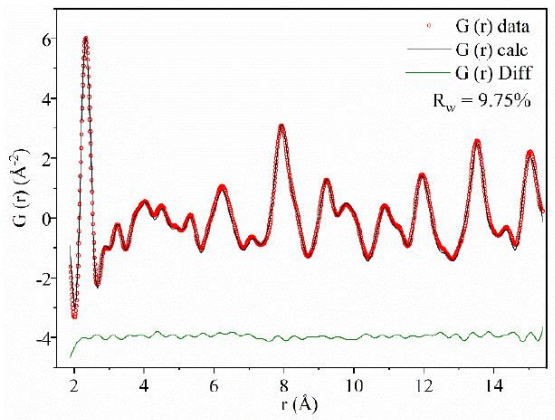

Figure 3: PDF refinement of Schlippe's Salt with Smartlab Rigaku.

powdered sample was loaded into a quartz capillary (0.4 mm in diameter) and measured in transmission mode using a HyPix3000 detector. Data were collected from 3 to 112° using four different speed-time, depending on the angular range (3° to 35°: 4 °/min; 34° to 65°: 1.5 °/min; 64° to 95°: 0.7 °/min, and 94° to 112°: 0.2 °/min). The experimental PDF was extracted using the program PDFgetX3 (21) and analyzed using the program PDFgui.(22) The total scattering structure-function, *S(Q)*, was produced in PDFgetX3 by subtracting the quartz container scattering and utilizing the appropriate sample composition. The pair distribution function pattern, *G(r)*, displayed in figure 3, was calculated via the Fourier transform of the total scattering data utilizing a maximum $Q_{MaxInst}$ = 14.6431 Å^{-1}. Values of Q_{damp} = 0.02 Å^{-1} and Q_{broad} = 0.08 Å^{-1} have been extracted from the refinement of a LaB_6 standard in PDFgui software and were used for further refinement.(22)

Imaging, mapping, and elemental analysis were performed using a Scanning Electron Microscope (SEM; JEOL - JCM7000) equipped with an Energy Dispersive Spectrometer (EDS). The samples were measured at an operating voltage of 15 kV.

The study of water inside the crystal structure was performed through Thermo-Gravimetric Analysis (TGA). The data was collected on a Netzsch TGA apparatus (STA 449 F3 Jupiter) over

the temperature range of 300 °C with 3 °C/min. An N_2 flux (100 mL/min) and air (N_2 80 mL/min - O_2 20 mL/min) were used during the acquisition.

Results and discussion

Structural analysis

This new rapid and scalable synthesis method presented herein resulted in a satisfying yield of around 90% in mass for only a four hours long process, which is far higher than the 30% yield obtained by a multiple-day-long protocol of dissolution, precipitation, and recrystallization.(13) As varying traces of the mopungite phase ($NaSb(OH)_6$) can appear during the process due to the decomposition under light (12), it is recommended to use the least amount of water possible during washing and have a powerful vacuum for the process to be done as fast as possible.

The room temperature XRD pattern of Schlippe's Salt obtained from the Bruker D8 ADVANCE diffractometer is shown in Figure 2. The one obtained through the Rigaku SmartLab diffractometer is shown in Figure 3.

The devices' attributes used, as well as the unit cell characteristics, determined with these patterns, are reported in Table 1.

Atomic positions and isotropic displacement parameters, obtained from the refinement of the D8 ADVANCE pattern, are reported in Table 2.

It will be noted that atomic positions and isotropic displacement parameters of hydrogen atoms have been set (all B_{Iso} being considered at 3.2 Å²) and the refinement of oxygen parameters have been processed with distances set to 0.9584 Å and a standard error allowed of 0.0020 Å while angles in the water structure were set to 106.45° with a standard error: 2.0000° (these settings were based on water molecules parameters(23) and following the decisions made by Mereiter *et al.*(16)). Refinements without these constraints have led to non-physical results (abnormal distances and angles for water molecules) from the software with little improvement on the reliability factors such as the R-Factor.

Table 1: Crystal data for Schlippe's Salt at 293K.

Chemical Formula	$Na_3SbS_4.9H_2O$	
Molecular weight (g/mol)	481.12	
Space Group	P 2_1 3 (198)	
Refinement	Rietveld (D8 ADVANCE)	PDF (Rigaku Smartlab)
Radiation	Cu 1.54059 Å	Mo 0.71146 Å
Cell Parameters		
a (Å)	11.959(2)	11.966(8)
α (°)	90°	90°
V (Å³)	1710.438(5)	1713.710(1)
Calculated density (g/cm³)	1.868	1.864

Table 2: Atomic coordinates and isotropic displacement parameters (B_{Iso}) obtained from D8 diffractometer (* are fixed atoms).

Atom	*x*	*y*	*z*	B_{Iso} (Å²)
Na1	0.2893(4)	0.2893(4)	0.2893(4)	3.6932(9)
Na2	0.4512(2)	0.4512(2)	0.4512(2)	2.9442(3)
Na3	0.6031(3)	0.6031(3)	0.6031(3)	4.7133(1)
Sb	0.0366(3)	0.0366(3)	0.0366(3)	2.1683(5)
S1	0.9205(3)	0.9205(3)	0.9205(2)	2.6582(2)
S2	0.1521(1)	0.1479(2)	0.9230(2)	2.3399(8)
O1	0.9748(1)	0.3673(6)	0.9245(7)	1.6732(1)
O2	0.1826(1)	0.6950(4)	0.9937(3)	1.6392(3)
O3	0.1028(6)	0.2602(2)	0.3252(4)	2.5602(4)
H1*	0.0246(1)	0.3049(1)	0.9276(0)	3.2
H2*	0.9280(9)	0.3598(1)	0.8602(0)	3.2
H3*	0.2515(1)	0.6614(1)	0.0193(0)	3.2
H4*	0.1665(1)	0.7573(1)	0.0405(0)	3.2
H5*	0.0553(1)	0.2304(1)	0.2681(0)	3.2
H6*	0.0593(1)	0.3107(1)	0.3702(0)	3.2

Table 3: Atomic coordinates and isotropic displacement parameters (B_{Iso}) obtained from the Rigaku Smartlab diffractometer (* are fixed atoms).

Atom	*x*	*y*	*z*	B_{Iso} (Å²)
Na1	0.2892(9)	0.2892(9)	0.2892(9)	6.2798(7)
Na2	0.4424(3)	0.4424(3)	0.4424(3)	1.1511(9)
Na3	0.5951(9)	0.5951(9)	0.5951(9)	2.0016(6)
Sb	0.0363(3)	0.0363(3)	0.0363(3)	1.2064(6)
S1	0.9236(4)	0.9236(4)	0.9236(4)	0.7381(6)
S2	0.1485(7)	0.1401(5)	0.9241(7)	1.9186(5)
O1	0.9781(3)	0.3477(5)	0.9283(1)	0.9209(5)
O2	0.1640(1)	0.6965(6)	0.9923(4)	0.7658(8)
O3	0.0941(5)	0.2395(5)	0.3292(7)	2.0694(5)
H1*	0.0246(1)	0.3049(1)	0.9276(1)	3.2
H2*	0.9280(9)	0.3598(1)	0.8602(1)	3.2
H3*	0.2515(1)	0.6614(1)	0.0193(1)	3.2
H4*	0.1665(1)	0.7573(1)	0.0405(1)	3.2
H5*	0.0553(1)	0.2304(1)	0.2681(1)	3.2
H6*	0.0593(1)	0.3107(1)	0.3702(1)	3.2

Atomic positions obtained from the PDF refinement of the Rigaku SmartLab pattern are reported in Table 3.

Both X-Ray and PDF refinements were performed using the $P2_13$ space group (198). All peaks have been adequately considered (as it can be seen in Figures 2 & 3), and no extra peaks may be observed over the full angular range, thus confirming the high purity of the sample.

When comparing results, our crystallographic parameters are quite similar to those previously reported.(16)

Indeed, the *a* cell parameter obtained through X-Ray diffraction and PDF refinement, 11.959(2) Å and 11.966(8) Å respectively, are very similar to those reported by K. Mereiter *et al.* (11.957(3) Å) and S. Haussühl *et al.* (11.957(2) Å). (16,24)

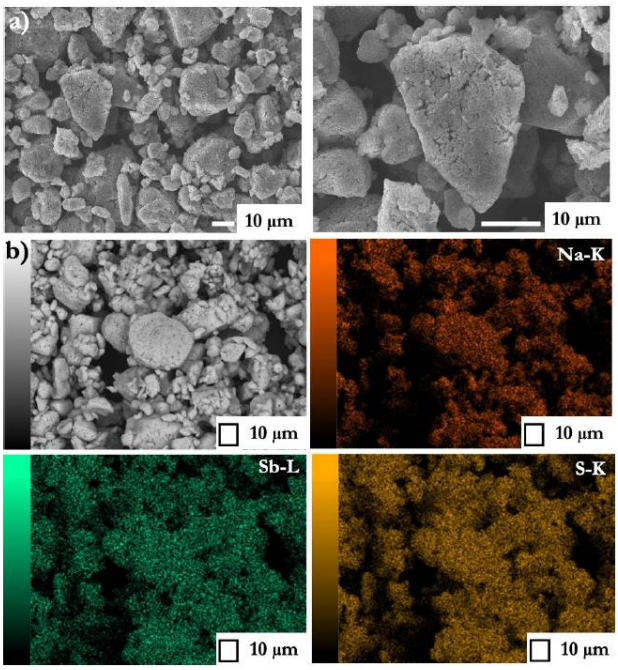

Figure 4: SEM images a) with x1000 and x2500 magnification b) with EDS-Elemental mapping of Na, Sb and S.

The deduced values confirm once again the high purity of the sample as well as the water amount because the dehydrated compound (Na_3SbS_4) crystallizes in the $P\bar{4}2_1c$ space group (a = 7.1653 Å). (25)

Just as cell parameters, atomic coordinates of all atoms (despite hydrogen) have also been compared to those obtained through X-Ray and neutron diffraction, previously published by K. Mereiter *et al.* Apart from the coordinates of the H atoms, the X-Ray results are more precise for Na, Sb, and S than the neutron results, and nearly as precise for the O atoms. Thus, the relative distances between the published data and those obtained from X-Ray diffraction (this study) highlight very similar coordinates.

Indeed, the biggest difference, which may be observed for the yO_3 position is around 0.43%.

As aforementioned, light element analysis is notoriously challenging because of the small number of form factors light elements generate which may explain the lowest accuracy provided by the X-Ray diffraction technique regarding the oxygen atoms.

On another hand, atomic coordinates deduced from the PDF refinement also exhibit similar values for the heavy atoms while slight deviations may be observed for the oxygen ones. It might also be pointed out that no constraints were applied to set the distance (and angle) of the water molecules. Therefore, the highest relative gap between the coordinates might be observed for yO_1 (1.87% deviation), xO_2 (2.00% deviation), and yO_3 (1.64 % deviation).

Elemental composition

As SEM analysis shows in figure 4.a), particles formed through this synthesis method average at 12.4 µm with a range between 2 and 33 µm. The particles themselves appear to be quite porous. Additionally, EDS allows checking of the elemental composition to ensure its homogeneity, as presented in figure 4.b), and estimate the proportions of sodium, antimony, and sulfur present in these particles.

On average, it was estimated that experimental composition was of 36%, 14%, and 50% which is rather close compared to the 37.5%, 12.5%, and 50% expected in theory for Na, Sb, and S respectively.

Dehydration

TGA results are shown in Figures 5 and 6, where each horizontal line represents the number of water molecules present in the structure (9 at 100%, 0 at 66.16%). From those results, it can be determined that water in the structure evaporates as soon as 30°C up to approximately 100°C in both tests. Differences are visible at approximately 200°C where, while the powder stays unchanged under N_2, oxidation clearly happens under air. The

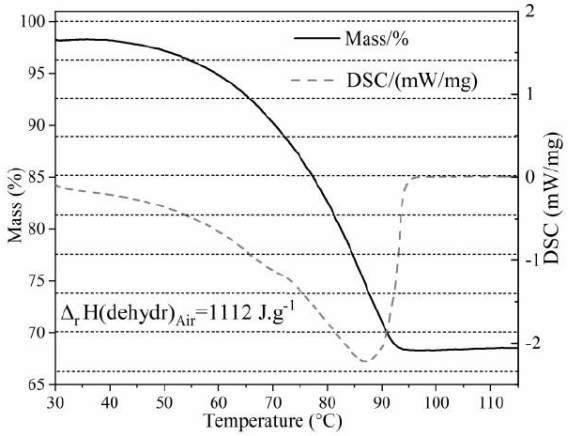

Figure 5: DSC-TGA curves of Schlippe's Salt in air. Heating rate = 3 °C/min.

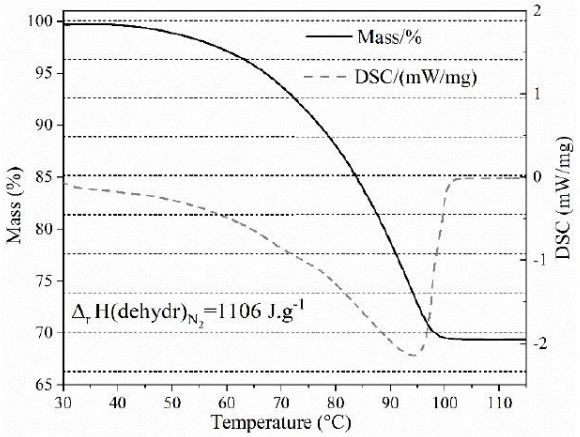

Figure 6: DSC-TGA curves of Schlippe's Salt in nitrogen. Heating rate = 3 °C/min.

compounds formed are Sb_2S_3, Sb_2O_3, and Na_2SO_4. In the case of the dehydrated compound, it rapidly reabsorbs water from ambient air and returns to its original $Na_3SbS_4 \cdot 9H_2O$ composition. The experimental value of enthalpy of the dehydration process can be calculated from DSC. Both values obtained are rather close, (-1106 $J \cdot g^{-1}$ and -1112 $J \cdot g^{-1}$). However, it can be noticed that not all the water is exactly extracted from the compound. It could be assumed that the leftover water is the last molecule still maintaining Schlippe's Salt structure before a rearrangement into the anhydrous compound as other works already show that the formation of Na_3SbS_4 is more complicated than a simple heating of its hydrated form.(4)

Conclusions

Here, a fast and highly efficient synthesis process of Schlippe's Salt was described. Using a ball mill and rotary evaporator in order to bring the energy for a complete reaction and a fast recovery of the compound to guarantee its high purity. The method has proved to be more efficient than those used so far for the synthesis of this compound since it is no longer available for commercial purchase.

The compound has also been characterized with X-Ray diffraction, coupled with pair distribution function analysis to assess its crystal structure. Both methods lead to similar results and concur with those that can be found in the literature. A brief exploration of the salt's behaviour under heating with thermogravimetric analysis and differential scanning calorimetry shows that the salt decomposes under air and stays stable under nitrogen. However, it is difficult to fully extract the remaining water present in the structure.

Conflicts of interest

There are no conflicts of interest to declare.

Acknowledgements

- The authors acknowledge the financial support provided by the ANR LISBON (ANR-20-CE05-0022-01) project and the Normandy region.
- The authors would like to thank the ENSICAEN engineering school and staff for providing the rotary evaporator

Notes and references

1. Kalhoff J, Eshetu GG, Bresser D, Passerini S. Safer Electrolytes for Lithium-Ion Batteries: State of the Art and Perspectives. ChemSusChem. 2015 Jul 8;8(13):2154–75.

2. Manthiram A, Yu X, Wang S. Lithium battery chemistries enabled by solid-state electrolytes. Nat Rev Mater. 2017 Apr;2(4):16103.

3. Yabuuchi N, Kubota K, Dahbi M, Komaba S. Research Development on Sodium-Ion Batteries. Chem Rev. 2014 Dec 10;114(23):11636–82.

4. Banerjee A, Park KH, Heo JW, Nam YJ, Moon CK, Oh SM, et al. Na $_3$ SbS $_4$: A Solution Processable Sodium Superionic Conductor for All-Solid-State Sodium-Ion Batteries. Angew Chem Int Ed. 2016 Aug 8;55(33):9634–8.

5. Jalem R, Gao B, Tian HK, Tateyama Y. Theoretical study on stability and ion transport property with halide doping of Na 3 SbS 4 electrolyte for all-solid-state batteries. J Mater Chem A. 2022;10(5):2235–48.

6. Shimoda M, Maegawa M, Yoshida S, Akamatsu H, Hayashi K, Gorai P, et al. Controlling Defects to Achieve Reproducibly High Ionic Conductivity in Na3SbS4 Solid Electrolytes. Chem Mater [Internet]. 2022 Jun 6 [cited 2022 Jun 27]; Available from: https://doi.org/10.1021/acs.chemmater.2c00944

7. Won Kim T, Ho Park K, Eun Choi Y, Yeon Lee J, Seok Jung Y. Aqueous-solution synthesis of Na 3 SbS 4 solid electrolytes for all-solid-state Na-ion batteries. J Mater Chem A. 2018;6(3):840–4.

8. Zhang J. Synthesis via an organic molten salt solvent route and characterization of PbS nanocrystals. Cryst Res Technol. 2011 Oct;46(10):1058–64.

9. Jalem R, Hayashi A, Tsuji F, Sakuda A, Tateyama Y. First-Principles Calculation Study of Na+ Superionic Conduction Mechanism in W- and Mo-Doped Na3SbS4 Solid Electrolytes. Chem Mater. 2020 Oct 13;32(19):8373–81.

10. Rush LE, Hood ZD, Holzwarth NAW. Unraveling the electrolyte properties of ${\mathrm{Na}}_{3}{\mathrm{SbS}}_{4}$ through computation and experiment. Phys Rev Mater. 2017 Dec 11;1(7):075405.

11. Zhao C, Liu L, Qi X, Lu Y, Wu F, Zhao J, et al. Solid-State Sodium Batteries. Adv Energy Mater. 2018;8(17):1703012.

12. Anderer C, Delwa de Alarcón N, Näther C, Bensch W. A Strategy for the Preparation of Thioantimonates Based on the Concept of Weak Acids and Corresponding Strong Bases. Chem - Eur J. 2014 Dec 15;20(51):16953–9.

13. Danker F, Engesser TA, Broich D, Näther C, Bensch W. The cation and anion bonding modes make a difference: an unprecedented layered structure and a tri(hetero)nuclear moiety in thioantimonates(v). Dalton Trans. 2021;50(48):18107–17.

14. Danker F, Anderer C, Poschmann M, Terraschke H, Näther C, van Leusen J, et al. [Mn(terpy)Sb2S4]n, a 1D Network of MnSb4S5 Rings Exhibiting a Pronounced Magnetocaloric Effect and Luminescence. Eur J Inorg Chem. 2020;2020(18):1751–8.

15. Zotov A, Shikina ND, Akinfiev N. Thermodynamic properties of the Sb(III) hydroxide complex Sb(OH)3(aq) at hydrothermal conditions. 2003;

16. Mereiter K, Preisinger A, Guth H. Hydrogen bonds in Schlippe's salt: refinement of the crystal structures of Na3SbS4.9H2O by X-ray diffraction and Na3SbS4.9D2O by neutron diffraction at room temperature. Acta Crystallogr B. 1979 Jan 15;35(1):19–25.

17. Rodríguez-Carvajal J. Recent advances in magnetic structure determination by neutron powder diffraction. Phys B Condens Matter. 1993 Oct;192(1–2):55–69.

18. Roisnel T, Rodríquez-Carvajal J. WinPLOTR: A Windows Tool for Powder Diffraction Pattern Analysis. Mater Sci Forum. 2001 Oct;378–381:118–23.

19. Schmidtmann M, Coster P, Henry PF, Ting VP, Weller MT, Wilson CC. Determining hydrogen positions in crystal engineered organic molecular complexes by joint neutron powder and single crystal X-ray diffraction. CrystEngComm. 2014 Jan 23;16(7):1232–6.

20. Müller P, Herbst-Irmer R, Spek AL, Schneider TR, Sawaya MR. Crystal Structure Refinement: A Crystallographer's Guide to SHELXL [Internet]. Oxford: Oxford University Press; 2006 [cited 2022 Apr 28]. 232 p. (International Union of Crystallography Texts on Crystallography). Available from: https://oxford.universitypressscholarship.com/10.1093/acprof:oso/9780198570769.001.0001/acprof-9780198570769

21. Juhás P, Davis T, Farrow CL, Billinge SJL. *PDFgetX3* : a rapid and highly automatable program for processing powder diffraction data into total scattering pair distribution functions. J Appl Crystallogr. 2013 Apr 1;46(2):560–6.

22. Farrow CL, Juhas P, Liu JW, Bryndin D, Božin ES, Bloch J, et al. PDFfit2 and PDFgui: computer programs for studying nanostructure in crystals. J Phys Condens Matter. 2007 Aug 22;19(33):335219.

23. Hoy AR, Bunker PR. A precise solution of the rotation bending Schrödinger equation for a triatomic molecule with application to the water molecule. J Mol Spectrosc. 1979 Jan 1;74(1):1–8.

24. Haussühl S. Isotopie-Effekte in den optischen, elektrischen, elastischen und thermischen Eigenschaften der Schlippeschen Salze Na3SbS4 · 9H2O und Na3SbS4 · 9D2O. Z Für Krist - Cryst Mater. 1970 Dec 1;132(1–6):255–65.

25. Gamo H, Phuc NHH, Muto H, Matsuda A. Effects of Substituting S with Cl on the Structural and Electrochemical Characteristics of Na3SbS4 Solid Electrolytes. ACS Appl Energy Mater. 2021 Jun 28;4(6):6125–34.

RÉSUMÉ EN FRANÇAIS

Ces travaux de thèse portent sur la mise en œuvre de plusieurs méthodes de synthèse pour la formation du composé thioantimoniate $Ag_4MnSb_2S_6$, aussi connu sous le nom de samsonite. Ce composé n'a jamais été synthétisé jusqu'à aujourd'hui via des conditions de laboratoire. De nombreuses voies de synthèse dites « hors équilibre » ont donc été expérimentées afin d'obtenir ce composé monophasé et ainsi de déterminer ses propriétés structurales et de transport.

La structure cristalline de la samsonite est complexe, elle cristallise dans une maille monoclinique (groupe d'espace : $P2_{1/n}$) avec comme paramètres de maille : a = 10.3861 Å, b = 8.1108 Å, c = 6.6637 Å, and β = 92.639 °. Cette structure est composée d'atomes d'argent très mobiles (Ag1 et Ag2 – position de Wyckoff : *4e*), mais sans que cela ne provoque de conductivité ionique. Les atomes d'antimoine sont quant à eux (Sb1 – position de Wyckoff *4e*) en configuration AX_3E_1, présentant donc un doublet non-liant. Des études ont d'ores et déjà montrés que cette configuration de l'antimoine permet une amélioration des propriétés thermoélectriques grâce notamment à la diminution de la conductivité thermique de réseau. La structure complexe de ce composé, associée au doublet non liant de l'antimoine pourrait donc faire de ce matériau un excellent candidat pour des applications thermoélectriques.

Ces travaux de thèse impliquent donc des synthèses (voie solide, sels fondus, solvo/hydro-thermale, et polyol), ainsi que le traitement des poudres ainsi obtenues. Des caractérisations structurales et microstructurales ont été réalisées par diffraction des rayons X et microscopie électronique à balayage. Des méthodes de frittage (Spark Plasma Sintering, presse isostatique…) ont ensuite été expérimentées afin d'obtenir des échantillons denses, indispensables aux caractérisations de transport (résistivité électrique, coefficient Seebeck et conductivité thermique).

Mots-clés : Synthèse, Sulfures, Samsonite, Hydrothermal, Polyol, Sels Fondus

Titre : Nouveaux composes sulfures pour la production efficace d'énergie

SUMMARY IN ENGLISH

This Ph.D. project revolves around the setup of multiple synthesis methods to form the quaternary sulfide compound $Ag_4MnSb_2S_6$, also known as samsonite. This mineral, to this day, was never synthesized in a laboratory setting. Many "out-of-equilibrium" process methods have been tried out to obtain the compound as a single phase and evaluate its structural and physical properties.

Additionally, the crystal structure of the phase is quite complex (space group: $P2_{1/n}$ with cell parameters: a = 10.3861 Å, b = 8.1108 Å, c = 6.6637 Å, and β = 92.639 °). It is composed of strongly mobile silver atoms (Ag1 and Ag2 – Wyckoff position: 4e) that, however, do not induce ionic conductivity, and antimony atoms (Sb1 – Wyckoff position: 4e) in an AX_3E_1 configuration, implying the presence of an electron lone pair. Many studies have already been done to show that such a configuration allows for an improvement of the thermoelectric properties thanks to a decrease in the thermal conductivity in the structure. These properties may lead to characteristics of a good candidate for applications in this domain of energy production.

This manuscript revolves around concepts such as synthesis (solid-state, molten salt, solvo/hydrothermal, polyol), and powder treatment. An analysis of the structure and microstructure (X-Ray diffraction, scanning electron microscopy…). Sintering processes (Spark Plasma Sintering, isostatic pressing, …) have also been experimented on, to obtain a densified powder, a pre-requisite to study transport properties. Said transport properties (electric resistivity, Seebeck coefficient, and thermal conductivity) are consequently assessed and discussed.

Keywords: Synthesis, Sulfides, Samsonite, Hydrothermal, Polyol, Molten Salt

Title: New Sulfur Based Compounds for Efficient Energy Production